2-2013

Proximal Sensing as a Means of Characterizing *Phragmites australis*

Travis Yeik
University of Nebraska – Lincoln, tyeik@huskers.unl.edu

PROXIMAL SENSING AS A MEANS OF CHARACTERIZING

PHRAGMITES AUSTRALIS

By

Travis C. Yeik

A THESIS

Presented to the Faculty of

The Graduate College at the University of Nebraska

In Partial Fulfillment of Requirements

For the Degree of Master of Arts

Major: Geography

Under the Supervision of Professor Donald C. Rundquist

Lincoln, Nebraska

February, 2013

PROXIMAL SENSING AS A MEANS OF

CHARACTERIZING OF *PHRAGMITES AUSTRALIS*

Travis Yeik, M.A.

University of Nebraska, 2013

Advisor: Donald C. Rundquist

Phragmites australis is an invasive wetland weed found throughout much of the United States. Documenting and mapping the growth and spread of this emergent macrophyte can be an important step in developing and implementing successful management strategies. Characterizing the phenology of a vegetation species with a sensor capable of hyperspectral resolution, positioned at close proximity to the canopy of interest, is often a first step necessary for understanding the basic species-specific reflectance patterns, and for quantifying the manner in which light interacts with the plants comprising particular communities. Spectral data over a *P. australis* canopy were collected during 22 field campaigns in 2011. Research was aimed at characterizing the spectral responses of a *P. australis* canopy throughout a growing season, and then relating the acquired reflectance data to individual stages in the life cycle, as well as changes in the vegetation fraction associated with the plant canopy. A deconvolution of primary constituents comprising the spectral signal upwelling from the canopy aided in understanding the temporal variations in reflectance. Analyses of both spectra and digital photographs of the canopy led to the development of a new transformation, termed the

"Albedo Corrected Vegetation Index" (ACVI), aimed at increasing the accuracy in estimating vegetation fraction. Seed production and shoot density, both of which are closely linked with the invasive qualities of *P. australis*, were estimated using methods involving a simple digital camera as well as dual spectroradiometers. Additionally, considerations and procedures for collecting spectral data in the field were reviewed, and a procedure was developed, based upon concurrently acquired pyranometer data, to correct for incongruities that often occur due to the variable environmental conditions encountered during field campaigns. The findings of this research provide the necessary fundamental steps in the effort to monitor invasive species such as *P. australis* by means of remote sensing.

ACKNOWLEDGEMENTS

I would express my sincere appreciation to my committee advisor, Dr. Donald Rundquist for his guidance and patience in assisting me with my thesis writing. Not only has he immensely aided in my development of writing and research skills, but his instruction in the classroom, as well as outside of the university environment, have been most valued. I would also like to thank my other committee members, Dr. Sunil Narumalani and Dr. Stephen Young, for their support in my educational achievements.

Further thanks are extended to CALMIT for providing me with the opportunity and resources necessary for obtaining my educational goals. This includes many of my peers, especially David Gibbs, who spent relentless hours enduring the hot Nebraskan summer while aiding me with my data collection. It also includes Dr. Art Zygielbaum, for his valuable instruction in research protocols and data handling, and Bryan Leavitt for his counseling and insight on much of the research equipment I used.

Finally, my gratitude reaches out to my friends and family who have supported me along the way. Most of all, I would like to thank my wife Alyssa for the inspiration she has provided and the sacrifices that she has endured over the last three years. I would also like to thank my family members for their continued encouragement throughout my educational career.

TABLE OF CONTENTS

Chapter 1: Introduction

Chapter 2: Refining Methods for Spectral Calibration in the Field

Chapter 3: Remote Monitoring of Phenology and Vegetation Fraction in *Phragmites australis*

Chapter 4: Remote Sensing of Seed Production and Plant Density in *Phragmites australis*

Chapter 5: Conclusion

LIST OF TABLES

Chapter 2

Chapter 3

LIST OF FIGURES

Chapter 3

LIST OF APPENDICES

CHAPTER 1

INTRODUCTION

PROBLEM STATEMENT

The rapid expansion of an invasive, yet non-native haplotype of common reed, *Phragmites australis* (Cav.) Trin. ex Steudel (hereafter referred to as *P. australis*) throughout Midwestern U.S. States is cause for growing concern to resource managers. *P. australis* has been considered a progressively invasive machrophytic species, especially in the eastern U.S. (Rudrappa et al., 2007); however, as recently as the last 150 years, there has been a surge of *P. australis* populations which have expanded westward (Saltonstall, 2002 and 2003). The invasion of *P. australis* through riparian habitats has caused a number of negative consequences due to its ability to establish dense, near mono-specific stands that typically outcompete native vegetative species (Kettenring et al., 2009; Kiviat, 2010), thus endangering the diversity of floral and faunal habitats (Meyerson et al., 2000; Minchinton and Bertness, 2003). Further expansion of these dense stands may potentially block the drainage of waterways (Montiero et al., 1999), which then leads to sediment build-up and flooding (Weinstein and Balletto, 1999), as well as disrupting normal ecosystem processes (Chambers et al., 1999).

Timely and detailed monitoring of invasive species provides critical information necessary for land managers to make knowledgeable decisions about allocating resources for control efforts. This monitoring is an important step in deterring further expansion of *P. australis* (Blossey, 1999; Ailstock et al., 2001).

Remote sensing offers many beneficial advantages when attempting to monitor an emergent macrophyte species such as *P. australis*. Satellite and aerial remote sensing platforms are capable of providing reliable, cost-effective, and timely data on invasive species which are otherwise difficult to monitor in large, and often inaccessible, geographical locations. The introduction of hyperspectral systems for studying wetlands offers the ability to identify specific plant species such as *P. australis* in order to analyze its distribution patterns (Pengra et al., 2007). Moreover, data acquired by hyperspectral sensors have been used to analyze the growth, vigor, and biophysical characteristics of *P. australis* (Ullah et al., 2000; Hodgson, 2002; Lu et al., 2009).

Past studies, including Ullah et al. (2000) and Hodgson (2002), have investigated the seasonal growth of *P. australis*, by relating biophysical characteristics such as LAI, biomass, percent cover, and stem length to hyperspectral reflectance measurements. My study differs from these others primarily in terms of a greater length of time period for the field study. While Ullah (2000) and Hodgson (2002) collected spectral signatures of *P. australis* canopies a total of four and seven times respectively over the growing season, I provided an extremely detailed and accurate spectral library of the vegetation canopy by providing reflectance data 22 times over the growing season. Moreover, I investigated various other biophysical properties of *P. australis* by attempting to spectrally estimate seed production and stem densities.

OBJECTIVES

The overall objectives of this study were as follows:

1) Characterize the seasonal growth of *P. australis* by means of hyperspectral reflectance data acquired at close-range

2) Quantify two biophysical attributes, seed production and stem density, using proximal sensing methods.

ARRANGEMENT OF THE THESIS

This thesis consists of 5 chapters. Chapter 1 discusses the problem statement and overarching objectives of the study.

Due to unfortunate problems in the data collection process during 2011, some of the spectral reflectance data were found to be incongruent of a typical vegetation spectra. Thus, chapter 2 of this thesis focuses on applying correction techniques in order to provide useful data for the subsequent chapter. Therefore, a third objective was added to the thesis:

3) Provide a method for correcting error in reflectance data acquired by spectroradiometers.

Although this objective was unintentionally introduced during the beginning of the data analysis period, it was included as a necessary requirement for preventing data loss.

Chapter 3 investigates the seasonal variations in the growth of the *P. australis* canopy through spectral measurements, and comparison to measured fraction of cover. Further analysis in this chapter examines the potential utility of a newly developed spectral index for estimating percent canopy cover.

Chapter 4 investigates the relationship between spectral data acquired by either a digital camera or a hyperspectral radiometer placed at close-range to the vegetation canopy in order to estimate seed production and stem density.

Chapter 5 summarizes the conclusions of the work and recommendations for future research.

REFERENCES

Ailstock, M. S., C. M. Norman, and P. J. Bushmann. 2001. Common Reed *Phragmites australis*: Control and Effects Upon Biodiversity in Freshwater Nontidal Wetlands. *Restoration Ecology*, 9 (1): 49–59.

Blossey, B. 1999. Before, During and After: The Need for Long-term Monitoring in Invasive Plant Species Management. *Biological Invasions*, 1 (2): 301–311.

Chambers, R. M., L. A. Meyerson, and K. Saltonstall. 1999. Expansion of *Phragmites australis* into Tidal Wetlands of North America. *Aquatic Botany*, 64 (3-4): 261–273.

Hodgson, A. B. 2002. Characterizing Wetland Plant Communities: An Analysis of Hyperspectral and Biophysical Relationships in Three Taxa of Wetland Macrophytes. Ph.D. Thesis. The Graduate College, University of Nebraska, Lincoln, Nebraska, USA.

Kettenring, K. M., M. K. McCormick, H. M. Baron, and D. F. Whigham. 2009. *Phragmites australis* (Common Reed) Invasion in the Rhode River Subestuary of the Chesapeake Bay: Disentangling the Effects of Foliar Nutrients, Genetic Diversity, Patch Size, and Seed Viability. *Estuaries and Coasts*, 33 (1): 118–126.

Kiviat, E. 2010. *Phragmites* Management Sourcebook for the Tidal Hudson River and the Northeastern States. Annandale, NY: Hudsonia Ltd. hudsonia.org.

Lu, S., Y. Shimizu, J. Ishii, S. Funakoshi, I. Washitani, and K. Omasa. 2009. Estimation of Abundance and Distribution of Two Moist Tall Grasses in the Watarase

Wetland, Japan, Using Hyperspectral Imagery. *ISPRS Journal of Photogrammetry and Remote Sensing*, 64 (6): 674–682.

Meyerson, L. A., K. Saltonstall, L. Windham, E. Kiviat, and S. Findlay. 2000. A Comparison of *Phragmites australis* in Freshwater and Brackish Marsh Environments in North America. *Wetlands Ecology and Management*, 8 (2): 89–103.

Minchinton, T. E. and M. D. Bertness. 2003. Disturbance-Mediated Competition and the Spread of *Phragmites australis* in a Coastal Marsh. *Ecological Applications*, 13 (5): 1400–1416.

Monteiro, A., I. Moreira, and E. Sousa. 1999. Effect of Prior Common Reed (*Phragmites australis*) cutting on Herbicide Efficacy. *Hydrobiologia*, 415 (0): 305–308.

Pengra, B. W., C. A. Johnston, and T. R. Loveland. 2007. Mapping an Invasive Plant, *Phragmites australis*, in Coastal Wetlands Using the EO-1 Hyperion Hyperspectral Sensor. *Remote Sensing of Environment*, 108 (1): 74–81.

Rudrappa, T., J. Bonsall, J. L. Gallagher, D. M. Seliskar, and H. P. Bais. 2007. Root-secreted Allelochemical in the Noxious Weed *Phragmites australis* Deploys a Reactive Oxygen Species Response and Microtubule Assembly Disruption to Execute Rhizotoxicity. *Journal of Chemical Ecology*, 33 (10): 1898–1918.

Saltonstall, K. 2002. Cryptic Invasion by a Non-native Genotype of the Common Reed, *Phragmites australis*, into North America. *Proceedings of the National Academy of Sciences*, 99 (4): 2445–2449.

Saltonstall, K. 2003. Genetic Variation Among North American Populations of *Phragmites australis*: Implications for Management. *Estuaries and Coasts*, 26 (2): 444–451.

Ullah, A., D. C. Rundquist, and D. P. Derry. 2000. Characterizing Spectral Signatures for Three Selected Emergent Aquatic Macrophytes: A Controlled Experiment. *Geocarto International*, 15 (4): 31–42.

Weinstein, M. P. and J. H. Balletto. 1999. Does the Common Reed, *Phragmites australis*, Affect Essential Fish Habitat? *Estuaries*, 22 (3): 793.

CHAPTER 2

REFINING METHODS FOR SPECTRAL CALIBRATION IN THE FIELD

ABSTRACT

It is necessary, when employing concurrently operating, but separate, upward- and downward looking spectroradiometers in a field setting, to make sure that the radiometric and spectral sensitivities of the two instruments are exactly the same. It seems clear that the instrument collecting the irradiance downwelling through the atmosphere must be precisely matched with the instrument collecting the radiance upwelling from the target of interest. Upon completion of the 2011 field season and during the analysis of acquired spectra, inconsistencies were noted in the reflectance profiles. In an effort to avoid loss of important data, the characteristics of the spectral reflectance information were examined in great detail. The analysis led to the development of a procedure to correct data acquired by mismatched spectroradiometers by normalizing the incident irradiance to the photon flux acquired by a pyranometer operating simultaneously with the spectroradiometer scanning. The approach reduced variation in the sensitivities between the two hyperspectral field radiometers by 72%. Even so, minor irregularities remained in the near-infrared portions of the re-processed spectra, which highlights the need for further research. After carefully reviewing field procedures to be implemented when undertaking proximal sensing for scientific purposes and scrutinizing all possible sources of error in the 2011 dataset, it was determined that the problem was very likely introduced due to moisture condensing under the cosine

diffuser attached to the upward-looking spectroradiometer. Material presented in this paper should be helpful for ensuring proper data collection methods are followed in future campaigns focused on close-range spectroscopy.

INTRODUCTION

Remote sensing, in general, is defined as the art and science of obtaining information about an object without being in direct physical contact with the object (Jensen, 2000). Throughout its history, there have been many definitions of 'remote sensing' (see Fussell et al., 1986) and how it is applied; however, in the context of this paper, remote sensing is limited to a sensor acquiring visible and near-infrared energy, in a large number of individual wavelengths, as reflected from the Earth's surface.

Typically, a "remote sensor" collects data from a platform operating at aircraft or satellite altitudes, whereas a "proximal sensor" involves collecting information from a ground-based platform that is in close proximity to the target or object of interest (Price, 1986). Three commonly used synonyms for the term proximal sensing include "in-situ sensing," "close-range sensing" and "field spectroscopy." The current paper is aimed at refining one procedural component generally associated with proximal sensing, that of calibrating instruments in the field.

One proximal sensing method of acquiring data from a target involves use of a "spectroradiometer," a non-imaging field radiometer capable of providing the researcher with both the intensity and spectral distribution of energy radiating from within the sensor's field of view. The data, acquired in many narrow, discrete channels within the electromagnetic spectrum, allow construction of "spectral profiles" or "spectral curves," which are graphs illustrating the intensity and spectral distribution parameters noted above. The graphs typically depict wavelength on the x-axis and percent reflectance on the y-axis (see example of Figure 2.1).

Spectroradiometers are "hyperspectral," that is they provide reflectance information in hundreds or even thousands of individual, narrow wavebands. Such an instrument uses a charge-coupled device (CCD), often chips made of silicon, to capture incoming photons in a capacitor and convert them to an electrical charge proportional to the light intensity at the many wavelengths of sensitivity. That voltage created can then be converted to a digital number, and then radiance, or the amount of radiant flux per unit incident angle scattered or emitted by the target object.

There are many reasons to employ proximal spectroradiometers for data collection, including the quantitative assessment of the interrelationship between the field collected spectral data and biophysical characteristics of a target object. Such an approach is an important component of scientific research in both the sensor sciences and the vegetation sciences. Multi-temporal field campaigns aimed at collecting spectral data have provided for the estimation and modeling of numerous biophysical characteristics associated with terrestrial vegetation such as chlorophyll content, absorbed photosynthetically active radiation, plant biomass, vegetation fraction, gross primary production, and leaf area index (Kim et al., 1994; Broge and Mortensen, 2002; Huete et al., 2002; Gitelson et al., 2002; and Wu et al., 2009).

Field spectroscopy has also been employed to corroborate with findings derived from other types of electronic systems, most generally sensors that are truly remote (i.e., aircraft and satellite instruments). Thus, spectra collected by portable field spectroradiometers are useful for validating and verifying the results of satellite and airborne data collection missions. The specific types of applications may include

atmospheric correction, spectral end-member identification, and accuracy assessment (O'Neill et al., 1997; Plaza et al., 2004; and Coll et al., 2005).

Spectral Calibration

In order to not only produce reliable scientific results but also establish data compatibility among different remote sensing research groups, incident radiation measured by a spectroradiometer must be calibrated to a known and widely accepted reflectance standard. Over the years, researchers have used a variety of bright white, very diffuse target materials as calibration standards ranging from inexpensive, readily available substances such as housing-insulation materials or Kodak gray cards to expensive, laboratory prepared substances such as barium sulfate.

Today's technology related to calibration generally involves the use of "Spectralon" (Labspere, Inc., North Sutton, NH), a molded material made of polytetraflourethylene. It has become established as a leading material for calibration panels because it is a nearly perfect Lambertian reflector, insuring a diffuse reflection that radiates equally in all directions and at all wavelengths. Spectralon holds up well in harsh environmental conditions, it is washable, and it is traceable to a reference surface held by the U.S. National Institute of Standards and Technology (Milton et al., 2009). The barium sulfate reference panels and Kodak cards used in the past were relatively poor Lambertian reflectors, were incapable of being cleaned, and were inconsistent when comparative tests were done (Jackson et al., 1992; Soffer et al., 1995).

Besides the "purely scientific" reasons for undertaking calibration of field spectral instruments, there are practical considerations. Examples include the fact that data are often acquired at a variety of illumination conditions, sun-target-sensor geometries, and with somewhat diverse instrument types. Therefore, it was important that a procedure be developed to "standardize" the spectral measurements made in the field by researchers.

In order to quantify the spectral response of a target object by means of field spectroscopy, a 'reflectance factor' should be calculated (Nicodemus et al., 1977). The reflectance factor is defined as the ratio of the radiant flux reflected by a target to that which would be reflected into the same reflected-beam geometry by an isotropic diffuse (i.e., Lambertian) standard surface irradiated in exactly the same way as the sample. In practice, this measure is expressed simply as percent reflectance; that is the ratio of the upwelling radiance from a target to the downwelling atmospheric irradiance acquired at the time of the corresponding radiance measurement. Typically, the upwelling measurement is acquired by scanning a reference panel (Spectralon) using a spectroradiometer. Percent reflectance, a convenient unit of measure, is calculated because it is an inherent property of an object and is independent of the intensity and nature of illumination, unlike radiance and irradiance (Peddle et al., 2001).

Spectral reflectance of objects in the field is typically measured using a single radiometer, which must be calibrated periodically to compensate for variations in sky conditions. The "rule of thumb" here was to "calibrate at least every 20 minutes." Many studies were published over the years using such a procedure, where the researcher typically scanned a white reference surface, and then scanned the target of interest, trying

to minimize the time delay between the two measurements. The goal was generally to calculate a percent reflectance for each of the wavelengths to which the instrument was sensitive. The measured reflectance at each wavelength was then graphed to create the spectral profile for the target of interest, as noted above. The basic problem, though, was that any change in sky conditions, such as the occurrence of rapidly moving cirrus clouds, invalidated the measurement. If the sky was not completely clear and stable, and if even a relatively small amount of time elapsed between the scanning of the reference panel and the scanning of the target, the scientific basis for the spectral result was lost. Typically, these changes in solar irradiance were caused by rapidly moving clouds and other atmospheric particulates, and they occurred within a time period from seconds to minutes.

Duggin (1981) proposed a method of alleviating the problem concerning the time delay between the scanning of a target in the field and a calibration panel. His suggested approach involved the use of two spectroradiometers; one for capturing the downwelling irradiance and the other for capturing the upwelling radiance concurrent with the former. A main point here was that the two instruments should be activated at the same time. Of course, there are a number of technical issues that need to be addressed before operationalizing such an approach, most of which are related to the precise matching of the two instruments. But, if these nontrivial technical considerations can be properly addressed, the result should be a powerful data collection system.

Only a few research groups actually tried to develop the approach described by Duggin, and some problems were identified. The author himself (Duggin, 1981)

acknowledged that the "dual headed" radiometer system was not perfect and produced ~10% discrepancy in the reflectance factor, or perhaps more when non-uniform irradiation conditions existed (Milton, 1981). Bolsenge and Kistler (1982) also found variations in the ratio between the sensor collecting irradiance and the sensor collecting radiance of the calibration panel over a period of five data collection days. They concluded that most of the variations in calibration ratios are due to variations in sensitivity between the two units. To reduce uncertainties in their data, they applied correction factors to spectral data collected under clear skies in order to adjust for differences in cosine diffuser responses (i.e., the downwelling irradiance). Similarly, Anderson et al. (2006) found variability in the correction of the two radiometers even over a four hour time period around solar noon. They pointed out multiple variables contributing to the change in reflectance factor between the two radiometers including the solar zenith angle, warm-up times, and detector sensitivity responses to environmental conditions.

One group, at the Center for Advanced Land Management Information Technologies (CALMIT), University of Nebraska-Lincoln, has been using such an approach since the early 1990's. Originally constructed using a pair of Spectron SE-590 spectroradiometers (Denver, CO), CALMIT scientists more recently based their system on twin Ocean Optics (Dunedin, FL) USB-2000 instruments, where one fiber-optic is pointed upward while the other is pointed downward during concurrent scanning. They developed algorithms to precisely match the two instruments, both in terms of band centers and sensitivities. This paper is linked to the well-known CALMIT system for

collection of spectral data in the field (e.g., Rundquist et al., 2001; 2004). Several CALMIT studies conducted using the dual-headed fiber-optic approach have successfully demonstrated the relationship between various biophysical vegetation characteristics and spectral transformations (i.e., indices). For example, Gitelson (2005) showed how the chlorophyll red-edge index was closely correlated to canopy chlorophyll content in maize and soybeans. Other studies have utilized the dual-fiber optics approach and have effectively linked several vegetation indices to leaf area index, plant biomass, fraction of absorbed photosynthetically active radiation, green vegetation fraction, and the CO2 flux at canopy level (Gitelson et al., 2003a; 2003b; Viña et al., 2004; Viña and Gitelson, 2005). Overall, the dual radiometer approach is one of the most effective methods for acquiring accurate reflectance data in support of field studies.

Objectives

Following data collection during the 2011 field season, some inconsistencies were noticed in the spectral profiles associated with sampled plots in a canopy of common reed (*Phragmites australis*, hereafter referred to simply as *P. australis*). The broad-band reflectance of the *P. australis* canopy, as collected using the dual-fiber Ocean Optics approach over the course of the 2011 growing season (as shown by day-of year, DOY, on the x-axis), in the blue (400-500 nm), green (500-600 nm), red (600-700 nm), and near-infrared (NIR, 750-850 nm) spectral regions is displayed in Figure 2.2. In general, the curves are in agreement with what one would expect from a vegetation canopy; specifically, there is a decrease in reflectance for the three components in the visible

(VIS) spectrum (400-700 nm) and an increase reflectance in the NIR during the middle of the growing season (DOY 151 – 263) due to an increase in vegetative biomass. The curves shown are in contrast to normal vegetation phenology, as seen by noticeable fluctuations in the reflectance at all wavelengths evident between DOY 181 and 213. Specifically, there is a sharp reflectance minimum associated with all wavelengths studied between DOY 181 and 188, then a sharp maximum between DOY 188 and 193 followed by another reflectance minimum between DOY 193 and 213. The peak increase in reflectance (noted previously) is particularly distinct and is associated with a 1.8% increase in the blue region, 3.7% in the green, 2.6% in the red, and a substantial 36.8% in the NIR. Remarkably large changes in reflectance within a week are unusual unless environmental conditions (e.g., hail or frost) caused a decrease in the amount of green vegetation present; however, such did not occur during the 2011 growing season. Figure 2.2 caused the realization that error was inadvertently introduced into the dataset during the temporal period noted above, and an investigation was undertaken in an effort to develop a satisfactory procedure for preventing data loss.

The consequences of this error, caused by some unknown inequality between the two radiometers during the 2011 field season, and the potential for leading to erroneous conclusions, were recognized. Therefore, purpose of this paper was to solve the problem by 1) reviewing the challenges in matching inter-calibrated radiometers; 2) locating the cause of the problem of sensor inequality (which leads to measurement errors); and 3) suggesting a potential method to correct the errors in acquired spectral data (i.e., thus preventing data loss).

METHODS

Field Site

During the 2011 growing season, a study was undertaken using four manmade wetland plots at the CALMIT field research facilities, located near Mead, Nebraska, USA. These facilities are part of the University of Nebraska-Lincoln Agricultural Research Development Center (ARDC) located approximately 56 km northeast of Lincoln, Nebraska.

Five to six sample areas (depending on the total size of the area available for data collection within the plot) in each of the four wetland plots were selected as representative of a *P. australis* canopy. To facilitate repetitive sampling, flags were used to mark the target areas very clearly for subsequent spectral scanning. Each of the four plots was less than 100 m apart and it took approximately five minutes to position equipment and set up for scanning from one plot to the next. Calibrations were acquired systematically in the same location every field campaign day less than 200 m from the plots and were away from corner reflecting objects in order minimize scattering from non-target objects.

Hercules

Spectral characterization of the *P. australis* life cycle requires repetitive collection of reflectance data over the sample plots of vegetation, and in this case, those data were acquired using field spectroradiometers mounted on the boom of "Hercules," an all-terrain, motorized platform (Appendix A). Hercules, similar to its predecessor "Goliath"

(Rundquist et al., 2004), provides an ideal platform for collecting remotely sensed data because the configuration of the instrument position is relatively rigid, thus minimizing noise from vibration, and the approach allows repeatable orientation of sensors from one sample site to the next. Once the height of the boom is set relative to the top of the canopy, it remains at that fixed vertical distance above the target. The boom, which may also be rotated to ensure that the sensors are continuously in the principal plane of the sun, extends to 10 m from the machine, ensuring that reflectance from non-target objects, such as colored clothing worn by an operator, is eliminated. Additionally, Hercules is painted a flat-black color to reduce extraneous scattering of photons from the platform itself. During data collection, Hercules was positioned directly north of the target canopy being acquired with the boom pointed south to eliminate spurious reflectance measurements caused by shadowing from the platform.

Procedure for Measuring Spectral Reflectance and Collecting Ancillary Data

Spectral reflectance measurements of *P. australis* were acquired weekly from late April through the middle of October, for a total of 22 field campaigns during the 2011 growing season. Spectral data were collected using a dual-fiber optic system, which employs two inter-calibrated Ocean Optics (Dunedin, FL) USB2000 hyperspectral radiometers, as noted previously. The system records spectral data in approximately 2000 bands between 400 – 900 nm (visible and near-infrared) with a band interval of ~.3 nm and a spectral resolution of ~1.5 nm. One radiometer, equipped with an optical fiber and cosine diffuser, is pointed upward to measure incident irradiance at each wavelength

(E_λ) within a hemispherical field-of-view. The other radiometer, equipped with an optical fiber capable of acquiring radiation in a 25° field-of-view, is pointed downward to measure radiance upwelling at each wavelength from the target (L_λ). A correction factor (CF) is necessary to match the transfer functions and for inter-calibration of the radiometers. This was accomplished by acquiring a spectral measurement of upwelling radiance (L_λ^{cal}) from a Spectralon reference panel (Labsphere, Inc., North Sutton, NH) which is calibrated to approximately 99% Lambertian reflectance, simultaneously with the measure of incident irradiance (E_λ^{cal}). The CF can then be calculated as

$$CF_\lambda = \frac{P_\lambda^{cal} \times E_\lambda^{cal}}{L_\lambda^{cal}} \qquad\qquad [1]$$

where P_λ^{cal} is the Lambertian reflectance calibrated at each wavelength from the Spectralon panel and linearly interpolated in order to correlate the band centers of the two radiometers. A CF value was calculated at each band center by calculating the median reflectance of daily scans from the calibration panel.

To calibrate the radiance collected from spectral instruments (i.e., acquire L_λ^{cal} and E_λ^{cal}), the downward-looking specroradiometer was positioned at a height of approximately 30 cm above a 30.5 x 30.5 cm (12 in. x 12 in.) white Spectralon panel. A minimum of eight spectral measurements of upwelling radiance and downwelling irradiance were taken concurrently during an interval of approximately 16 seconds, and the median values for each individual band were calculated. For each data collection campaign during the growing season, multiple spectral scans of the calibration panel

were acquired during a 15 minute interval near solar noon (11:00 and 13:00 local time),
when diurnal variations in the incoming radiation are nearly constant due to a near-
vertical zenith angle. Solar zenith angle is calculated at the time of the scan to correct for
non-Lambertian reflectance from the Spectralon panel when angles above 60° were
observed (Rollin et al., 2000).

Once the scans of the reference panel were completed, during each of the field
campaigns, spectral reflectance measurements over the five sample areas within the *P.
australis* experimental plot were acquired at a height of 5.8 m above the vegetation
targets, yielding a 2.7 m instantaneous-field-of-view (IFOV) at the top of the canopy.
For each of the scanning sessions per sample area, a minimum of eight spectral
measurements of upwelling *P. australis* radiance and downwelling irradiance from the
atmosphere were taken concurrently, and the median values for each band were
calculated. Percent reflectance from the *P. australis* canopy (ρ_λ) was determined by the
following equation:

$$\rho_\lambda = \frac{L_\lambda}{E_\lambda} \times CF_\lambda \times 100 \qquad [2]$$

Simultaneously during the data collection process, measurements were also
obtained (once per second) from both a pyranometer (LI-200, LI-COR Inc., Lincoln,
Nebraska) and a quantum sensor (LI-190, LI-COR Inc., Lincoln, Nebraska), both of
which were attached to the boom of Hercules. The pyranometer and quantum sensors,
which collected incoming flux in the 400-1100 nm and the 400-700 nm range

respectively, were sampled concurrently with one another using a Campbell Scientific 21X datalogger (Logan, UT). An average value was then calculated for each sensor for the entire duration of the corresponding spectral scan.

RESULTS AND DISCUSSION

Correction Technique Suggested by Past Literature

The CF values between the two spectroradiometers over the course of the season varied considerably (average coefficient of variation, CV, between 400-900 nm = 25.4%; also depicted in Figure 2.3), thus suggesting that the sensitivities of the two sensors were unstable. The CF and CV values calculated from the 2011 and previous field seasons using the dual-headed sensor system (over corn and soybeans) were compared (Figure 2.3). Between 2005 and 2008 (there was no acquisition of field data with Hercules in 2009 and 2010), average CV values between 400-900 nm ranged from 5.1% (2007) to 22.1% (2005); however, in 2005 the deviation is large due to a broken fiber optic which occurred midway through the field season. Nevertheless, the variation noted above may cause considerable error in spectral reflectance and data collection methods apparently needed adjustment.

Anderson et al. (2006) suggested a method to substitute inaccurate CF values at each wavelength with those collected both geographically and temporally close to one another; thus, minimizing anisotropic effects caused by changing sun/sensor geometries. This method was tested by substituting CF values calculated on field outings before and after the observed fluctuations between DOY 181 and 213; as a result, the spectral

reflectance curve characterizing *P. australis* per wavelength was merely shifted vertically (i.e., the reflectance spectra were adjusted along the y-axis), but spurious reflectance measurements were still apparent. The result of the Anderson et al. (2006) technique did not provide a suitable quantitative solution to the problem because the multi-temporal spectral curve visually fluctuates over a relatively large time period (25 days), and selecting an appropriate CF for substitution was difficult if not impossible.

Causes for Uncertainty in Spectral Reflectance

A field technician must be aware of and understand the nature of inconsistencies in acquired spectral data, whether they are caused by instrument fluctuations, environmental conditions, human error, or other. It would seem that such awareness and understanding could allow for correcting problems with data acquired in the past as well as adjusting field procedures to eliminate errors from occurring during the future field campaigns.

A multitude of potential problems surround hardware configurations operating in field settings. Fiber optics should be examined carefully to ensure they do not contain breaks or cracks. Also, dual linked radiometers need to be spectrally calibrated to ensure that the array of CCD sensors in one spectroradiometer is concomitant with the other, thus matching the band centers of the two devices. Additionally, the two instruments must be identical in terms of levels of sensitivity (i.e., the radiometry must match). The CCD and other electrical components within each spectroradiometer may be sensitive to external factors such as variable ambient temperatures, high humidity, or voltage inputs

from the battery. Although some of the noted impacts are wavelength specific (e.g., air temperature), radiometric noise is nevertheless generated, which in turn produces differences between the two sensors in the quantification of the incoming signals (Anderson et al., 2006).

Another important issue is linked to how the sensors are deployed in the field setting. Specifically, considerable variability is introduced into spectra acquired by means of an investigator holding a sensor (or sensors) and simply "pointing" the device at the target. The spectra compiled by sensors positioned on a mechanical boom are much more reliable and contain considerably less variation (Rundquist, et al., 2004).

There are environmental complications that exacerbate the challenge of precisely matching dual spectroradiometers. Because the intensity of irradiation from a bright sky (as received by the upward looking radiometer) is sufficiently greater than the upwelling radiation (as received by the downward-looking radiometer), there is a lag time of milliseconds between the integration times of the two radiometers. In other words, the sensor collecting the upwelling signal from a relatively dark target integrates for a slightly longer period of time than the sensor collecting the downwelling signal from the relatively bright sky. Unfortunately, a few milliseconds of difference in integration time between the two instruments may introduce error into the compiled spectral signal. This situation may be exacerbated during a field campaign when there are noticeable fluxes in the incoming irradiance (e.g., due to the occurrence of small, rapidly moving cirrus clouds). The matter of differing integration times, however, is one issue for which no solution has been brought forward. Automatic determination of necessary integration

times is built into field spectroradiometers, and when two different instruments are pointed at two targets that differ greatly in brightness, a "mismatch" is the inherent outcome.

Several errors may be introduced when the field researcher fails to implement consistent, systematic methods for acquiring spectral reflectance data. Duggin and Philipson (1982) and Milton (1987) outline several guidelines (discussed below) for ensuring proper collection of proximal sensing data. These guidelines, or techniques, should be followed closely in order to produce accurate and meaningful data, and perhaps more importantly, in order to establish standardization of data among researchers comprising the remote sensing community.

One important guideline requires the researcher to maintain a fixed geometry between the sun and sensor, which alleviates problems caused by bi-directional reflectance factors (BDRF). The BDRF are an anisotropic consequence of non-perfect Lambertian reflectance from the calibration panel, the cosine diffuser on an upward looking fiber optic (yielding a hemispherical view), and the target object of interest. For example, because both the cosine diffuser and the calibration panel are slightly non-Lambertian, which is especially noticeable at low solar zenith angles, they may produce dissimilar anisotropic characteristics and make it difficult to precisely match the dual radiometers (Rollins et al., 2000; Anderson, et al., 2006). Jackson et al. (1992) proposed calibration equations to minimize errors induced by BDRF related to several Spectralon panels; however, the reflectance properties from a supposed Lambertian reference panel

remain an approximation based, to some extent, on the solar angle, so uncertainties are still present (Lillesand and Kiefer, 2000).

Although the challenges of obtaining near-perfect Lambertian reflectance standards were more prevalent when Kodak gray cards and boards painted with barium sulfate were commonly used, there are several issues that remain to be addressed when calibrating with Spectralon panels. For instance, an unclean or scratched calibration panel is capable of producing exceptionally non-Lambertian reflectance, which alters the total amount of light available to the sensor. Moreover, impediments such as dust or water on the cosine diffuser, upwelling tip of the fiber optic, or calibration panel will inherently cause inaccurate measurements in the amount of irradiance/radiance measured; therefore, careful inspection of equipment should occur prior to scanning any object of interest. Not only should equipment be checked prior to scanning, but other "odd" and unanticipated happenings may lead to erroneous data during the data collection process. One example of such atypical occurrences include finding an insect perched comfortably on the tip of the fiber optic.

A guideline for obtaining accurate multi-temporal data, such as attempting to monitor spectral changes associated with a vegetation canopy throughout the course of the growing season, requires reproducing identical system configurations each time data are collected. For example, it is very important to maintain a constant distance between the target and the sensor, which thereby leads to a constant IFOV. Although relatively simple to implement, such a procedure ensures that any changes in the reflected signals accumulated over the course of a growing season are not a result of variations in the

sensor IFOV. Therefore, the researcher must make height adjustments to the sensor position concomitantly with the vertically growing plant canopy (i.e., *P. australis*) during a field season in order maintain a constant IFOV.

A researcher must also be aware of extraneous signals measured by the sensors that originate from non-targeted objects such as corner reflectors (i.e., trees and large buildings). Other non-targeted objects signals stemming from the sensing platform itself or the clothing worn by field researchers are capable of redirecting photons into the upwelling radiation stream (Rundquist, et al., 2004). A good rule of thumb is for technicians to remain at least five meters away from targets. There are certainly a number of variables which may cause problems in proximal sensing data collection, but with proper technique, most, if not all of the problems presented can be minimized or nearly eliminated.

Identifying the Source of Error

Prerequisite to correcting for the erroneous vegetation spectra acquired over the course of the 2011 growing season was a need to identify the specific factor (or factors) contributing to those errors. The first step was to simply cross-correlate digital numbers (DN's), or raw measurements of the light intensity acquired by the Ocean Optics sensors, with several environmental measurements occurring at the time of data collection in the field in order to determine whether those variables may have impacted sensor performance. Environmental data recorded during spectral scanning included ambient air temperature, relative humidity, and wind speed. Table 2.1 shows the correlation between

the DN's, as measured by both the upward-looking (measuring downwelling hemispherical irradiance from the sky) and downward-looking (measuring upwelling radiance from the calibration panel) spectroradiometer fiber optics in the VIS through the NIR spectrum with the environmental conditions extant during each calibration session in the field over the entire course of the growing season. As observed in Table 2.1, the correlations between air temperature (R^2 ranging from 0.003 [$\rho < 0.990$] to 0.079 [$\rho < 0.741$]) and wind speed (R^2 ranging from 0.000 [$\rho < 0.998$] to 0.020 [$\rho < 0.934$]) vs. radiance acquired by the upward-looking sensor and irradiance acquired by the downward-looking sensor in the VIS through NIR spectrums were non-significant and correlations pertaining to relative humidity vs. similar radiance/irradiance were non-significant and weak respectively (R^2 ranging between 0.286 [$\rho < 0.222$] and 0.544 [$\rho < 0.013$]). But, more important than the previous finding was that the correlations between irradiance acquired in two different ways (i.e., by the sensors pointed at the sky versus pointed at the white reference panel) varied substantially from one another. This unexpected finding leads one to conclude that the levels of radiometric sensitivities of the two Ocean Optics instruments were different.

The second step in the approach, aimed at examining the variability in sensitivity between the two Ocean Optics spectroradiometers, involved correlating the radiometric data acquired by the fiber-optic systems to other types of sensors operating concurrently with spectral scanning. In this case, both a pyranometer and a quantum sensor were also collecting photon-flux data downwelling from the atmosphere during the calibration scans (as noted in the Methods section). This procedure involved integrating the DN's

acquired by the downward and upward-looking Ocean Optics systems during calibration to the wavelength ranges of both the pyranometer (400 – 1100 nm) and quantum sensor (400 – 700 nm). In this way, radiant flux, or the total intensity of the energy downwelling from the atmosphere in the VIS and/or NIR spectra, was calculated; in other words, the Ocean Optics measurements of irradiance were compared directly with the irradiance recorded by the pyranometer and quantum sensor. The information acquired by the latter two sensors positioned on Hercules was verified by means of comparison with a similar sensor operated as part of a weather station configuration, and located only 3 km away (R^2 = 0.952 and 0.962 respectively).

One minor problem in the developed methodology was that the wavelength range of data selected for use in the research and acquired by the Ocean Optics sensors was slightly narrower than that of the pyranometer (400 – 900 nm versus 400 – 1100 nm respectively). However, the slight difference in wavelength ranges likely results in little, if any, difference in the correlations of radiant flux between the instruments because the radiant output per wavelength emitted by the sun (in the ranges noted) remains essentially the same, as demonstrated by Planck's curves. Therefore, the summation of the energy received by the Ocean Optics sensors in the wavelength range between 400 and 900 nm was used to correlate with the photon-flux data acquired by the pyranometer in the same wavelength range.

In the case of the quantum sensor, the range of sensitivity is, by the very nature of the instrument, restricted to the visible range, or photosynthetically active radiation (PAR). Therefore, the Ocean Optics data were integrated (i.e., summed) for the PAR

region of the spectrum for correlation with the photosynthetic photon-flux information acquired by the quantum sensor.

The relationship between calculated radiant flux as measured by both the upward and downward-looking Ocean Optics instruments vs. radiant flux measured by the pyranometer and quantum sensor is summarized in Figure 2.4 (a-b) and Figure 2.4 (c-d) respectively.   The figures show a strong positive correlation between radiant flux measured by the downward-looking radiometer (i.e., measuring the signal from the white reference panel) and the pyranometer/quantum sensor (R^2 = 0.973/0.989 respectively); and a weaker relationship between radiant flux acquired by the upward-looking sensor (i.e., measuring the downwelling atmospheric irradiance directly using a hemispherical cosine diffuser on the fiber optic) and the pyranometer/quantum sensor (R^2 = 0.657/0.638 respectively).   These latter, low correlations suggest that there was a problem associated with the upward-looking Ocean Optics sensor that led to inaccurate measurements of downwelling irradiance.   More specifically, the problem was identified, then, as a variation in the sensitivities of the two Ocean Optics sensors used during the course of the entire 2011 field season. That sensitivity difference led, in turn, to the fluctuations in the spectra recorded during the data collection campaigns, as documented in Figure 2.2.

Once it was established that a sensitivity difference was the root of the problem, it was determined that a detailed evaluation of the individual sensor responses for each of the 2011 field campaigns was necessary. A logical first step here seemed to be a careful comparison of the signal acquisitions by the upward-looking Ocean Optics fiber and the pyranometer for each field expedition.   Because of obvious redundancies between the

two instruments, and the greater wavelength range of the pyranometer, only the pyranometer data were used for subsequent steps. Radiant flux values calculated from the upward-looking sensor (as described above) and measured photon flux acquired by the pyranometer were standardized (measured as the number of standard deviations from the mean radiant flux acquired throughout the day) to a scale which could be compared to one another throughout each field collection day. These scaled values were then differenced from one another in order to analyze the stability or instability of the upward-looking sensor as compared to the pyranometer (which, as noted in the Methods section, was recording photon flux once every second during spectral scanning) as each sampled reflectance spectra of *P. australis* was subsequently acquired throughout the field collection day. Figure 2.5 depicts the absolute differences in acquired radiant flux between the upward-looking Ocean Optics sensor and the pyranometer on a per-spectral-scan basis between DOY 181 and DOY 213 when, as noted previously, the fluctuations in the spectral reflectance were greatest. Deviations from zero indicate that variation in measured radiance flux exists between the upward-looking fiber optic and the pyranometer. For example, DOYs 199, 206, and 213 were field days where the upward-looking sensor measured more incoming radiant flux than the pyranometer. In contrast, on DOYs 188 and 191, the upward-looking sensor measured less incoming radiant flux than the pyranometer. On DOY 181, though, the radiant fluxes as measured by both the upward-looking Ocean Optics sensor and the pyranometer were relatively equal to one another; a finding which suggests that sensitivity differences among sensors were

essentially non-existent on that day. A pertinent new objective, then, was to understand why the system performed well on some days and not so well on others.

Equipment Testing and Inspection

In attempting to address the pertinent objective noted immediately above, the first step was to isolate possible causes, or extraneous variables, which may have led to the instability in the upward-looking spectroradiometer. An obvious starting point was to test the instruments themselves and, consequently, seek to determine whether the initial instability in the system was a result of malfunctions in the spectroradiometers and/or the attached fiber optics. Therefore, at the end of the field season, all equipment, including the fiber optics and spectroradiometers, were removed from the boom of Hercules and brought back to the CALMIT spectroscopy laboratory where the sensitivities of the two radiometers were tested in a controlled setting. Spectra were continuously collected over a reference target for an 8 hour time period using the same fiber optics and the two spectroradiometers employed during the summer field campaigns. The results (not shown) documented the fact that the sensitivities of the two spectroradiometers were relatively constant, remained stable, and could not be linked to the spectral errors observed in the field data.

In contrast to the spectra collected in the laboratory setting, the differences between measured radiant flux captured by the upward-looking Ocean Optics radiometer and the pyranometer fluctuated erratically from one sample plot of *P. australis* to the next throughout a given field collection day (as seen in Figure 2.5). This suggests that some

extraneous variable linked to the upward-looking spectroradiometer existed, which was causing the discrepancies in acquired spectra and that that particular parameter varied erratically. Such a finding seems to rule out environmental variables that typically change more gradually over time (e.g., air temperature or relative humidity). As seen in Figure 2.5, there were several rather erratic deviations between radiant flux measured by the upward-looking spectroradiometer and pyranometer sensor which were observed repeatedly after the first scan and between samples seven and eight, samples 14 and 15, and samples 21 and 22 on different days. Upon closer inspection of the data-collection circumstances, it was determined that these consistent fluctuations between scanning sessions occurred during periods before and/or after Hercules (the sensing platform) was moved among the separate plots of *P. australis*. Prior to moving between individual plots of *P. australis*, fiber optic cables on the boom were routinely secured with straps to minimize vibrations and jarring. Nevertheless, a considerable amount of the variation in sensitivity between the upward-looking spectroradiometer and pyranometer sensor was observed immediately after the platform moved. Thus, it appears that, despite all the precautions taken to insure that platform movement could not influence data integrity, the travel of Hercules between sample points and plots apparently did cause some error.

Several other possibilities that may have caused fluctuations in the sensitivity between the upward-looking spectroradiometer and pyranometer sensor were suspected and ultimately examined, including minuscule cracks in the fiber optic cables which may have been shifting each time the cables were secured to the boom, changes in the voltage applied to the spectroradiometers, or impediments such as dirt or water on the tips of the

fiber optic cables. Cracks in the fiber optic cables were tested by repeatedly moving and bending the cables, then subsequently scanning a reference target. This potential problem was eliminated as the radiance acquired by fiber cables connected to both the upward and downward-looking spectroradiometers remained stable during testing. Another laboratory test was conducted to determine if varying voltage inputs to the spectroradiometers affected the measured reflectance. Figure 2.6 shows the CV (determined as ratio of the standard deviation of DN's to the mean of DN's) between 400 – 900 nm in the upward and downward-looking radiometers as voltage varied from 4.0 – 5.5 V (a voltage range much wider than experienced when the sensor system is operating on the boom of Hercules). The results showed that the CV in the VIS and NIR varied with changes in voltage less than 1.5% in the upward-looking radiometer and less than 1% in the downward-looking radiometer. Overall, the spectroradiometers remained stable during changes in voltage, and variations in acquired spectra were far less than the fluctuations observed in the field. However, through careful inspection, corrosion on the metal tip of the upward-looking fiber optic was discovered at the point where the cosine diffuser was attached, which may have been indicative of water accumulating there (i.e., condensation build-up). This corrosion was likely a result of equipment being stored in a shed during cool nights and operated in the warmth of the day, a situation which would be conducive to the occurrence of condensation.

In summary, the precise and irrefutable cause behind the spectral discrepancy in the upward-looking spectroradiometer was not determined. However, due to corrosion between the tip of the fiber optic cable and the cosine diffuser, it was suspected that

condensation was a likely source of this error. From the results presented, it was ascertained that equipment failure was not a likely source of error due to matching measurements of radiance acquired by both the upward and downward-looking spectroradiometers in a laboratory setting. Yet, to be certain, several other factors were eliminated as possible sources of error including variations in air temperature, wind speed, relative humidity, and voltage. It was useful to identify the probable cause of the problem, but that still did not serve to correct the spurious data collected during the 2011 growing season. Therefore, a procedure was needed in order to adjust the incongruity in the data so that they would be useful during analysis of the spectral-reflectance information from 2011.

Correcting CF Values

As a means of removing the variability observed in the data acquired by the Ocean Optics system, the downwelling incident irradiance during calibration was adjusted by means of the following equation:

$$E_\lambda^{cal-norm} = \frac{E_\lambda^{cal} \times Pyr}{E_{\Sigma 400-900}^{cal}} \qquad\qquad [3]$$

where $E_\lambda^{cal-norm}$ is the normalized incident irradiance during calibration; E_λ^{cal} is the downwelling irradiance acquired by the upward-looking radiometer during calibration, Pyr is the photon flux acquired by the pyranometer; and $E_{\Sigma 400-900}^{cal}$ is the summation of

irradiance between 400 and 900 nm during the calibration period, thus simulating photon-flux acquired by the upward looking Ocean Optics radiometer.

Similarly, actual downwelling incident irradiance acquired by the upward looking fiber optic during the target object scan was adjusted using the following equation:

$$E_\lambda^{norm} = \frac{E_\lambda \times Pyr}{E_{\sum 400-900}} \qquad [4]$$

where E_λ^{norm} is the normalized incident irradiance, E_λ is downwelling irradiance, and $E_{\sum 400-900}$ is the summation of irradiance between 400 and 900 nm acquired over the vegetation canopy.

Equations 1 and 2 were adjusted by substituting the original irradiance measured by the upward-looking radiometer with calculated normalized irradiance as shown in equations 5 and 6:

$$CF_\lambda = \frac{P_\lambda^{cal} \times E_\lambda^{cal-norm}}{L_\lambda^{cal}} \qquad [5]$$

$$\rho_\lambda = \frac{L_\lambda}{E_\lambda^{norm}} \times CF_\lambda \times 100 \qquad [6]$$

Figure 2.7 displays the results of the corrected spectra adjusted using normalized irradiance. As seen in the figure, the large deviations in reflectance, especially noticeable between DOY 181 and 213 were removed and the reflectance spectra appear to be more

congruent with that of a vegetation canopy. It was calculated that the CV of CF values between 400 – 900 nm acquired by the upward and downward-looking sensors during calibration were reduced by 72% after applying equations 5 and 6; thus, greatly minimizing the fluctuations in the reflectance of the vegetation canopy.

Scrutiny of Figure 2.7 revealed several peaks particularly noticeable in the NIR wavelengths on DOY 168, 193 and 242. In order to understand why those peaks occurred, further analysis was conducted by investigating the sensitivity between the pyranometer and the downward-looking sensor (collecting radiance from the calibration panel) over the course of the field season. This sensitivity was calculated as the ratio between radiant flux measured from the pyranometer and the integration of DN's between 400 – 900 nm from the downward-looking sensor acquired during calibration. Figure 2.8, which was constructed to clarify the matter, shows the changes in measured radiant flux between the pyranometer and the downward-looking sensor compared to changes in NIR reflectance of the plant canopy. As observed in the figure, days with greater sensitivity issues between the two instruments (i.e., radiant flux acquired by the pyranometer is comparably greater than radiant flux acquired by the downward-looking radiometer) are closely aligned with the peaks in the NIR reflectance.

Coincidentally, the peaks (described above) in the sensitivity between the pyranometer and the downward-looking sensor occur, typically, on days with moderately high relative humidity (Figure 2.9). Therefore, the slight variability observed between the pyranometer and the downward-looking radiometer may have been caused by changes in atmospheric water vapor. Yet, to influence the changes in the NIR reflectance

of the vegetation canopy, the sensitivity between the pyranometer and the downward-looking radiometer must have changed from the time of calibration until the scanning of the vegetation canopy. Therefore, the cause of the peaks in the NIR reflectance of the canopy may only be postulated since comparisons of photon flux acquired by both the pyranometer and downward-looking radiometer were only be measured during calibration, and not throughout the field collection process. Thus, further research should investigate the sensitivity between these two instruments.

CONCLUSIONS

Unexpected and sometimes erratic variability in the reflectance spectra of a proximally-sensed vegetation canopy brought about a need for a post-field-campaign method to correct error in data acquired by mismatched spectroradiometers. The research presented herein identified a few issues related to the relevant concepts and operation using dual inter-calibrated spectroradiometers. Some of those issues have been noted by previous investigators within our own research group during previous field seasons while others have been alluded to in the literature. Three specific objectives were identified and addressed.

First, there are many considerations in undertaking field research aimed at proximal sensing. A few of the complications that emerge have been presented and discussed in detail in this paper. The potential problems are numerous and involve issues related to instrument operation, including differences in sensitivity between radiometers. Guidelines for proper sensor deployment and data acquisition were also summarized.

Secondly, many of the issues alluded to in the first objective were investigated as possible causes behind the fluctuation in the canopy reflectance. In this study, it was discovered that radiant flux calculated from the upward-looking spectroradiometer, measuring irradiance downwelling via the atmosphere, varied considerably throughout the day as compared to measurements made by pyranometer and quantum sensors. Through further investigation, it was determined that instability in the upward-looking radiometer was likely caused by a) an instrumental-insulation defect which allowed moisture to enter the cosine diffuser, b) environmental conditions which were favorable to condensation, c) human error due to negligence in ensuring that equipment was properly cleaned and maintained prior to conducting scientific research, and d) platform movement between sample plots (to some extent).

Finally, a method for correcting variations in the reflectance spectra was offered. Calculated radiant flux collected by the upward-looking sensor was normalized to simultaneous measurements from a pyranometer, and, as a result, variation between the inter-calibrated radiometers decreased by 72%. However, some of the irregularities that existed in the acquired reflectance data, especially noticeable in the NIR, were still prevalent after modifications were made, quite possibly due to additional but minor amounts of variation that occurred between the pyranometer and downward-looking radiometer. Therefore, some residual error noticeable in the form of erratic peaks in reflectance of the NIR spectral region was observed in the resulting vegetation reflectance spectra on days with higher than normal relative humidity.

Appropriate field data collection procedures and sensor calibration techniques should be implemented when using dual spectroradiometers to ensure that the two instrument sensitivities remain constant throughout the field campaigns. Future investigators undertaking proximal sensing should be aware of the issues noted in this paper, and researchers should monitor the coincidence (or lack thereof) in spectral signals acquired by spectroradiometers and corresponding ancillary measurements such as radiant flux from a pyranometer. Such a carefully orchestrated approach is needed to avoid error propagation in spectral reflectance data collected at close-range in a field setting.

REFERENCES

Anderson, K., E. J. Milton, and E. M. Rollin. 2006. Calibration of Dual-beam Spectroradiometric Data. *International Journal of Remote Sensing*, 27 (5): 975–986.

Bolsenga, S. J. and R. D. Kistler. 1982. A Dual Spectroradiometer System for Measuring Spectral Reflectances. *Journal of Applied Meteorology*, 21 (5): 642–647.

Broge, N. H and J. V Mortensen. 2002. Deriving Green Crop Area Index and Canopy Chlorophyll Density of Winter Wheat from Spectral Reflectance Data. *Remote Sensing of Environment*, 81: 45–57.

Coll, C., V. Caselles, J. Galve, E. Valor, R. Niclos, J. Sanchez, and R. Rivas. 2005. Ground Measurements for the Validation of Land Surface Temperatures Derived from AATSR and MODIS Data. *Remote Sensing of Environment*, 97: 288–300.

Duggin, M. J. 1981. Simultaneous Measurement of Irradiance and Reflected Radiance in Field Determination of Special Reflectance. *Applied Optics*, 20 (22): 3816.

Duggin, M. J. and W. R. Philipson. 1982. Field Measurement of Reflectance: Some Major Considerations. *Applied Optics*, 21: 2833.

Fussell, J., D. Rundquist, and J. Harrington, Jr., 1986. On defining remote sensing. *Photogrammetric Engineering and Remote Sensing*, 52 (9): 1507-1511

Gitelson, A. A. 2003a. Remote Estimation of Leaf Area Index and Green Leaf Biomass in Maize Canopies. *Geophysical Research Letters*, 30 (5).

———. 2003b. Novel Technique for Remote Estimation of CO2 Flux in Maize. *Geophysical Research Letters*, 30 (9).

Gitelson, A. A. 2005. Remote Estimation of Canopy Chlorophyll Content in Crops. *Geophysical Research Letters*, 32 (8).

Gitelson, A. A., Y. J. Kaufman, R. Stark, and D. Rundquist. 2002. Novel Algorithms for Remote Estimation of Vegetation Fraction. *Remote Sensing of Environment*, 80: 76–87.

Huete, A., K. Didan, T. Miura, E. P. Rodriguez, X. Gao, and L. G. Ferreira. 2002. Overview of the Radiometric and Biophysical Performance of the MODIS Vegetation Indices. *Remote Sensing of Environment*, 83: 195–213.

Jackson, R. D., T. R. Clarke, and M. S. Moran. 1992. Bidirectional Calibration Results for 11 Spectralon and 16 BaSO4 Reference Reflectance Panels. *Remote Sensing of Environment*, 40 (3): 231–239.

Jensen, J. R. 2000. Remote Sensing of the Environment : an Earth Resource Perspective. Upper Saddle River, N.J.: Prentice Hall.

Kim, M. S., C. S. T. Daughtry, E. W. Chappelle, J. E. McMurtrey, and C. L. Walthall. 1994. The Use of High Spectral Resolution Bands for Estimating Absorbed Photosynthetically Active Radiation (A Par). *Proceedings of 6th International Symposium on Physical Measurements and Signatures in Remote Sensing*, p 299-306

Lillesand, T. M. and R. W. Kiefer. 2000. Remote Sensing and Image Interpretation. New York: John Wiley & Sons.

Milton, E. J. 1987. Principles of Field Spectroscopy. *International Journal of Remote Sensing*, 8: 1807–1827.

Milton, E. J. 1981. Does the Use of Two Radiometers Correct for Irradiance Changes During Measurements. *Photogrammetric Engineering and Remote Sensing*, 47: 1223–1225.

Milton, E. J., M. E. Schaepman, K. Anderson, M. Kneubühler, and N. Fox. 2009. Progress in Field Spectroscopy. *Remote Sensing of Environment*, 113: S92–S109.

Nicodemus, F. E., J. C. Richmond, J. J. Hsia, I. W. Ginsberg, T. Limperis, and W. R. Ott. 1977. Geometrical Considerations and Nomenclature for Reflectance. US Department of Commerce, National Bureau of Standards Washington, D. C

O'Neill, N. T., F. Zagolski, M. Bergeron, A. Royer, J. R. Miller, and J. Freemantle. 1997. Atmospheric Correction Validation of CASI Images Acquired Over the Boreas Southern Study Area. *Canadian Aeronautics and Space Institute*, 23 (2): 143–162.

Peddle R., D, H. P. White, R. J. Soffer, J. R. Miller, and E. F. LeDrew. 2001. Reflectance Processing of Remote Sensing Spectroradiometer Data. *Computers & Geosciences*, 27 (2): 203–213.

Plaza, A., P. Martinez, R. Perez, and J. Plaza. 2004. A Quantitative and Comparative Analysis of Endmember Extraction Algorithms from Hyperspectral Data. *IEEE Transactions on Geoscience and Remote Sensing*, 42: 650–663.

Price, M. 1986. The Analysis of Vegetation Change by Remote Sensing. *Progress in Physical Geography*, 10 (4): 473–491.

Rollin, E. M., E. J. Milton, and D. R. Emery. 2000. Reference Panel Anisotropy and Diffuse Radiation - Some Implications for Field Spectroscopy. *International Journal of Remote Sensing*, 21 (15): 2799–2810.

Rundquist, D., A. A. Gitelson, D. Derry, J. Ramirez, R. Stark, and G. P. Keydan. 2001. Remote Estimation of Vegetation Fraction in Corn Canopies. In: Grenier G, Blackmore S (eds) Proceedings of the Third European Conference on Precision Agriculture. Montpellier, France. 1: 301–306.

Rundquist, D., R. Perk, B. Leavitt, G. Keydan, and A. A. Gitelson. 2004. Collecting Spectral Data over Cropland Vegetation Using Machine-positioning Versus Hand-positioning of the Sensor. *Computers and Electronics in Agriculture*, 43 (2): 173–178.

Soffer, R., J. Harron, and J. Miller. 1995. Characterization of Kodak Grey Cards as Reflectance Reference Panels in Support of BOREAS Field Activities. *Proceedings 17th Canadian Symposium on Remote Sensing*, 357–362.

Viña, A. 2005. New Developments in the Remote Estimation of the Fraction of Absorbed Photosynthetically Active Radiation in Crops. *Geophysical Research Letters*, 32 (17).

Viña, A., A. A. Gitelson, D. C. Rundquist, G. Keydan, B. Leavitt, and J. Schepers. 2004. Monitoring Maize (L.) Phenology with Remote Sensing. *Agronomy Journal*, 96: 1139.

Wu, C., Z. Niu, Q. Tang, W. Huang, B. Rivard, and J. Feng. 2009. Remote Estimation of Gross Primary Production in Wheat Using Chlorophyll-related Vegetation Indices. *Agricultural and Forest Meteorology*, 149: 1015–1021.

	DW-NIR	DW-Red	DW-Green	DW-Blue	UP-NIR	UP-Red	UP-Green	UP-Blue	Wind Speed	Rel Hum	Air Temp
Air Temp	0.031	0.079	0.076	0.070	0.003	0.012	0.011	0.010	0.002	0.001	1.000
Rel Hum	0.544	0.502	0.494	0.484	0.295	0.287	0.286	0.279	0.211	1.000	
Wind Speed	0.020	0.014	0.011	0.008	0.000	0.002	0.003	0.004	1.000		
UP-Blue	0.593	0.568	0.555	0.544	0.989	0.997	0.999	1.000			
UP-Green	0.595	0.571	0.556	0.542	0.992	0.999	1.000				
UP-Red	0.591	0.567	0.550	0.535	0.993	1.000					
UP-NIR	0.569	0.534	0.516	0.501	1.000						
DW-Blue	0.977	0.991	0.997	1.000							
DW-Green	0.984	0.998	1.000								
DW-Red	0.986	1.000									
DW-NIR	1.000										

Table 2.1. Coefficients of determination among ambient air temperature (Air Temp), relative humidity (Rel Hum), wind speed, and incident radiance to both the upward-looking (UP) and downward-looking (DW) sensors in the blue (400 − 500 nm), green (500 − 600 nm), red (600 − 700 nm), and NIR (850 − 950 nm) regions of the electromagnetic spectrum. As observed in Table 1, the correlations between air temperature (R^2 ranging from 0.003 [$p < 0.990$] to 0.079 [$p < 0.741$]) and wind speed (R^2 ranging from 0.000 [$p < 0.998$] to 0.020[$p < 0.934$]) vs. radiance acquired by the upward-looking sensor/irradiance acquired by the downward-looking sensor in the VIS through NIR spectrums were non-significant and correlations pertaining to relative humidity vs. similar radiance/irradiance were non-significant and weak respectively (R^2 ranging between 0.286 [$p < 0.222$] and 0.544 [$p < 0.013$]). Also noticeable, correlation values between irradiance acquired by the downward-looking sensor aimed at the calibration panel and the upward-looking sensor are uncharacteristically weak.
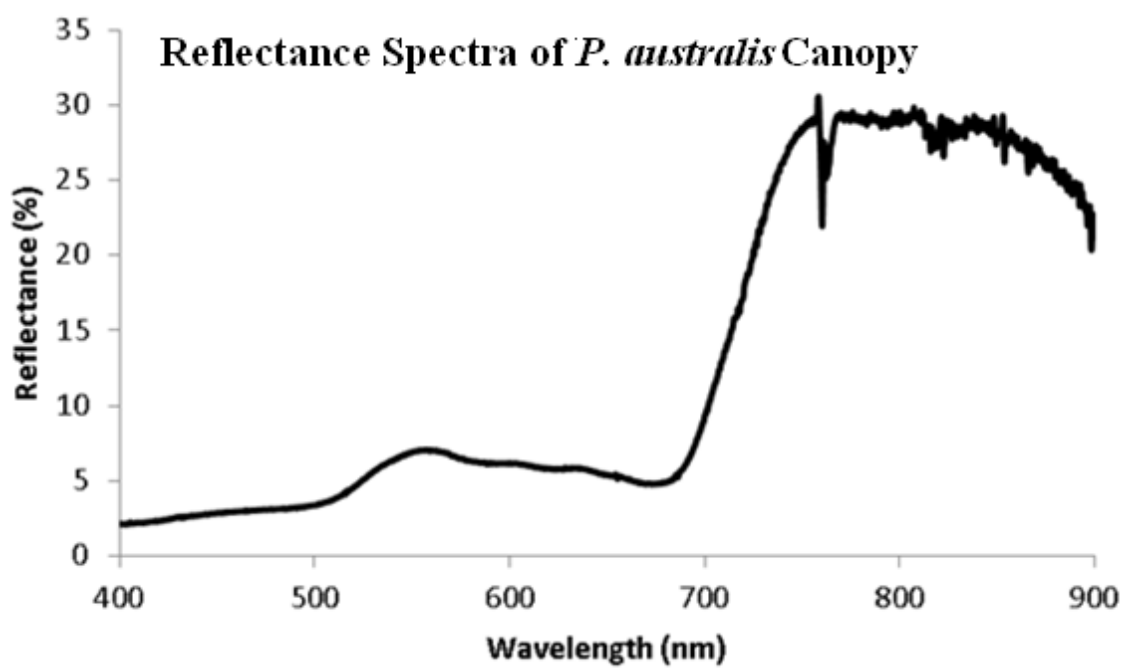
Figure 2.1. Example of reflectance spectra between 400 and 900 nm of *P. australis* canopy on DOY 269.
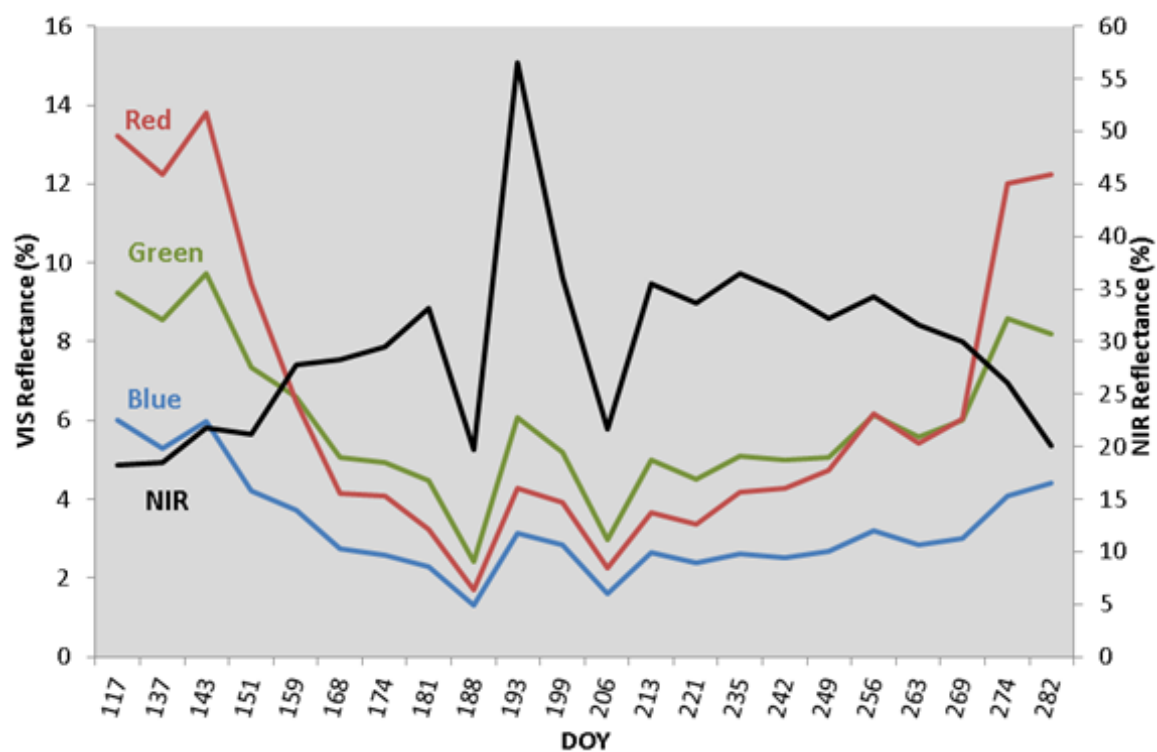
Figure 2.2.   Multi-temporal spectral reflectance curves of *P. australis* in the VIS and NIR regions of the spectrum.   Large variances in reflectance are visually apparent between DOY 181 and 213.
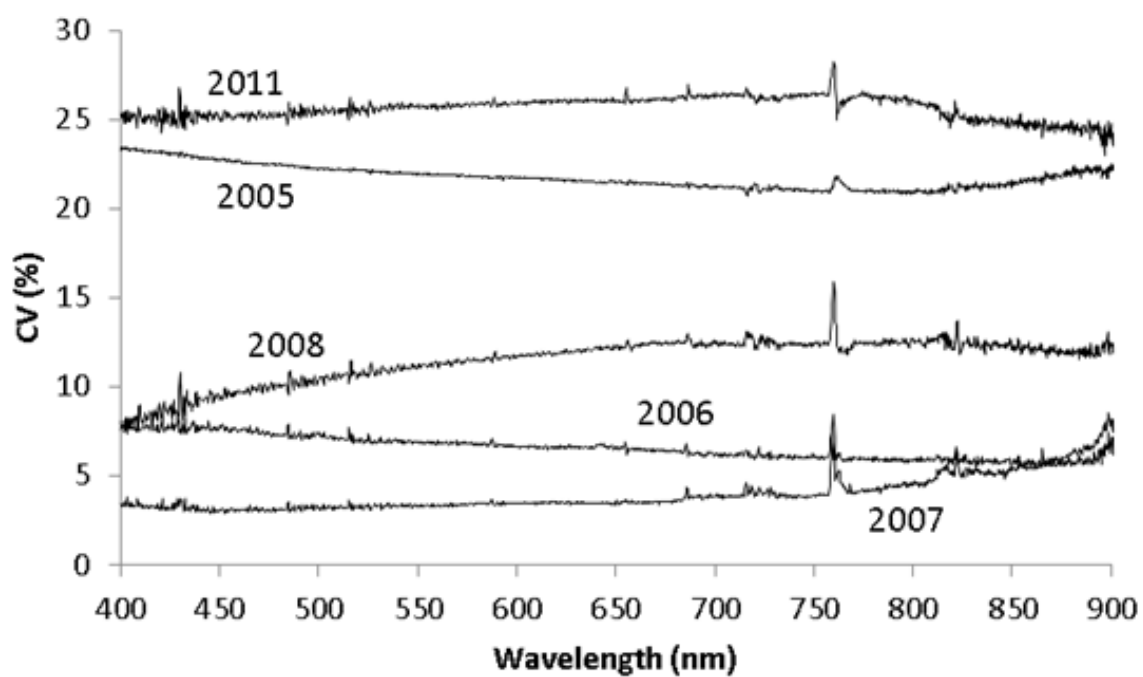
Figure 2.3. Coefficient of variation (CV) of seasonal CF values at each wavelength (400-900nm) between 2005 and 2008 and in 2011. During the 2011 field season, there were larger CV values than the previous field seasons.
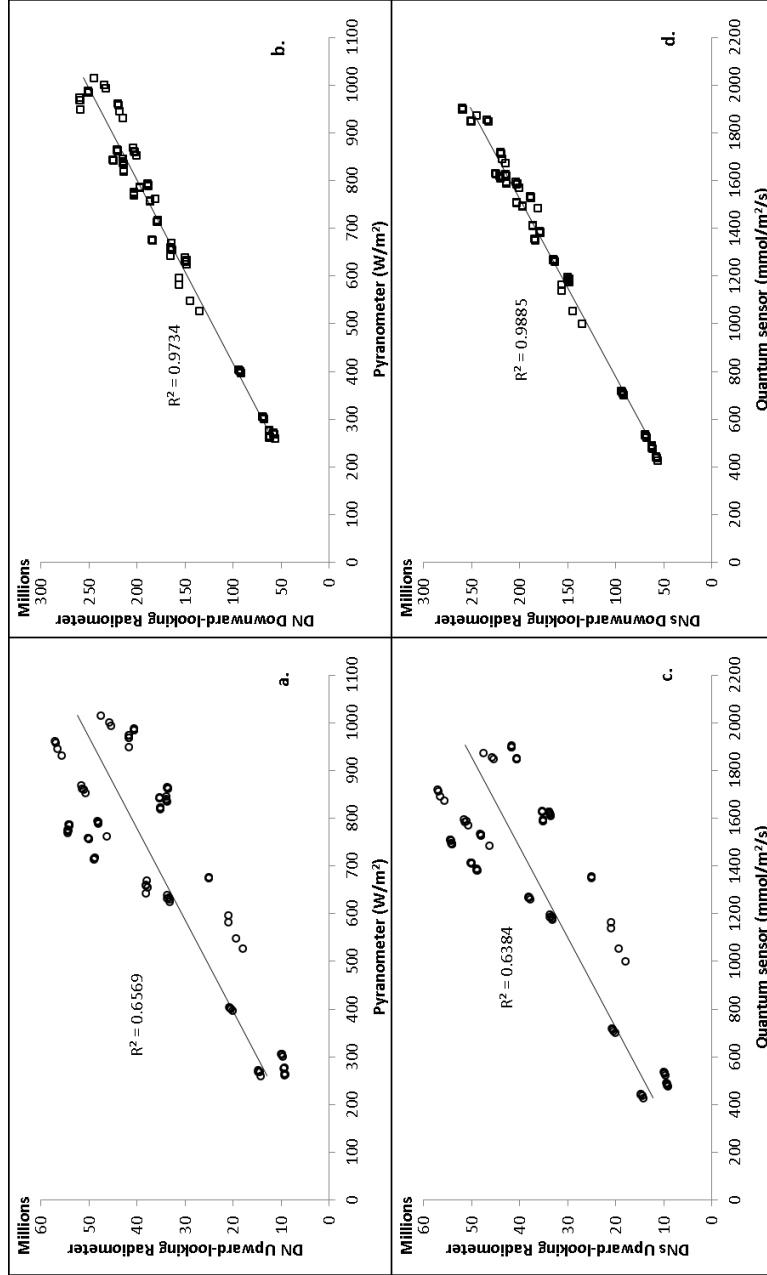
Figure 2.4 (a-d). Relationship between sum of DNs in the VIS – NIR spectrum for the upward-looking (a) and downward-looking (b) sensors on the y-axes to the radiant flux acquired by the pyranometer sensor on the x-axes. Relationship between sum of DNs in the VIS spectrum for the upward-looking (c) and downward-looking (d) sensors on the y-axes to the radiant flux acquired by the quantum sensor on the x-axes. The line of best-fit and R^2 shows the best correlation between the values of the upward/downward-looking sensors and the pyranometer/quantum sensor. There is a conspicuously lower correlation between the upward-looking sensor and the pyranometer/quantum sensor than between the downward-looking sensor and the pyranometer/quantum sensor.
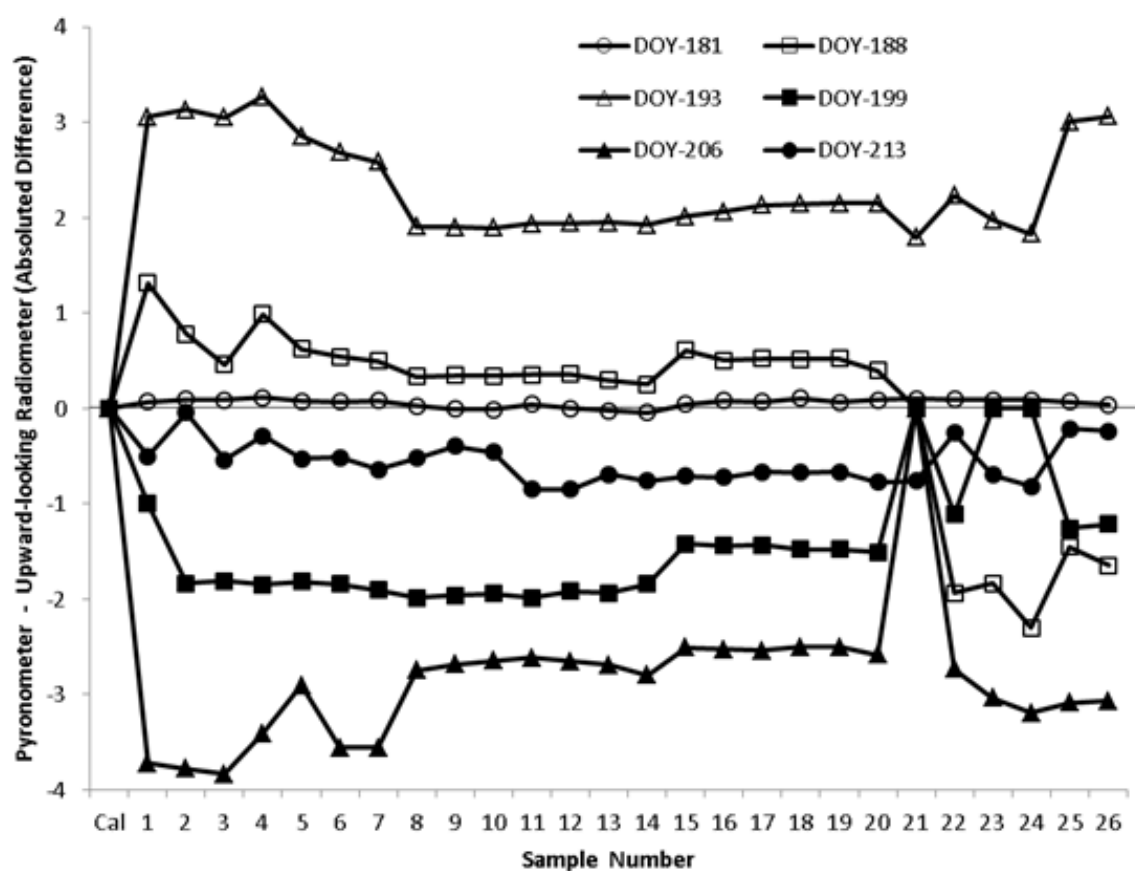
Figure 2.5. Graph shows the sensitivity between upward-looking sensor and the pyranometer throughout the field collection process between DOY 181 – 213. Positive changes from zero indicate spectral scans when the upward-looking sensor measured less radiant flux than the pyranometer and negative changes from zero indicate the upward-looking sensor measured greater radiant flux than the pyranometer. Also seen in the figure, changes in measured photon flux between the two instruments fluctuate erratically from sample to sample throughout the field collection process.
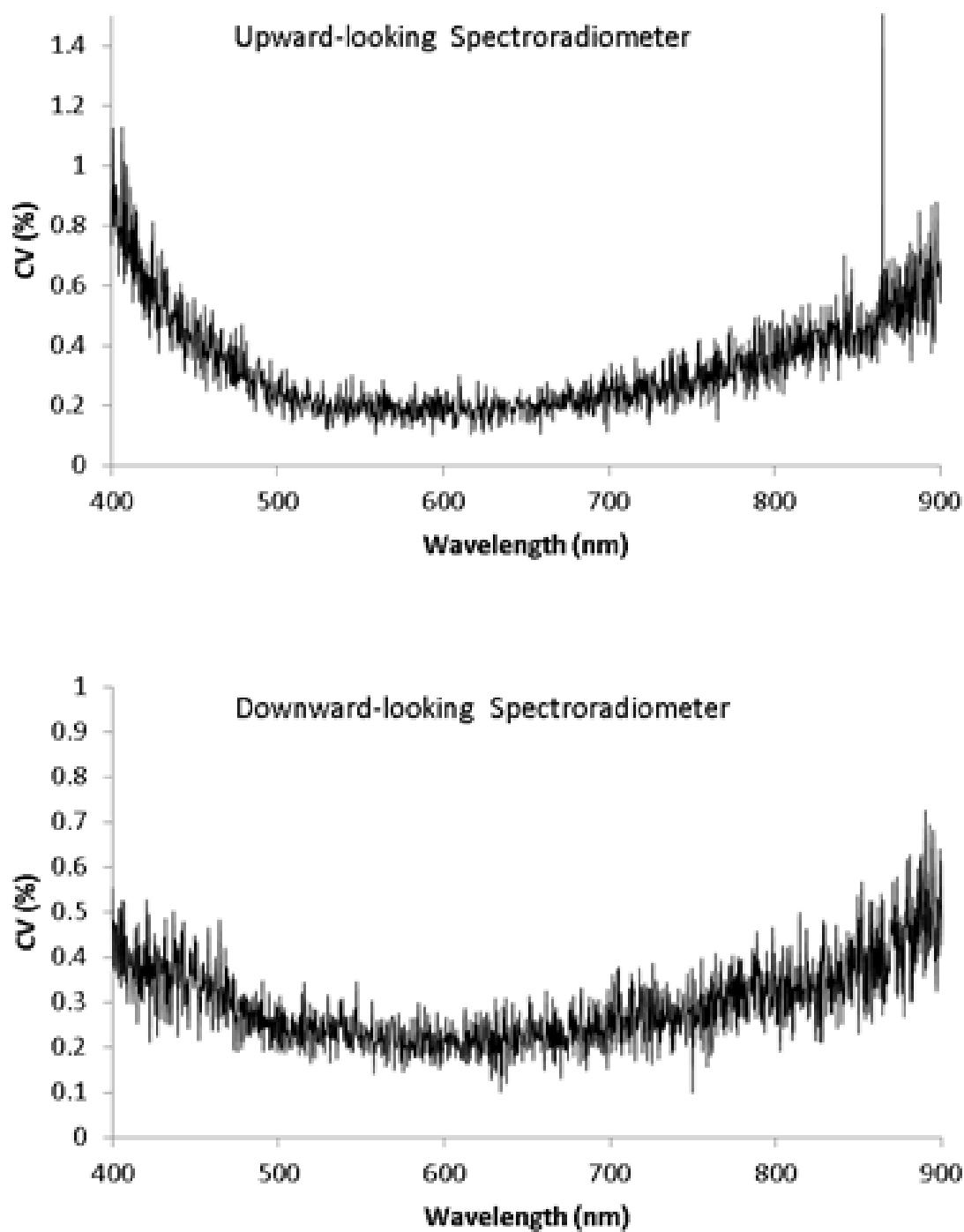
Figure 2.6. Sensitivity, as shown by the CV, of the upward and downward-looking spectroradiometers per wavelength to changes in voltage (4.0 – 5.5 V) applied to the instruments.
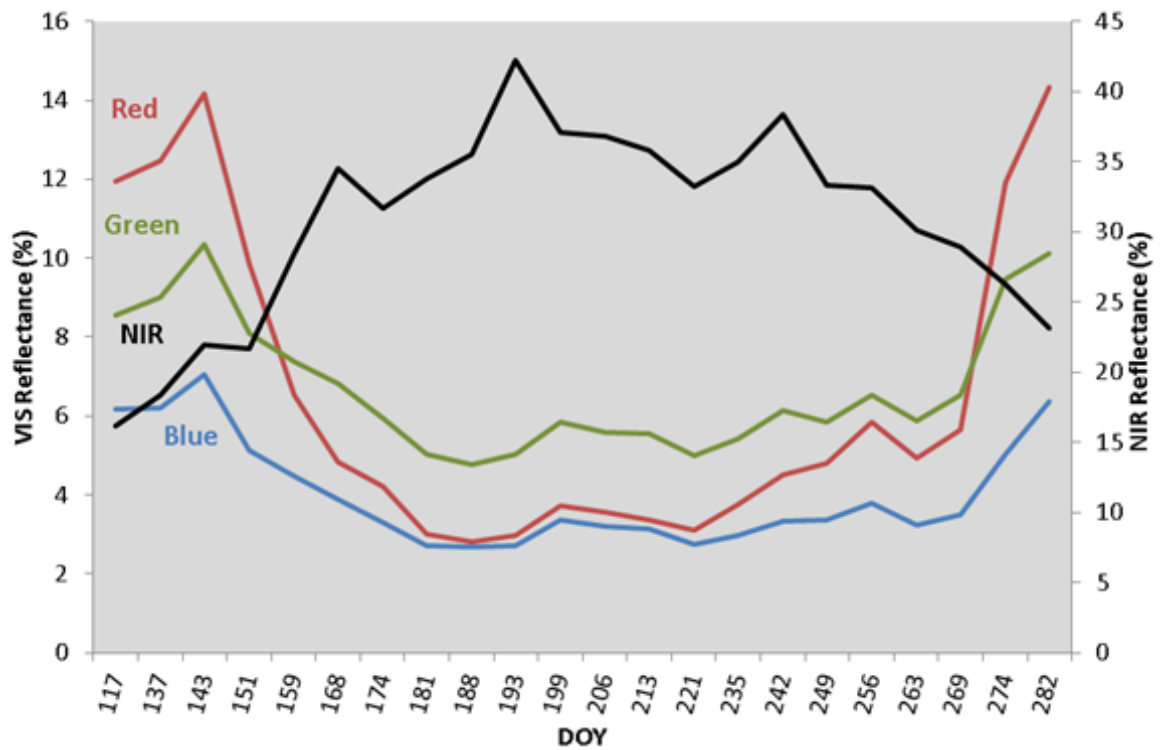
Figure 2.7. Reflectance spectra of the *P. australis* canopy after equations 3 and 4 were applied. As compared to Figure 2.2, spurious measurement in the reflectance at each wavelength of the vegetation canopy between DOY 181 and 213 no longer exist. Yet, several peaks are noticeable in the NIR which appear on DOY 168,193, and 242.
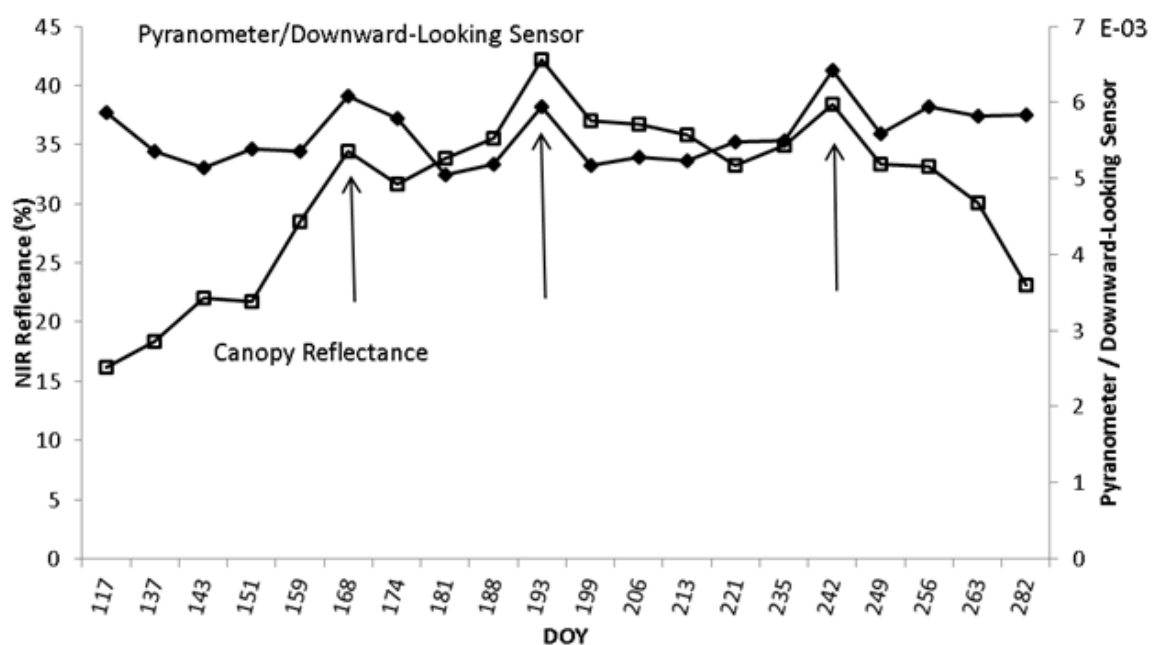
Figure 2.8. Graph of demonstrating differences between canopy reflectance and sensitivity of the pyranometer and the downward-looking sensor. Peaks in the NIR reflectance are closely aligned with peak sensitivities between the pyranometer and the downward-looking spectroradiometer.
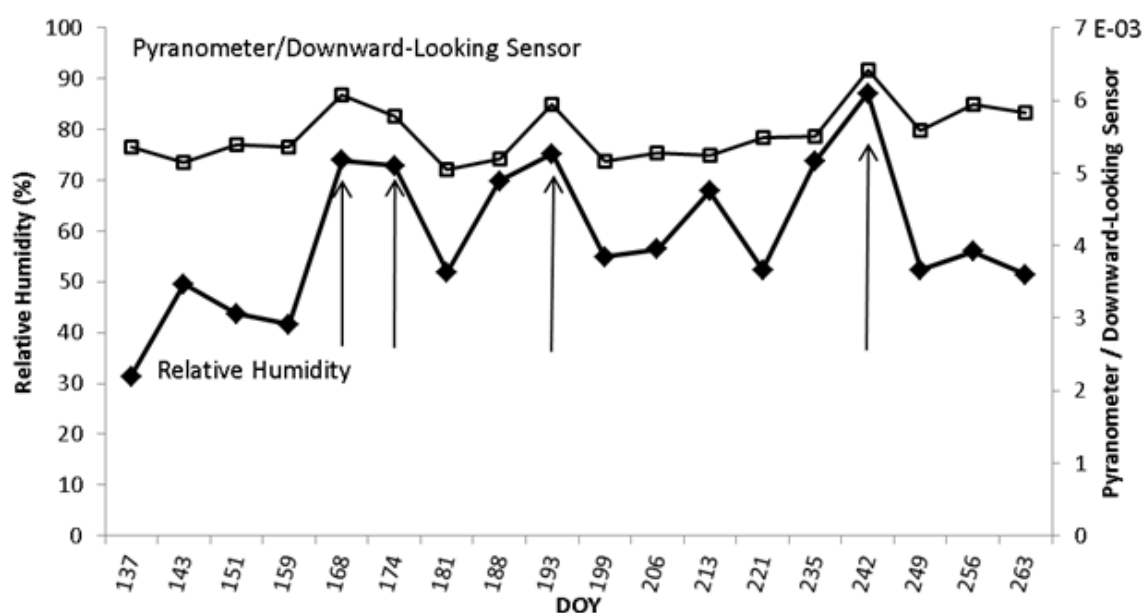
Figure 2.9. Graph of demonstrating differences between relative humidity and sensitivity of the pyranometer and the downward-looking sensor. Larger discrepancies between the pyranometer and downward-looking sensor as observed on DOY 168, 174, 193, and 242 correspond to days with greater relative humidity.

CHAPTER 3

REMOTE MONITORING OF PHENOLOGY AND VEGETATION FRACTION

IN *PHRAGMITES AUSTRALIS*

ABSTRACT

The rapid expansion of non-native common reed, *Phragmites australis*, into Midwestern wetland and riparian areas has threatened native plant communities and is a growing concern for resource managers. Monitoring and managing the invasive spread of weeds requires an accurate understanding of the plant's phenology. The growth and development of *P. australis* was spectrally characterized using close-proximity remote sensing instruments, and was quantified using changes in calculated vegetation fraction (%). The amount of green vegetation fraction was determined at each of four stages of plant development, which were distinguished by means of spectral characteristics. By deconvolving the primary constituents (vegetation, inflorescence, shadows, and background litter) comprising images of the plant canopy, it was determined that visible reflectance from both living and non-living plant material varied between phenological stages due to biophysical growth of the canopy. As a result, the estimation of vegetation fraction could not be accurately determined using previously published spectral indices. Therefore, an albedo corrected vegetation index (ACVI), which used spectral transformations in only the visible portion of the spectrum, was derived in order to adjust for phenological changes affecting the spectral reflectance from the plant canopies. Error

in predicted vegetation fraction using ACVI was less than other vegetation indices tested and remained sensitive to a wide range of fractions of cover. Further research is required in order to test ACVI in other vegetation canopies comprised of different plant structures and phenological cycles.

INTRODUCTION

Rationale for Studying *P. australis*

Rapid expansion of non-native common reed, *Phragmites australis* (Cav.) Trin. ex Steudel (hereafter referred to simply as *P. australis*), is causing negative impacts in Midwest wetlands including riparian areas along streams, ponds, lagoons, rivers, marshes, and roadside ditches. *P. australis* has the ability to establish dense, near mono-specific stands that typically outcompete native vegetative species (Kettenring et al., 2009; Kiviat, 2010) and expansion of these dense stands endangers the diversity of floral and faunal habitats (Meyerson et al., 2000; Minchinton and Bertness, 2003). Moreover, the establishment of *P. australis* in and around drainage channels is problematic because it typically expands into water-ways and disrupts the normal flow (Montiero et al., 1999), which can potentially cause build-up of sediments (Weinstein and Balletto, 1999) and lead to flooding, resulting in additional environmental and economic problems.

The Phenology of *P. australis*

Phenology is a physiological measurement of the rate of growth and development of a plant in an environment (Hodges, 1991). Therefore, plant species with similar morphological phenotypes may have different physiological life cycles depending on the environmental history.

Accurate and detailed monitoring of plant phenology is an important component for the management and control of invasive species (Ghersa and Holt, 1995). Generally, phenology is monitored in crop-weed management systems (Bhowmik, 1997) for

measuring and modeling specific phenotypic plasticity responses, within-field competition, plant discrimination, and seed bank populations (Acker et al., 1993; Deen et al., 1998; Swanton et al., 2000; Hegazy et al., 2005).

The notion of monitoring vegetation phenology in crops has also been extrapolated to wetlands containing stands of *P. australis*; for example, Bastlová et al. (2004) explained how environmental and geographical factors such as mineral nutrient dose, water availability, and latitudinal variation may affect the phenology and growth of *P. australis*. The authors concluded that environmental variables influencing the phenology of *P. australis* may play a vital role in its successful establishment and increased expansion. Seasonal variations in plant pigments, leaf water content, plant height, canopy cover, and leaf angle distribution have been useful characteristics in discriminating wetland plant species (Gilmore et al., 2008). Davies et al. (2010) indicated that the growth and phenology of *P. australis* was advantageous in competing with desirable vegetation. Boedeltje et al. (2004) provided insight explaining how the flowering phenology of many hydrochorous (i.e., seeds dispersed by water) plants influenced the discharge, seed release time, and buoyancy of seeds in wetland areas; thus, affecting the plant's ability to spread.

Phenological development of plant species may be assessed by measuring both spectral reflectance (in many discrete wavelengths, as discussed below) over an entire growing season and also by calculating the fraction of the green photosynthetic material present in the canopy of interest. Vegetation fraction (VF) is defined as the ratio of green vegetation in a horizontal plane relative to the amount of non-green material in the same

area; or in other words, the coverage of green vegetation as observed when looking downward, in a vertical view, from the top of the canopy. Estimation of VF is useful for monitoring other canopy biophysical properties such as photosynthesis, plant transpiration, and gross primary production (Aman et al., 1992; Gutman and Ignatov, 1998). Green VF can also help elucidate plant growth stages such as the seedling, leaf-out, flowering, and senescence stages. Altogether, detailed plant phenology data are useful in understanding the invasive characteristics of *P. australis* and its ability to establish and compete with native or other desirable vegetation.

Remote Sensing: A Potential Tool for Analyzing and Monitoring *P. australis*

Monitoring and inventorying wetland environments is potentially challenging because some study sites can be difficult to access and navigate. Such data-collection campaigns are time consuming as well as expensive in order to execute correctly. Remote sensing offers a potentially useful means of studying wetland ecosystems by providing a synoptic view, multi-spectral data collection, multi-temporal coverage, and cost effectiveness (Rundquist et al., 2001). These and other advantages are attractive when one is faced with examining a very dense, almost impenetrable canopy of invasive *P. australis*.

Prerequisite to employing remote sensing for the purpose of monitoring and managing stands of *P. australis* is the need to thoroughly understand its spectral properties. Therefore, the objectives of the study were 1) to characterize the spectral response of a canopy of *P. australis* over an entire growing season; 2) to relate the multi-

temporal spectra to changes in fraction of vegetative cover; 3) to deconvolve primary components in an image that make up the composite spectral signature of both living and non-living material; and 4) to examine selected spectral transformations (i.e., vegetation indices) for determining which appears best for continued monitoring of the canopies using remotely sensed data.

METHODS

Field Site

During the 2011 growing season, a study was undertaken using a manmade wetland at the Center for Advanced Land Management Information Technologies (CALMIT) field research site, located near Mead, Nebraska, USA. These facilities are part of the University of Nebraska-Lincoln Agricultural Research Development Center (ARDC), which is approximately 56 km northeast of Lincoln, Nebraska.

P. australis was planted at the ARDC site in 1994, and it has subsequently become a monoculture species in the constructed wetland. Prior to conducting research, the plot was burned in late March, 2011, before the *P. australis* had emerged, for the purpose of removing dead biomass which had accumulated during previous growing seasons. The wetland was built with geotextile beneath the soil to retain water; yet, due to sufficient rainfall during the 2011 growing season, it was not necessary to provide well water to the plot.

Design of Sample Plots

Five sample areas, or "mesocosms," considered representative of a *P. australis* canopy, were selected at a distance of approximately 2.25 m from the edge or outer boundary of the vegetated area. The test site also contained a wooden instrument platform (constructed for an earlier project) located in the middle of the plot (Figure 3.1). Three of the mesocosms were linearly juxtaposed next to one another in an east-to-west direction; the other two were positioned adjacent to and south of those three. Each mesocosm overlapped its neighbor by 1.35 m for a total ground area of 21.87 m^2. Therefore, the experimental design associated with the mesocosms was established in a non-random fashion; but nevertheless, was considered typical of the homogenous monoculture of *P. australis* canopy actively growing in the larger plot. The configuration of the mesocosms was developed to provide sampling areas of adequate size for proper reflectance measurements, and also to be representative of the plot. Other considerations included being able to position the sampling areas within easy reach of sensors, and to eliminate issues related to shadowing of the vegetation by either the sensor systems or the wooden platform. To facilitate repetitive sampling, flags were used to mark the target areas clearly for the subsequent spectral scanning.

Instrument Deployment

In order to spectrally characterize the life cycle of *P. australis*, reflectance data over the sample plots of vegetation were acquired using field spectroradiometers mounted on the boom of "Hercules," an all-terrain, motorized platform (Appendix A).

Hercules, similar to its predecessor "Goliath" (Rundquist, 2004), provides an ideal platform for collecting remotely sensed data because the configuration of the instrument position is relatively rigid, thus minimizing noise from vibration, and the approach allows repeatable orientation of sensors from one sample site to the next. Once the height of the boom is set relative to the top of the canopy, it remains at that fixed vertical distance above the target. The boom, which may also be rotated to ensure that the sensors are continuously in the principal plane of the sun, extends to a minimum distance of 10 m from the machine, ensuring that reflectance from non-target objects, such as colored clothing worn by an operator, is eliminated. Additionally, Hercules is painted a flat-black color to reduce extraneous scattering from the platform itself. During data collection, Hercules was positioned directly north of the target canopy being acquired by the sensor, with the boom pointed south to eliminate spurious reflectance measurements caused by shadowing from the platform.

Procedure for Measuring Spectral Reflectance and Collecting Ancillary Data

Spectral reflectance measurements of *P. australis* were acquired weekly from late April through the middle of October, for a total of 22 field campaigns during the 2011 growing season. Spectral data were collected using a dual-fiber optic system, which employs two inter-calibrated Ocean Optics (Dunedin, FL) USB2000 hyperspectral radiometers. The system records spectral data in 2023 individual bands ranging from approximately 350 to 1001 nm (visible and near-infrared) with a channel interval of ~.3 nm and a bandwidth of ~1.5 nm. One radiometer, equipped with an optical fiber and

cosine diffuser, is pointed upward to measure incident irradiance (E_λ) within a hemispherical field-of-view. The other radiometer, equipped with an optical fiber capable of a 25° field-of-view, is pointed downward to measure radiance upwelling from the target (L_λ). A correction factor (CF) is necessary to match the transfer functions and for inter-calibration of the radiometers. This was accomplished by acquiring a spectral measurement of upwelling radiance (L_λ^{cal}) from a Spectralon reference panel (Labsphere, Inc., North Sutton, NH) which is calibrated to approximately 99% Lambertian reflectance, simultaneously with the measurement of incident irradiance (E_λ^{cal}). The CF can then be calculated as

$$CF_\lambda = \frac{P_\lambda^{cal} \times E_\lambda^{cal}}{L_\lambda^{cal}} \qquad [1]$$

where P_λ^{cal} is the Lambertian reflectance calibrated at each wavelength from the Spectralon panel and linearly interpolated in order to correlate the band centers of the two radiometers. A CF value was calculated at each band center by calculating the median reflectance of daily scans from the calibration panel.

To calibrate the radiance collected from spectral instruments (i.e., acquire L_λ^{cal} and E_λ^{cal}), the downward-looking spectroradiometer was positioned at a height of approximately 30 cm above a 30.5 x 30.5 cm (12 in. x 12 in.) white Spectralon panel. A minimum of eight spectral measurements of upwelling radiance and downwelling irradiance were taken concurrently during an interval of approximately 16 sec, and the median values for each individual band were calculated. For each data collection

campaign during the growing season, multiple spectral scans of the calibration panel were acquired during a 15 minute interval near solar noon (between 11:00 and 13:00 local time), when solar diurnal variations in radiation are nearly constant due to a near-vertical zenith angle. Solar zenith angle was calculated at the time of the scan to correct for non-Lambertian reflectance from the Spectralon panel when angles above 60º were observed (Rollin et al., 2000).

A visual inspection of the recorded calibration spectra were carried out in order to identify anomalous scans, which were then removed from the dataset. The anomalies were caused by variations in illumination impinging on the calibration panel, which, in turn, was caused by slight movement of the Hercules boom and the attached fiber optic cables, due to the occasional windy conditions encountered during field campaigns. For this reason, the integration time for each spectral scan was lengthened by increasing the number of calibration scans acquired to ensure that data values were within the standard error. Median values were calculated at each wavelength of sensor sensitivity for both the radiance and irradiance datasets.

Once the scans of the reference panel were completed during each of the field campaigns, spectral reflectance measurements over the five sample areas within the *P. australis* experimental plot were acquired at a height of 5.8 m above the vegetation targets, yielding a 2.7 m instantaneous-field-of-view (IFOV) at the top of the canopy. For each of the scanning sessions per sample area, a minimum of eight spectral measurements of upwelling *P. australis* radiance and downwelling irradiance from the atmosphere were taken concurrently, and the median values for each band were

calculated. Measurements took three minutes in each of the five sample areas for a total of approximately 15 minutes of actual data collection per field campaign. Percent reflectance from the *P. australis* canopy (ρ_λ) was determined by the following equation:

$$\rho_\lambda = \frac{L_\lambda}{E_\lambda} \times CF_\lambda \times 100 \qquad\qquad [2]$$

During the spectral scans, an image of the vegetation canopy was acquired with an Olympus C-750 Ultra Zoom (Tokyo, Japan) digital camera attached to the boom of Hercules. Vegetation fraction was calculated for each image proportional to the IFOV of the upwelling sensor using the "excess green method" (Meyer and Neto, 2008). This technique applies a user-defined threshold to distinguish green and non-green pixels in an image, and separates them in binary fashion to create a new image. The VF was then determined as a percent based upon the ratio of green vegetative pixels to the total pixels in the image. An average value was then derived to establish the percent VF from each of the five mesocosms within the *P. australis* plot per sampling date.

Simultaneously during the data collection process, measurements were also obtained (once per second) from both a pyranometer (LI-200, LI-COR Inc., Lincoln, Nebraska) and a quantum sensor (LI-190, LI-COR Inc., Lincoln, Nebraska), both of which were attached to the boom of Hercules. The pyranometer and quantum sensors, which collected incoming flux in the 400-1100 nm and the 400-700 nm range, respectively, were sampled concurrently using a Campbell Scientific 21X data logger

(Logan, UT). An average value was then calculated for each sensor for the entire duration of the corresponding spectral scan.

Correction of Spectral Data

After the 2011 field campaigns were finished and data analysis was underway, errors were noticed in the resulting *P. australis* spectra. Detailed and exhaustive examination of the datasets led to the conclusion that the problem was caused by daily variations in CF, which were the result of instability in the sensitivity of the upward-pointing sensor (i.e., the one measuring downwelling irradiance). A solution, as described in Chapter 2, was developed involving normalizing the response from each wavelength of sensitivity in the upward-pointing sensor to the pyranometer data collected during the integration time of the spectral scan.

Vegetation Indices Used to Describe Phenology and for Estimating Fraction of Green Vegetation Cover

Mathematical combinations of reflectance from multiple wavelengths are commonly used in remote sensing as indicators of the presence and condition of vegetation (Rouse et al., 1973; Tucker, 1979; Huete et al., 2002). These spectral indices are calculated based upon the amounts of radiation reflected back to the sensor at various wavelengths, and consist of composite signals of various intensities from not only the vegetation canopies themselves, but also "background objects" such as soils and litter.

The normalized difference vegetation index, known as NDVI, (Rouse et al., 1973) is the most widely used transformation for monitoring various biophysical parameters associated with vegetation. An alternative spectral transformation, proposed for remote estimation of VF, is the visible atmospherically resistant index (VARI), which displays a linear relationship with green VF (Gitelson et al., 2002; Viña et al., 2004). NDVI and VARI$_{Green}$ were calculated by the following equations:

$$NDVI = \frac{(\rho_{NIR} - \rho_{Red})}{(\rho_{NIR} + \rho_{Red})} \qquad [3]$$

$$VARI_{Green} = \frac{(\rho_{Green} - \rho_{Red})}{(\rho_{Green} + \rho_{Red} - \rho_{Blue})} \qquad [4]$$

where ρblue, ρgreen, ρred, and ρNIR were integrated to the band passes of the Landsat Thematic Mapper (TM) as shown in Table 3.1.

Algorithm Calibration and Validation

P. australis spectra collected from the five mesocosms were integrated to obtain an average value per data collection campaign, thus yielding a total of 22 samples for the growing season (n = 22). Because of this small n-size, coefficients of the vegetation indices used to estimate VF were obtained using a "leave-one-out" cross-validation method. To calibrate the indices, training datasets were produced by generating regression models summarizing the relationship between an individual vegetation index

and measured VF. The 22 training datasets were created by sequentially subsetting a single sample from the entire dataset (*n*-1). Validation of each model was then accomplished using the remaining sample in each of the calibrations. By iteratively validating the dataset *n* times, each observation was used exactly once. Root mean square error (RMSE) and correlation coefficients (R^2) were calculated from the average of all validations and were then used to assess the accuracy of the algorithms.

RESULTS AND DISCUSSION

Variation in Reflectance Spectra throughout Growing Season

Spectra (generated from vegetation reflectance at wavelengths between 400 and 900 nm) of the *P. australis* canopy are shown in Figure 3.2(a-d), along with annotated maximum and minimum ranges of VF for each phenological stage. On day-of-year (DOY) 117 (Figure 3.2a), VF equaled 0%, as evidenced by the spectral curve depicting increasing reflectance with increasing wavelength. Such a profile is indicative of soil and/or litter (i.e., dead vegetation from the previous year's growth). Over the following 26 day period, characterized as the "emergence period," VF increased at a slow rate to a maximum of 5%. The resulting minimal increase in visible (VIS) reflectance, shown in Figure 3.2(a), can be partially attributed to the composite signal comprised of leaf surfaces and soil background. Larger variations, such as the increased reflectance at all wavelengths between DOY 137 and 143, may be caused by changing soil conditions (i.e., variability in moisture content).

From DOY 151 to DOY 213 (Figure 3.2b), here termed the "vegetative growth stage," the *P. australis* stand experienced considerable above-ground development, including shoot elongation and leaf expansion. The *P. australis* reached its maximum canopy coverage on DOY 193 at 95% VF. This increase in coverage caused a decrease in reflectance in the green (3.3%) and blue (2.5%) regions of the spectrum due to increased photosynthetic activity and absorption by chlorophyll and carotenoids (Zur et al., 2000). Similarly, red reflectance decreased sharply (7%) due to increased absorption by chlorophyll in the canopy leaves (Gitelson, 2005). Consequently, the red region was more sensitive to changes in *P. australis* growth as compared to the green and blue regions. In contrast to the diminishing reflectance in the VIS spectrum during vegetative growth, NIR reflectance increased sharply, as expected, from about 20% to nearly 45%.

The canopy progressively flowered after DOY 221, causing VF to decrease by 27% (Figure 3.2c) as the *P. australis* developed a reddish inflorescence. Consequently, reflectance in the VIS increased while reflectance in the NIR decreased.

Beginning on DOY 263, leaf necrosis was visually observed in the canopy, indicative of the onset of senescence. The decline in the total amount of green vegetation caused *P. australis* reflectance in the NIR to decrease while the VIS increased (Figure 3.2d). Between DOY 269 and 274, the first frost occurred, which caused a steep decline in VF as a result of both necrosis and leaf fall.

Another perspective related to the phenology of *P. australis* is provided by Figure 3.3 where changes in blue, green, red, and NIR reflectance are shown according to the DOY. Variations in the frequency and amplitude of the reflectance at each of these

wavelength regions throughout the warm season are linked closely to the physiological processes associated with annual plant growth and ultimate decline. For instance, the large change in the slope between the vegetative growth and flowering stages indicate a transition in the manner in which *P. australis* processes light associated with the various growth stages. Slight changes in the amplitude of VIS and NIR reflectance, for example after DOY 188 and through flowering (around DOY 262), are mainly caused by changes in the distribution of plants and flowers in the canopy, which, in turn, affects the interactions involving solar energy and the plants themselves. These changes in amplitude are more exaggerated in the NIR due to the flowers constituting an altered canopy structural component.

Relative Changes in Blue, Green, Red, and NIR Reflectance with Changes in VF

The relationship between the *P. australis* reflectance in the blue, green, red, and NIR vs. VF is presented in Figure 3.4. In general, as VF increased, reflectance in the VIS decreased while reflectance in the NIR increased. This outcome, as expected, is caused by increased absorption in VIS wavelengths and an increase in scattering of NIR energy due to an increase in plant biomass. The steeper slope associated with the red reflectance is indicative of a wider dynamic range of values than is the case for blue and green. Thus, the red remained more sensitive to all changes in VF than reflectance in the blue and green.

Changes in Albedo with Changes in VF between Flowering and Reproductive Stages

The total spectral reflectance from the *P. australis* canopy in the VIS portion of the spectrum varied somewhat among the phenological stages and was dependent on plant characteristics and the nature of the target background filling the sensor IFOV.

Figure 3.5 depicts the general differences in integrated reflectance in the blue, green, and red spectral regions (i.e., spectral albedo) against VF during the phenological stages of vegetative growth versus flowering/senescence. The figure shows, for similar VF values between the respective phenological stages, that the VIS reflectance during the vegetative growth stage was higher than that for flowering/senescence when VF was 45-90%. This suggests, somewhat surprisingly, that photosynthetically active radiation (PAR) albedo, which consists of the sum of reflectance in blue, green, and red wavelengths, was absorbed to a slightly greater extent during inflorescence than during vegetative growth when VF was the same between the two periods.

The disparity in reflectance values between the vegetative growth and flowering/senescence stages was more prevalent in the VIS portion of the spectrum than the NIR, thus introducing error into the calculation of VF by the vegetation indices studied. More specifically, it was observed that the index using only the visible spectrum (i.e., $VARI_{Green}$) was more susceptible to error than the index employing the NIR (i.e., NDVI). To clarify this finding, Figure 3.6 was developed to illustrate the slight disparity in values calculated from the numerator of $VARI_{Green}$ ($\rho Green - \rho Red$) between the vegetative growth and flowering/senescence periods. It was observed that the absolute difference between green and red reflectance was greater during the vegetative

growth stage, when considering equal values of VF, as compared to the denominator of VARI$_{Green}$ (ρGreen + ρRed − ρBlue). The latter calculation showed no disparity in the resulting values. Therefore, it appears that there was a minor bias in the amount of estimated VF calculated by VARI$_{Green}$ between the vegetative growth and flowering periods. As a result, in order to estimate VF as accurately as possible, it became necessary to deconvolve the composite upwelling spectral signature in order to understand what factors influence the change in VIS reflectance between the two phenological stages.

In order to fully understand why reflectance behaved distinctly differently between vegetative growth and flowering stages, it was necessary to determine the total proportion of each component (i.e., green vegetation, inflorescence, shadows, and background) comprising the spectral signature. Such information may clarify the manner in which spectral constituents within the IFOV contribute to the overall reflectance. The combination of primary constituents comprising the spectral signature was deconvolved in the downward-looking image of the *P. australis* canopies in the following manner.

The amount of inflorescence present at the time of scanning was estimated using similar methods described earlier for calculating VF. After some considerable trial and error, it was determined that the equation (2 * Red − Green), resulted in the best approach for separating plant inflorescence from both green vegetation and other background materials (Figure 3.7a-b). This equation contrasts the differences in overall spectral reflectance where constituents have greater red reflectance than green reflectance. However, when senescence occurred and the amount of non-photosynthetically active

vegetation increased, there was greater spectral mixing involving plant inflorescence and "yellow" vegetation. In order to separate these two components of the composite signal, the image was further refined by applying a second transformation.

Visual observation indicated that the *P. australis* flower had less yellow hue than the darker necrosed (but also yellow) leaves. In order to more fully elucidate the spectral mixing of primary components within the IFOV, hue variations in yellow components in the photograph were spectrally separated by the following equation: (Red / Green) / (Green / Blue). Figure 3.8(a-b) shows the results of the second transformation, which contrasts the differences between the yellow hue variations in plant inflorescence and necrosed leaves on DOY 274.

Finally, background components, which were classified as neither green photosynthetic material nor plant inflorescence, were disintegrated to separate shadows from background soil and litter by applying a user-defined threshold to each image (which varied depending on fluxes in sky conditions) based upon the formula (Blue + Green + Red). The resulting "classified images" provide a seemingly definitive dissolution of primary image components as considered throughout the course of an entire growing season. Seasonal changes in the visual coverage of each constituent, as observed from the top of canopy, influence the composite reflectance measured by the sensor. Thus, an understanding of the fraction each component contributes to the overall reflectance through the season may determine to what extent other components besides VF contribute to the increased reflectance observed during the vegetative growth stage as compared to the flowering/senescence stage, when equal VF is observed at both times.

Once the procedure was implemented, the amount of plant inflorescence was then calculated as a percent of the total area within the sensor IFOV. The fundamental assumption was that the total upwelling signal is the sum of reflected photosynthetically active vegetation (i.e., VF), inflorescence (IF), shadow fraction (SF), and non-photosynthetic background components such as bare soils and litter (BF). Thus, the proportion of any one of the four primary components can be calculated by simple subtraction.

Figure 3.9 summarizes the fraction that the four different image constituents contributed to the composite signal, as measured over time throughout an entire growing season. The amount of background information received by the sensor decreased inversely to the increase in VF, as expected, up to DOY 221, or when plant inflorescence began to develop. Between DOY 221 and 274, BF varied between 2 and 6%, whereas IF increased steadily to comprise a full 22% of the reflected signal by DOY 256. There was a noticeable increase in SF during the beginning of the season (DOY 114 – 159) due to an increase in plant height and biomass; however SF varied from 2-16% beyond this date and was no doubt mainly influenced by changes in solar illumination (i.e., cloud dynamics). For example, diffuse light, caused by cloudy conditions, allowed further penetration of light into the canopy by reducing "hard shadows" (Milton, 1981). Therefore, the minimal variations in SF after the emergence stage are proportional to changes in the amount of VF and BF as viewed from the top of the canopy.

During the vegetative growth stage, the measured spectral signal was comprised of a mixed reflectance from green vegetation and background soils and litter. However,

during flowering, IF was three times greater than BF, and thus, the signal was mainly a combination of reflectance from the green vegetation and plant inflorescence. Upon extensive comparison of pixel values in the photographs between the vegetative growth and flowering stages, it was determined that there was greater reflectance from the background soils than from plant inflorescence. Therefore, visually brighter background soils (as compared to plant inflorescence) between the two stages likely caused the increased PAR albedo, considering the amounts of VF were equal.

Algorithm Development

Structural changes in the developing plant canopy, in turn, led to major variability in the light climate (i.e., reflectance, absorption, transmission) within that canopy. Additional variations in the upwelling signal from the canopy can be caused by changes in cloud conditions, which influence the proportion of reflected visible light from vegetation, background, and the nature of the shadows that occur in response to fluxes in illumination. Thus, such variability in downwelling irradiance and subsequent conditions must be considered in order to accurately estimate VF over the course of a growing season, and alternate approaches may be necessary. An initial step in developing a "compensating algorithm" was to correct for variations in reflected VIS light from the canopy; thus, any developed index should include a term for reflected PAR (R_{PAR}). Effectually, the reciprocal of reflected PAR $(R_{PAR})^{-1}$ may be used to reduce measured variations in VIS light upwelling from the canopy, caused either by changes in the developing canopy itself or by fluxes in atmospheric conditions.

Reflected PAR from the vegetation stand is linearly (and inversely) correlated to the percent canopy cover as documented in Figure 3.10. In other words, the amount of VIS light reflected from the vegetation stand decreases (i.e., it becomes absorbed) proportionally to the amount of increasing VF. As a result, R_{PAR} may serve to reduce variations in VIS albedo as well as provide a means for correlating to the fraction of vegetation cover.

As seen in Figure 3.10, the variance in the recorded points of R_{PAR} from the best-fit function is likely caused by fluctuations in cloud conditions, which in turn influences the amount of light penetrating through the various levels of the canopy. The objective then, was to reduce this uncertainty in order to quantify the vegetation coverage more effectively and more accurately.

Gitelson et al. (2002) demonstrated the high correlation that exists between reflectance at blue and red wavelengths acquired over canopies of corn and soybeans. Likewise, the *P. australis* reflectance at blue and red wavelengths were closely correlated ($R^2 = 0.95$, $p < 0.001$) and consequently, the assumption may be made that reflectance in the blue region of the spectrum yields nearly identical information with that in the red (ρBlue $\propto$ ρRed). Therefore, in reality, there are two independent (i.e., less correlated) VIS bands, green and red, which provide most of the quantitative information about a growing stand of vegetation.

A normalized differenced ratio, accomplished by means of simple mathematical transformation, may aid in accounting for soil (e.g., moisture content) and other background variations occurring throughout the growing season (Hanan et al., 1991).

With the considerations noted above in mind, it seemed appropriate that the numerator should be composed of ρGreen – ρRed. Yet, as demonstrated earlier in Figure 3.6, the absolute difference between green and red reflectance creates large dissimilarities in estimated VF from one phenological cycle to the next. There is also a hyperbolic relationship caused by the increasing sensitivity of red reflectance to low amounts of chlorophyll. In order to reduce the influence of subtle physiological changes within the canopy, such as diminished amounts of chlorophyll and the associated spectral response in the red region, it seems necessary to minimize the slope of the absolute difference of green and red reflectance to VF. If it can be done, then the remaining variance between the absolute difference of green and red reflectance should be caused solely by the variance in irradiance due to fluxes in the atmospheric conditions at the time of scanning.

It was discovered that in the case of increasing green reflectance, the slope of the absolute difference between green and red reflectance vs. VF decreased. This slope approaches zero when ρGreen is multiplied by a factor between 2.0 to 2.8. Figure 3.11 shows the CV of ρGreen – ρRed as ρGreen is multiplied from 2.0 to 2.8 throughout the 22 field campaign days. The variance of ρGreen – ρRed reaches a minimum when ρGreen is multiplied by 2.4. The relationship (not shown), therefore, between (2.4 * ρGreen – ρRed) and VF is nearly invariable ($R^2 = .011$).

Therefore, the resulting vegetation index (2.4 * ρGreen – ρRed) $(R_{PAR})^{-1}$, hereafter termed the "albedo corrected vegetation index" (ACVI) can be expressed as

$$ACVI = \frac{(2.4 * \rho_{Green} - \rho_{Red})}{(\rho_{Green} + \rho_{Red} + \rho_{Blue})}$$ [5]

Calibration and validation of ACVI was performed in a manner similar to the approaches applied to the NDVI and VARI indices, using the leave-one-out cross-validation.

Measured vs. predicted VF using NDVI, VARI$_{Green}$, and ACVI are presented in Figure 3.12. As shown in the graphic, NDVI behaves asymptotically with regard to measured VF, and as a result, becomes relatively insensitive beyond VF = 60% (Gitelson, 2004). In contrast to the behavior of NDVI, VARI$_{Green}$ displayed a linear relationship with green VF. The performance of these indices is comparable to the results reported by Viña et al. (2004) and Gitelson et al. (2002). In the case of ACVI, the numerator of the transformation ($2.4 * \rho$Green $- \rho$Red) remained nearly invariant to changes in VF while the denominator (ρBlue $+ \rho$Green $+ \rho$Red) decreased linearly to VF. As a result, ACVI remains linear to the entire range of VF.

The error of predicted vs. observed VF, as presented by the sum of squares, was much smaller with ACVI than in both NDVI and VARI$_{Green}$ from DOY 151 through 274, which was the duration of the vegetative growth and flowering stages (Figure 3.13). This suggests that ACVI performed exceptionally well at correcting for variability in the light climate of the canopy between the two phenological stages. The result of corrected PAR albedo reflected from the vegetation canopy improved the RMSE of estimated VF when ACVI (1.51) was applied as compared to both NDVI (2.94) and VARI$_{Green}$ (3.27).

Noise Equivalence (NE), which allows comparison among several vegetation indices with difference scales of dynamic ranges (Viña and Gitelson, 2005), can be expressed as

$$NE\Delta VF = \frac{RMSE(VI \; vs. \; VF)}{d(VI)/d(VF)}$$ [6]

where RMSE is the error of the predicted vs. observed VF and d(VI)/d(VF) is the slope of the best-fit function of the vegetation index to VF (Govaerts et al., 1999). The NE of ACVI to VF exceeded all vegetation indices tested and other widely used indices including Wide Range Dynamic Vegetation Index (WDRVI, α=0.2) and Enhanced Vegetation Index (EVI; Figure 3.14).

CONCLUSIONS

By collecting spectral reflectance of *P. australis* over the course of an entire growing season, one can quantitatively assess the phenological development of the vegetation canopy. In this study, four objectives were fulfilled using proximal remote sensing of a *P. australis* canopy.

Four stages of development (emergence, vegetative growth, flowering, and senescence) were identified and distinguished by evaluating the changes in amplitude of the reflected light. Reflectance spectra varied characteristically per wavelength among the four stages of plant development.

The amount of vegetation present during each phenological stage may be used to monitor and manage the invasive characteristics of *P. australis*. Therefore, the four phenological stages of development identified were further evaluated by calculating VF over the course of the growing season. Those VF values were characteristic of *P. australis* growth and development.

Variations in canopy reflectance between and among phenological stages were, at times, a limiting factor in accurately estimating the amount of VF over the course of a growing season. It was determined that variations in VIS reflectance from non-green vegetative material such as background soil, litter, and plant inflorescence between the vegetative growth and flowering/senescence stages contributed to inaccuracies in VF estimation when using $VARI_{Green}$.

As a solution to the problem identified in the previous conclusion, a new algorithm (ACVI) was developed to normalize variations in the R_{PAR} from the *P. australis* canopy. Tests demonstrated that ACVI was superior to other indices examined. Despite the subtle differences in improved RMSE for estimated VF with the new index, its sensitivity to low VF is comparable to that of NDVI.

Although, the spectral features of *P. australis* may be different from those in an agricultural field site, ACVI, which corrects for variations in PAR albedo, may be extrapolated to other vegetation canopies with growing characteristics that are similar to *P. australis*. Further analysis concerning the validation of the results should be investigated to assess the robustness of ACVI when applied to other vegetation types.

REFERENCES

Acker, R. C. V., C. J. Swanton, and S. F. Weise. 1993. The Critical Period of Weed Control in Soybean [*Glycine max* (L.) Merr.]. *Weed Science*, 41 (2): 194–200.

Aman, A., H. P. Randriamanantena, A. Podaire, and R. Frouin. 1992. Upscale Integration of Normalized Difference Vegetation Index: The Problem of Spatial Heterogeneity. *IEEE Transactions on Geoscience and Remote Sensing*, 30 (2): 326–338.

Bastlová, D., H. Čížková, M. Bastl, and J. Květ. 2004. Growth of *Lythrum salicaria* and *Phragmites australis* Plants Originating from a Wide Geographical Area: Response to Nutrient and Water Supply. *Global Ecology and Biogeography*, 13 (3): 259–271.

Bhowmik, P. C. 1997. Weed Biology: Importance to Weed Management. *Weed Science*, 45 (3): 349–356.

Boedeltje, G., J. P. Bakker, A. Ten Brinke, J. M. van Groenendael, and M. Soesbergen. 2004. Dispersal Phenology of Hydrochorous Plants in Relation to Discharge, Seed Release Time and Buoyancy of Seeds: The Flood Pulse Concept Supported. *Journal of Ecology*, 92 (5): 786–796.

Davies, Richard J.-P. D., D. A. Mackay, and M. A. Whalen. 2010. Competitive Effects of *Phragmites australis* on the Endangered Artesian Spring Endemic *Eriocaulon carsonii*. *Aquatic Botany*, 92 (4): 245–249.

Deen, W., T. Hunt, and C. J. Swanton. 1998. Influence of Temperature, Photoperiod, and Irradiance on the Phenological Development of Common Ragweed (*Ambrosia artemisiifolia*). *Weed Science*, 46 (5): 555–560.

Ghersa, C. M. and J. S. Holt. 1995. Using Phenology Prediction in Weed Management: a Review. *Weed Research*, 35 (6): 461–470.

Gilmore, M. S., E. H. Wilson, N. Barrett, D. L. Civco, S. Prisloe, J. D. Hurd, and C. Chadwick. 2008. Integrating Multi-temporal Spectral and Structural Information to Map Wetland Vegetation in a Lower Connecticut River Tidal Marsh. *Remote Sensing of Environment*, 112 (11): 4048–4060.

Gitelson, A. A. 2004. Wide Dynamic Range Vegetation Index for Remote Quantification of Biophysical Characteristics of Vegetation. *Journal of Plant Physiology*, 161 (2): 165–173.

———. 2005. Remote Estimation of Canopy Chlorophyll Content in Crops. *Geophysical Research Letters*, 32 (8).

Gitelson, A. A., Y. J. Kaufman, R. Stark, and D. C. Rundquist. 2002. Novel Algorithms for Remote Estimation of Vegetation Fraction. *Remote Sensing of Environment*, 80 (1): 76–87.

Govaerts, Y. M., M. M. Verstraete, B. Pinty, and N. Gobron. 1999. Designing Optimal Spectral Indices: A Feasibility and Proof of Concept Study. *International Journal of Remote Sensing*, 20 (9): 1853–1873.

Gutman, G. and A. Ignatov. 1998. The Derivation of the Green Vegetation Fraction from NOAA/AVHRR Data for Use in Numerical Weather Prediction Models. *International Journal of Remote Sensing*, 19 (8): 1533–1543.

Hanan, N. P., S. D. Prince, and P. H. Y. Hiernaux. 1991. Spectral Modelling of Multicomponent Landscapes in the Sahel. *International Journal of Remote Sensing*, 12 (6): 1243–4258.

Hegazy, A. K., G. M. Fahmy, M. I. Ali, and N. H. Gomaa. 2005. Growth and Phenology of Eight Common Weed Species. *Journal of Arid Environments*, 61 (2): 171–183.

Hodges, T. 1991. Predicting Crop Phenology. Boca Raton: CRC Press.

Huete, A., K. Didan, T. Miura, E. P. Rodriguez, X Gao, and L. G. Ferreira. 2002. Overview of the Radiometric and Biophysical Performance of the MODIS Vegetation Indices. *Remote Sensing of Environment*, 83 (1-2): 195–213.

Kettenring, K. M., M. K. McCormick, H. M. Baron, and D. F. Whigham. 2009. *Phragmites australis* (Common Reed) Invasion in the Rhode River Subestuary of the Chesapeake Bay: Disentangling the Effects of Foliar Nutrients, Genetic Diversity, Patch Size, and Seed Viability. *Estuaries and Coasts*, 33 (1): 118–126.

Kiviat, E. 2010. *Phragmites* Management Sourcebook for the Tidal Hudson River and the Northeastern States. Annandale, NY: Hudsonia Ltd.

Meyer, G. E. and J. C. Neto. 2008. Verification of Color Vegetation Indices for Automated Crop Imaging Applications. *Computers and Electronics in Agriculture*, 63 (2): 282–293.

Meyerson, L. A., K. Saltonstall, L. Windham, E. Kiviat, and S. Findlay. 2000. A Comparison of *Phragmites australis* in Freshwater and Brackish Marsh Environments in North America. *Wetlands Ecology and Management*, 8 (2): 89–103.

Milton, E. J. 1981. Does the Use of Two Radiometers Correct for Irradiance Changes During Measurements. *Photogrammetric Engineering and Remote Sensing*, 47: 1223–1225.

Minchinton, T. E. and M. D. Bertness. 2003. Disturbance-Mediated Competition and the Spread of *Phragmites australis* in a Coastal Marsh. *Ecological Applications*, 13 (5): 1400–1416.

Monteiro, A., I. Moreira, and E. Sousa. 1999. Effect of Prior Common Reed (*Phragmites australis*) cutting on Herbicide Efficacy. *Hydrobiologia*, 415 (0): 305–308.

Rollin, E. M., E. J. Milton, and D. R. Emery. 2000. Reference Panel Anisotropy and Diffuse Radiation - Some Implications for Field Spectroscopy. *International Journal of Remote Sensing*, 21 (15): 2799–2810.

Rouse, J. W., R. H. Haas, J. A. Schell, and D. W. Deering. 1973. Monitoring Vegetation Systems in the Great Plains with ERTS. *In Third ERTS Symposium, ed. S. C. Freden and M. A. Becker*, 1:309–317. NASA SP-351.

Rundquist, D. C., S. Narumalani, and R. M. Narayanan. 2001. A Review of Wetlands Remote Sensing and Defining New Considerations. *Remote Sensing Reviews*, 20 (3): 207–226.

Rundquist, D. C., R. Perk, B. Leavitt, G. Keydan, and A. A. Gitelson. 2004. Collecting Spectral Data over Cropland Vegetation Using Machine-positioning Versus Hand-positioning of the Sensor. *Computers and Electronics in Agriculture*, 43 (2): 173–178.

Swanton, C. J., J. Z. Huang, A. Shrestha, M. Tollenaar, W. Deen, and H. Rahimian. 2000. Effects of Temperature and Photoperiod on the Phenological Development of Barnyardgrass. *Agronomy Journal*, 92 (6): 1125–1134.

Tucker, C. J. 1979. Red and Photographic Infrared Linear Combinations for Monitoring Vegetation. *Remote Sensing of Environment*, 8 (2): 127–150.

Viña, A. and A. A. Gitelson. 2005. New Developments in the Remote Estimation of the Fraction of Absorbed Photosynthetically Active Radiation in Crops. *Geophysical Research Letters*, 32 (17).

Viña, A., A. A. Gitelson, D. C. Rundquist, G. Keydan, B. Leavitt, and J. Schepers. 2004. Monitoring Maize (L.) Phenology with Remote Sensing. *Agronomy Journal*, 96: 1139.

Weinstein, M. P. and J. H. Balletto. 1999. Does the Common Reed, *Phragmites australis*, Affect Essential Fish Habitat? *Estuaries*, 22 (3): 793.

Zur, Y., A. A. Gitelson, O. B. Chivkunova, and M. N. Merzlyak. 2000. The Spectral Contribution of Carotenoids to Light Absorption and Reflectance in Green Leaves. *Proceedings of the 2nd International Conference Geospatial Information in Agriculture and Forestry*, Buena Vista, FL, January 10-12, 2000, 2:1-7.

Band	Wavelength (nm)
ρBlue	450 – 515
ρGreen	525 – 605
ρRed	630 – 690
ρNIR	750 – 900

Table 3.1. Bands and wavelengths of Landsat Thematic Mapper used to calculate vegetation indices.

Diagram of Experimental Plot Setup

Legend

IFOV's of Phragmites

Sample 1
Sample 2
Sample 3
Sample 4
Sample 5

Hercules research vehicle postitioned directly north of target canopy

Plot of Phragmites Canopy (1,882 m^2)

5.4 m

4.05 m

Platform for miscellaneous data collection
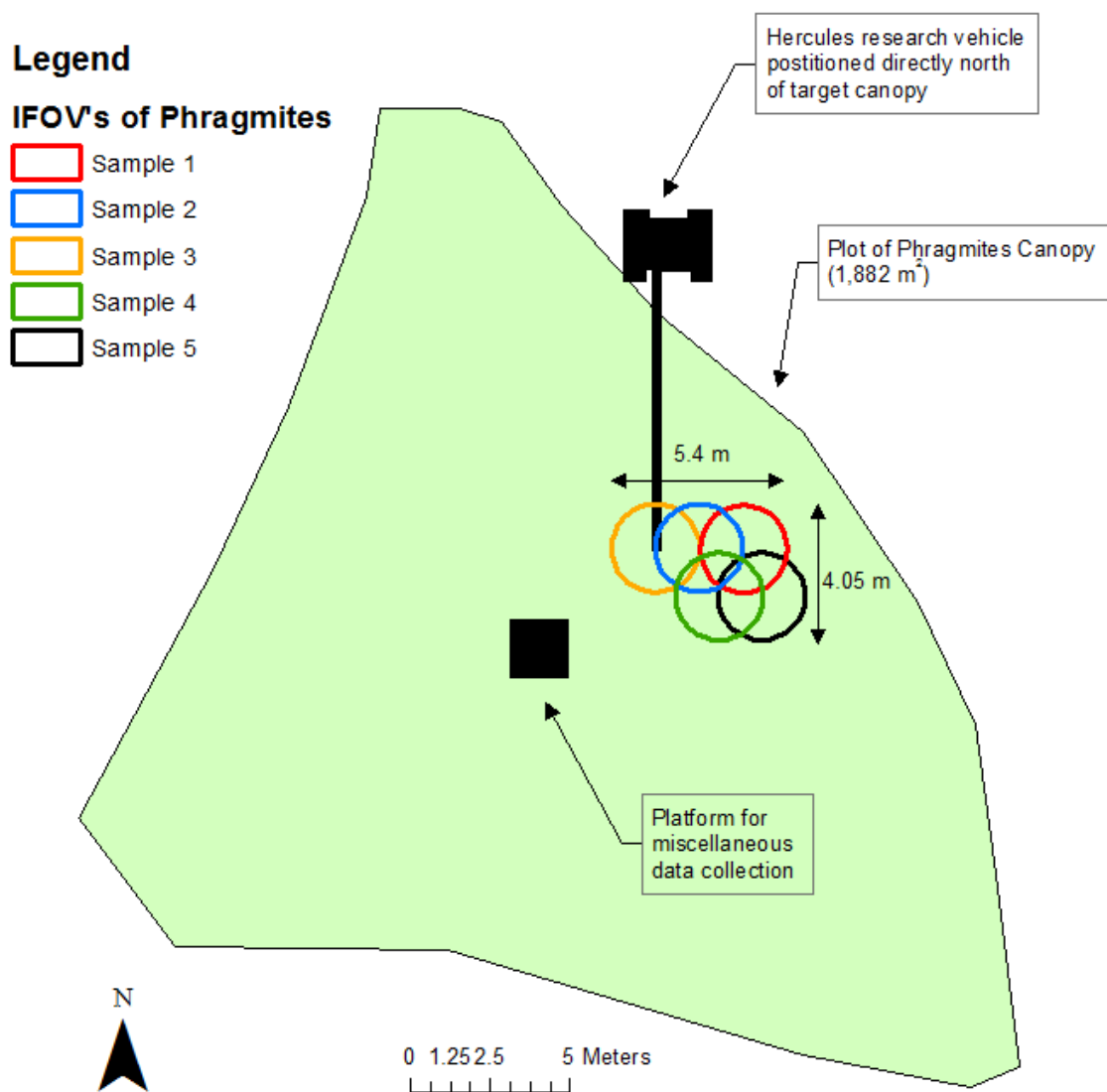
N

0 1.25 2.5   5 Meters

Figure 3.1. Diagram of *P. australis* plot and sampling configuration.
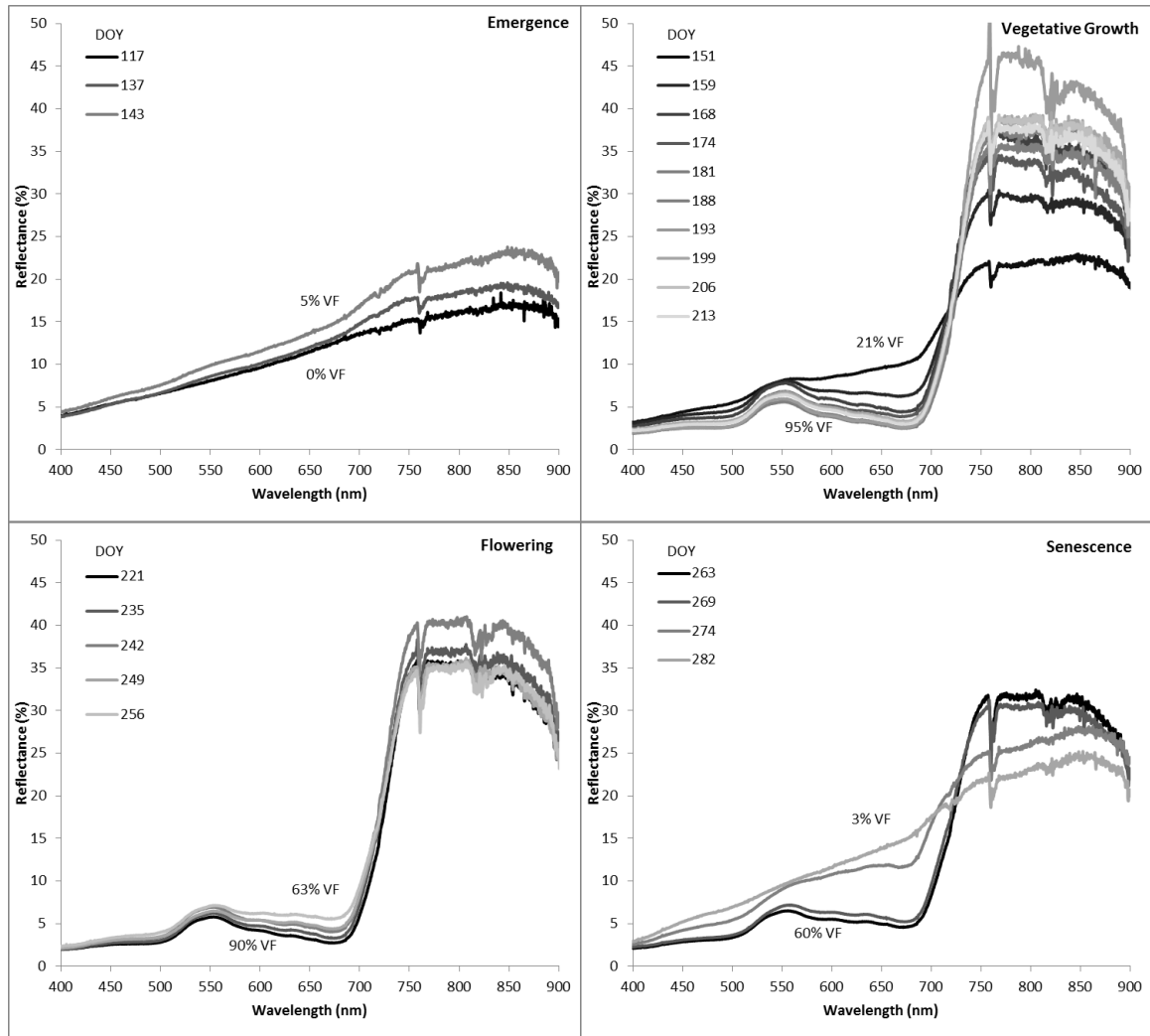
Figure 3.2 (a-d). *P. australis* reflectance in the range 400 – 900 nm during the (a) emergence, (b) vegetative growth, (c) flowering, and (d) senescence stages.
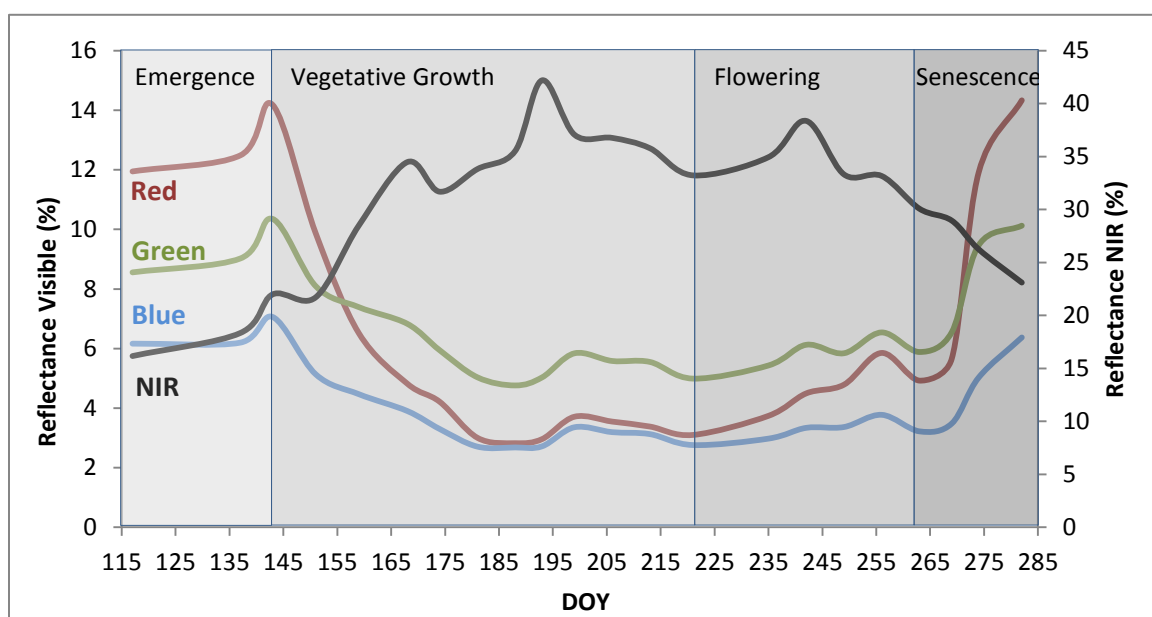
Figure 3.3. *P. australis* reflectance in the VIS and NIR wavelengths over the course of the growing season (DOY 117 – 282).
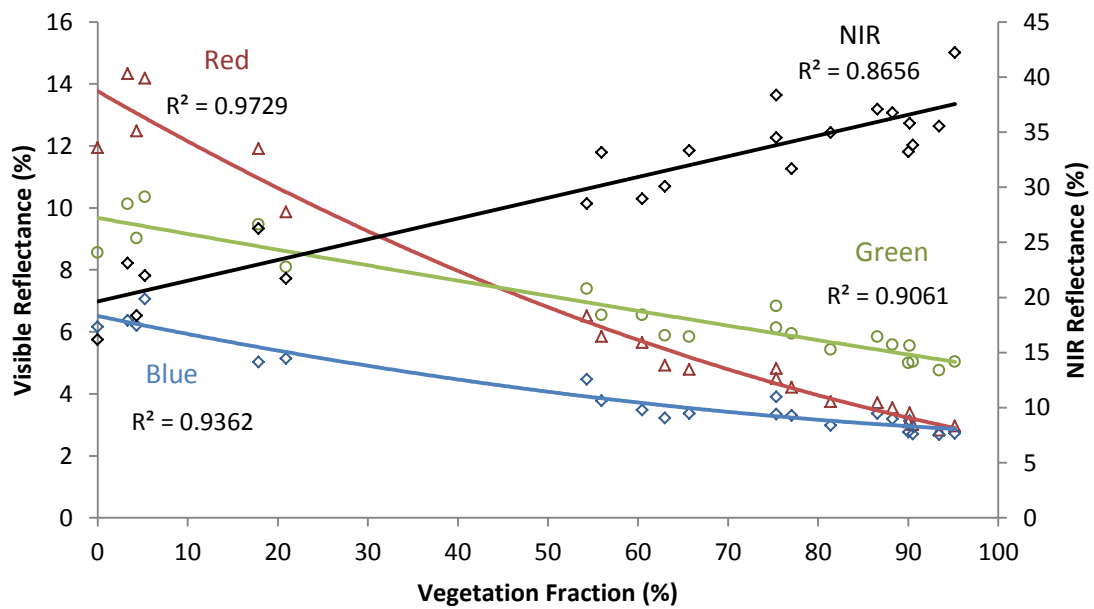
Figure 3.4. Reflectance in the blue, green, red, and NIR vs. VF for *P. australis.* As VF increased, reflectance in the VIS region decreased and reflectance in the NIR increased. Reflectance in the red had a wider dynamic range of values and remained more sensitive to all changes in VF than reflectance in the green and blue.
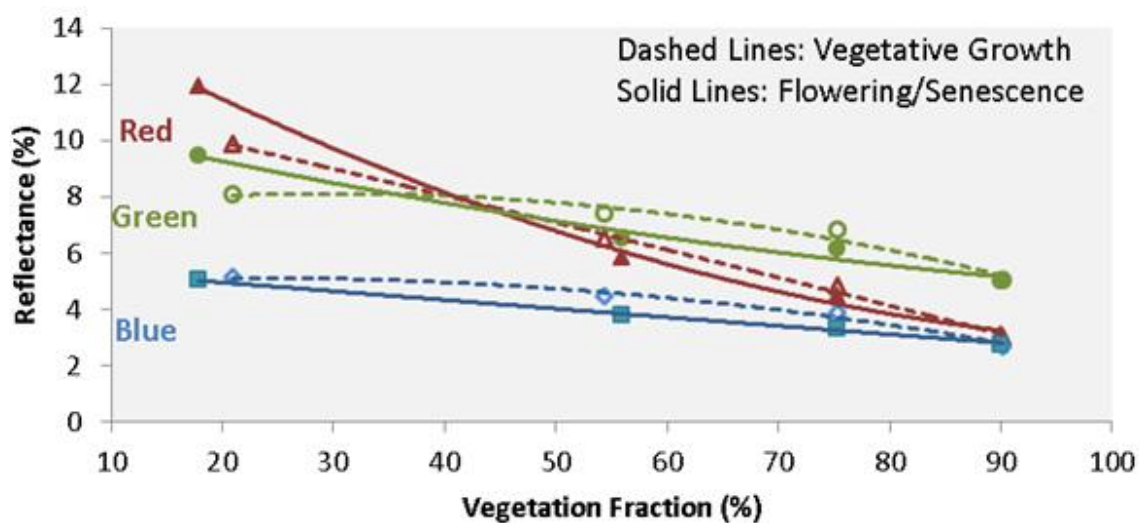
Figure 3.5. Changes in reflectance for the VIS spectrum between the vegetative growth and flowering stages (DOY 151-274) relative to changes in VF. Between VF of 45-90%, reflectance in the blue, green, and red regions of the spectrum were 18%, 13%, and 11% greater (as a ratio to total amount reflected) during the vegetative growth stage than the flowering stage.
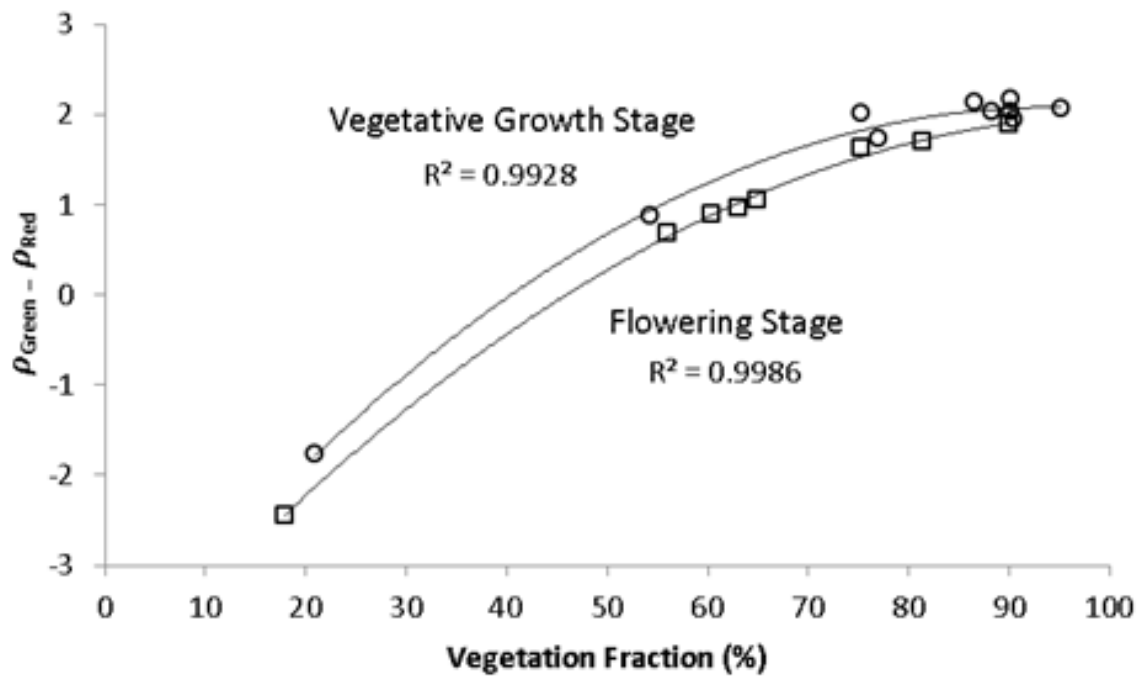
Figure 3.6. Changes in $\rho_{Green} - \rho_{Red}$ to changes in percent VF between Vegetative Growth and Flowering Stages. For similar amounts of VF, $\rho_{Green} - \rho_{Red}$ in the numerator of VARI$_{Green}$ had higher values during the vegetative growth stage as compared to the flowering/senescence stage.

Figure 3.7 (a)
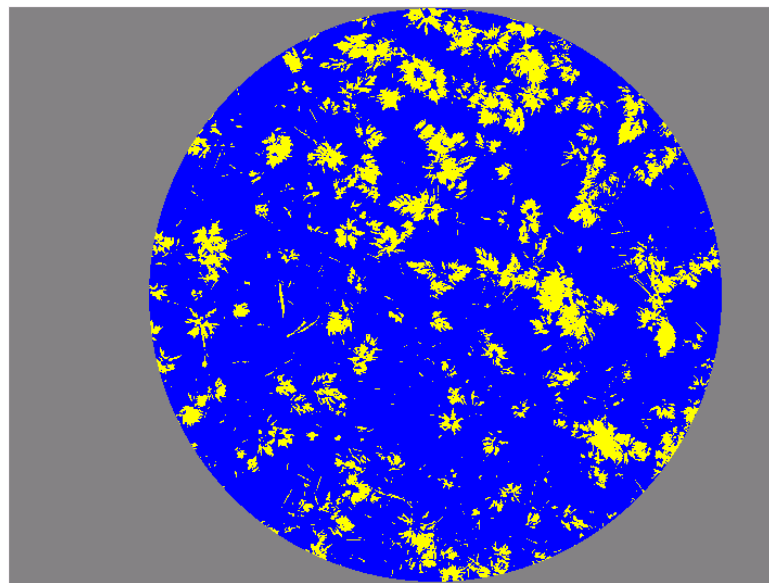
Figure 3.7 (b)

Figure 3.7 (a) shows a photograph taken over the *P. australis* canopy on DOY 256. Figure 3.7 (b) is the result of "digital classification" of the photograph by applying a user defined threshold to the image after the 2 * Red − Green transformation is applied. In Figure 3.7 (b), plant inflorescence is displayed in yellow, while vegetation/background is shown in blue.

Figure 3.8 (a)
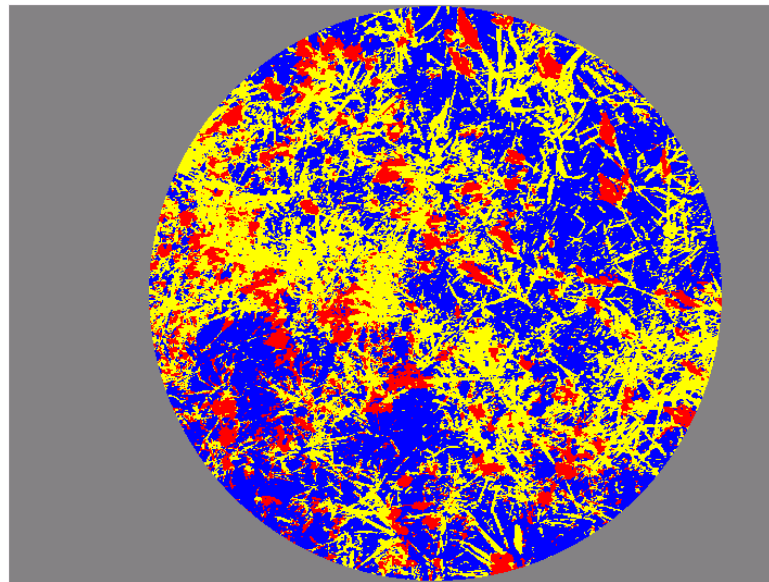
Figure 3.8 (b)

Figure 3.8 (a) shows a photograph taken over the *P. australis* canopy on DOY 274. Figure 3.8 (b) is the result of applying a user defined threshold to the image after the second transformation {(Red / Green) / (Green / Blue)} had been applied. The image is classified into three categories: blue representing green vegetation/background, yellow representing yellow leaves, and red representing plant inflorescence.
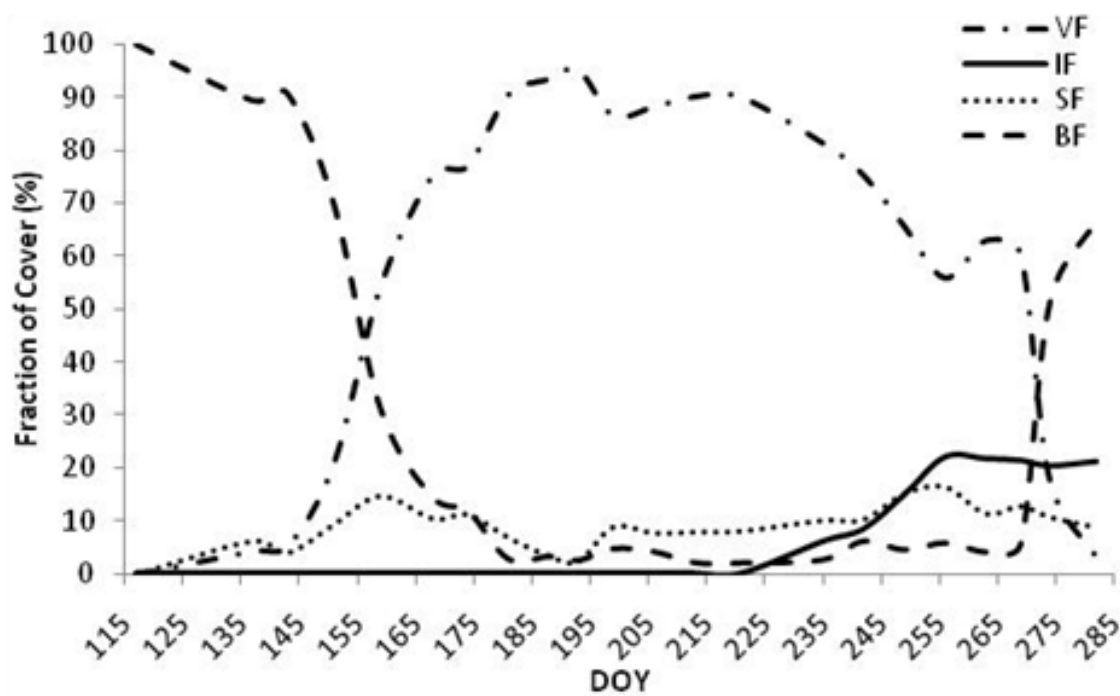
Figure 3.9. Calculated total percentage of VF, IF, SF, and BF classified in each image through the growing season.

The chart shows a scatter plot with:
- Y-axis labeled R_{PAR} ranging from 0 to 35
- X-axis labeled VF (%) ranging from 0 to 100
- Equation: $y = -0.2027x + 29.142$
- $R^2 = 0.951$
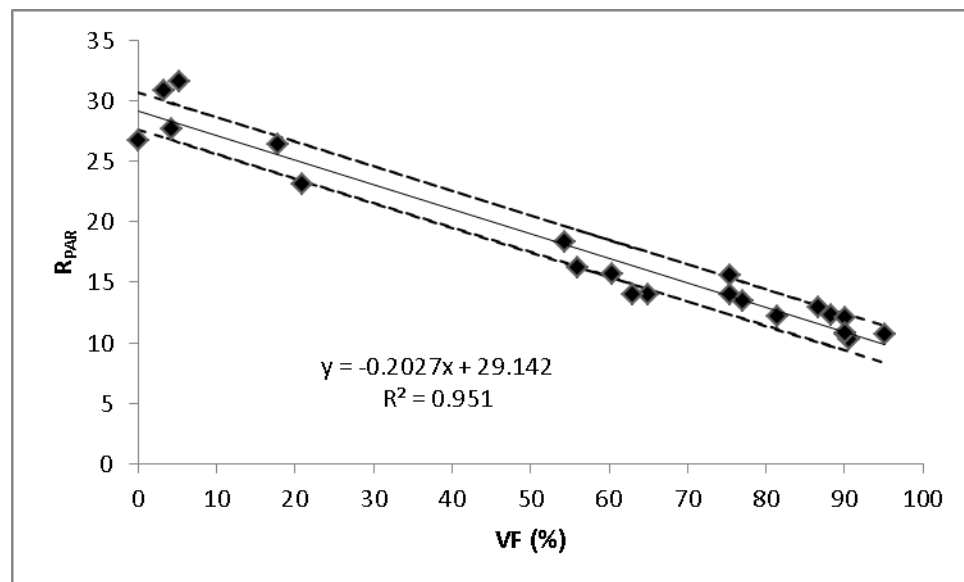
Figure 3.10. Relationship between R_{PAR} vs. VF. The solid line is the best fit function. The smaller, dashed lines show the root-mean square deviation of sample points from the best fit function. For VF from 0 to 95%, R_{PAR} is strongly correlated.
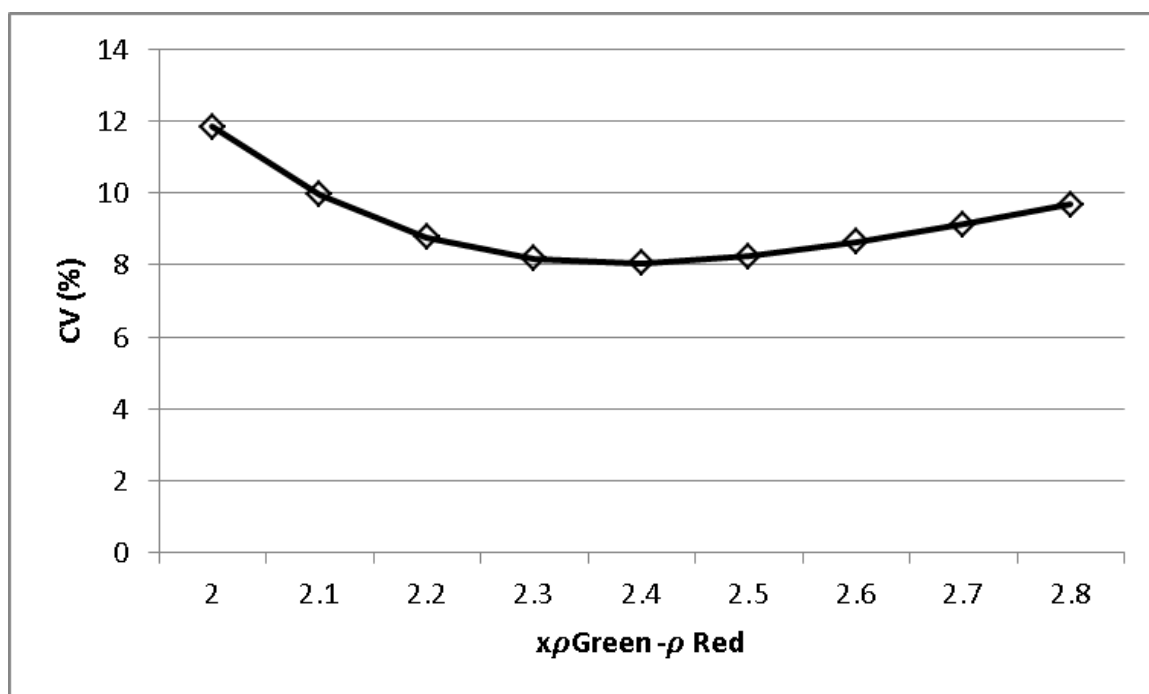
Figure 3.11. CV of the absolute difference between green and red reflectance throughout the 22 field campaign dates as green is multiplied by a factor of 2.0 - 2.8. The variation is at a minimum when ρGreen is multiplied by 2.4, which suggests that any additional variations are caused by changes in the irradiance from the atmosphere.
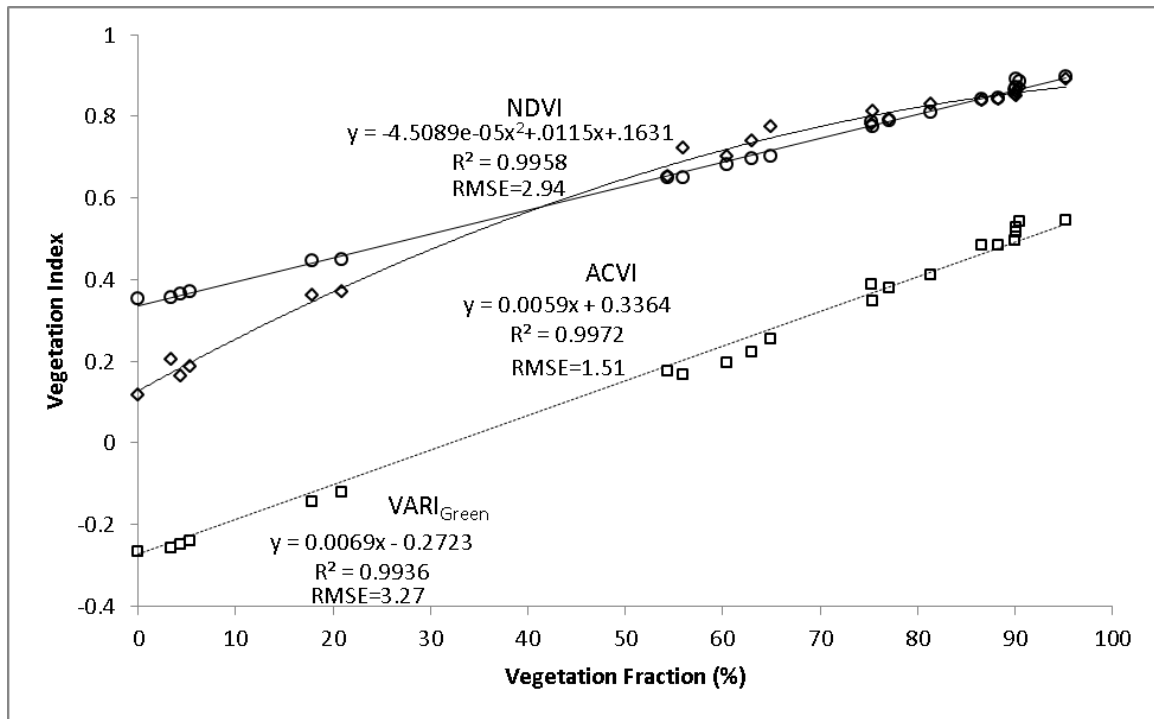
Figure 3.12. Vegetation indices NDVI, VARI$_{Green}$ and ACVI vs. VF. The lines show the best-fit functions of the sample points. NDVI begins to saturate with an increase in VF beyond 75% as compared to the linear relationship with VARI and ACVI at all VF values. Correlations (R^2) are significantly high (>.99; p-value < 0.001) in all indices vs. VF, however, ACVI performs slightly better with a lower RMSE value.
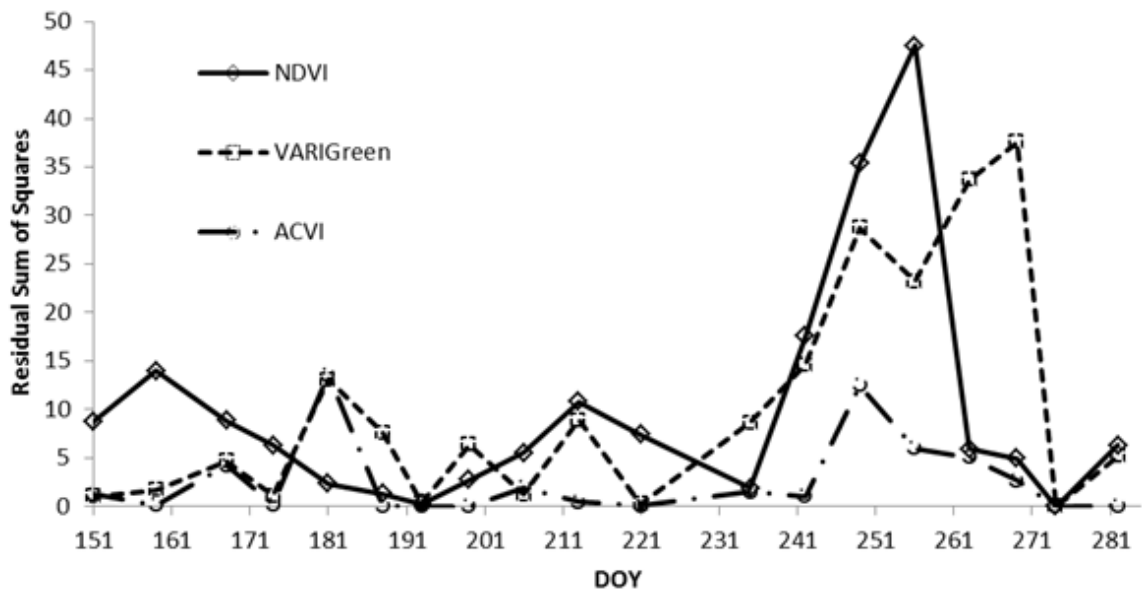
Figure 3.13. Residual squared-sums of NDVI, VARI$_{Green}$, and ACVI vs. VF during the vegetative growth and flowering/senescence stages. Plant inflorescence was observed on DOY 235, which corresponds to a trend of increasing error of predicted VF through flowering (DOY 235-269) in both NDVI and VARI$_{Green}$.
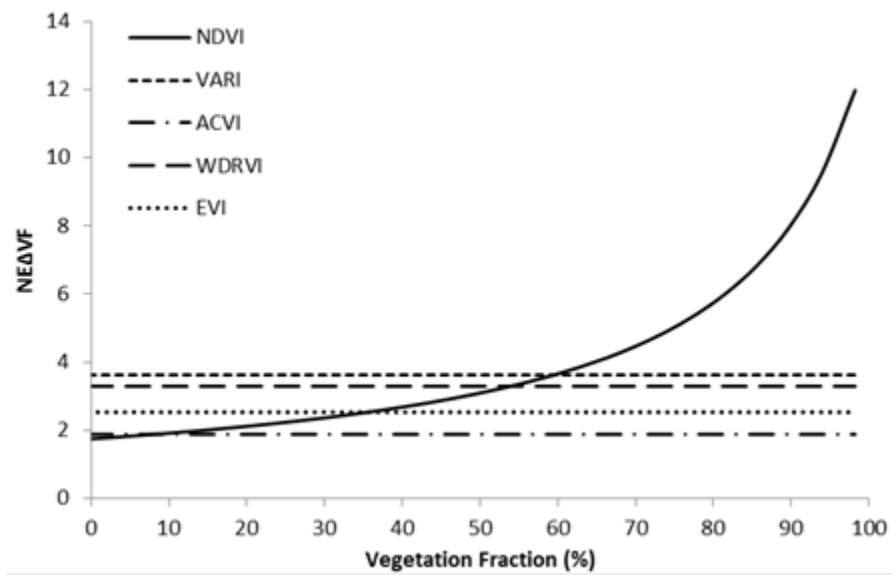
Figure 3.14. Sensitivity of NDVI, VARI$_{Green}$, ACVI, WDRVI, and EVI tested to estimate VF in *P. australis*. ACVI remains more sensitive for all VF values > 2%.

CHAPTER 4

REMOTE SENSING OF SEED PRODUCTION AND PLANT DENSITY IN

PHRAGMITES AUSTRALIS

ABSTRACT

The emergent macrophyte, *Phragmites australis*, has the ability to expand and colonize new habitats quite successfully. Understanding the population dynamics of this invasive plant species is an important diagnostic tool for creating a management strategy that will help thwart its rapid expansion. The quantification of two factors contributing to the rapid distribution of *P. australis*, inflorescence density (which was a surrogate for total seed production) and shoot density, are investigated using data collected by a simple digital camera and a much more complex system which utilizes two connected hyperspectral radiometers. Inflorescence fraction, which was determined as the area of inflorescence calculated from a binary classification of a digital image captured by the digital camera, correlated well to both inflorescence density ($R^2 = 0.924$) and shoot density ($R^2 = 0.724$). Correlations of two widely known vegetation indices (NDVI and GNDVI) derived from spectral data collected from the radiometers versus both inflorescence density and shoot density were non-significant. Factors such as the spatial resolution and the method in which the biophysical attributes were estimated likely contributed to the greatest differences in correlations between the two data collection systems. Further study on the topic should be aimed at extending the temporal period

wherein the inflorescence and shoot density are investigated, examining the *P. australis* canopy under various growing conditions, and exploring the methods used in this study to other vegetation types with canopy structures similar to *P. australis*.

INTRODUCTION

Overview of *P. australis* as an Invasive Weed

The non-native haplotype of common reed, also known as *Phragmites australis* (Cav.) Trin. ex Steudel (hereafter *P. australis*), has invasively expanded across riparian areas throughout North America. *P. australis* is a rapidly growing emergent macrophyte that establishes dense, near mono-specific stands which typically out-compete native vegetative species (Kettenring et al., 2009; Kiviat, 2010). As a result, there has been a growing interest in monitoring and managing this invasive species.

Importance of Population Dynamics

Weed scientists, resource managers, and conservation biologists often seek successful, long-term management strategies to control invasive species using targeted, low input systems, which depend on evaluating the population dynamics of the species of concern (Lutman, 2002). Population dynamics and demographic models may help identify instances where control efforts should be implemented for the purpose of reducing the spread of invasive species (Sakai et al., 2001). Furthermore, studies have shown that understanding the population dynamics of invasive species can help identify strategies for reducing frequent and repeated use of herbicides (Gonzalez-Andujar and Fernandez-Quintanilla, 1991; Buhler et al., 1997).

Population Dynamics of *P. australis*

An important factor contributing to the population dynamics of *P. australis* is its ability to reproduce and rapidly colonize new habitats. However, the primary means of reproduction of this invasive plant, which contributes to its rapid expansion, has been the subject of considerable disagreement. For example, many studies have suggested that *P. australis* predominantly spreads by clonal reproduction of rhizomes and stolons (Pellegrin and Hauber, 1999; Rice et al., 2000; Bart et al., 2006), and until recently, it was believed that *P. australis* produced very few viable seeds, especially in northern latitudes (Tucker, 1990; Gervais et al., 1993; Maheu-Giroux and de Blois, 2006). However, other studies have shown seed viability of *P. australis* to be highly variable and dependent on environmental conditions present at a particular site (McKee and Richards, 1996; Kettering and Whigham, 2009). At some sites, the possibility of *P. australis* colonization by vegetative diaspores was ruled out and it was determined that seed distribution was responsible for the primary establishment (Brisson et al., 2008; Belzile et al., 2009; McCormick et al., 2009). The recent research on seed dispersion for establishing satellite populations of *P. australis* highlights the importance of understanding and monitoring the population dynamics of this invasive species; and, more specifically, its seed production.

Fiala (1976) demonstrated the relationship between shoot density and root growth in *P. australis* stands. Other studies have shown how shoot density in *P. australis* affects the competition among various wetland species (Hara, 1994; Lenssen et al., 2004).

Monitoring the stand density in weed canopies is an important demographic variable necessary for managing the growth and competitiveness of an invasive species.

Remote Sensing as a Potential Tool in Understanding Population Dynamics

One approach in helping control the spatial extent of weed populations is through the development and use of weed maps which document both the aerial extent and density of invasive species. Such maps are useful for monitoring and understanding population dynamics and verifying model predictions (van Groenendael, 1988; Lamb and Brown, 2001). In environments where the collection of ground data for the compilation of weed maps and demographic models is both time consuming and labor intensive, remote sensing may be a potentially viable approach. Especially in wetland ecosystems, remote sensing may be an efficient approach because the technology offers a synoptic view, multi-spectral data collection for discriminating vegetation types, multi-temporal coverage, and cost effectiveness (Rundquist et al., 2001). These and other advantages are attractive when one is faced with examining the very dense, almost impenetrable canopies of invasive *P. australis*.

Objectives

If remote sensing is indeed the method of choice for mapping and understanding weed demographics, then an additional requirement is that the acquired aircraft or satellite imagery be high in not only spatial resolution but perhaps also spectral resolution (Brown and Noble, 2005). Problems for most resource managers, though, include the

facts that the acquisition of remotely sensed images is often an expensive proposition, the learning curve with regard to processing such digital data can be quite steep, and the necessary hardware and software are expensive. An alternative approach for collecting similar types of demographic weed data is to make use of a simple digital camera deployed in close proximity to the vegetation canopy of interest. One advantage of placing a camera in close proximity to the canopy itself is associated with the opportunity to produce digital images of very high spatial resolution. Whereas airborne and satellite borne sensors are capable of resolving Earth targets of approximately one meter, a digital camera placed within close proximity to the target of interest may provide images at resolutions ranging from centimeters to millimeters.

If available, a spectroradiometer deployed a few meters above a canopy can provide the advantage of collecting spectral data in hundreds to thousands of individual, very narrow spectral bands. Although it is a non-imaging device, the spectral profiles generated from data collected by such a system should be instructive at minimum, and, more importantly, they may provide a useful diagnostic mechanism for analysis.

The use of spectroradiometers for understanding weed demographic data has been limited in past research. Spectra acquired by spectroradiometers have been used to compute spectral indices, or mathematical combinations of reflectance from multiple wavelengths which may be then correlated to several weed modeling parameters. For example, Lu et al. (2009) successfully demonstrated the use of spectral indices for mapping and estimating specific shoot densities in several stands of invasive species, including *P. australis*. Also, Mirik et al. (2006) investigated the use of spectral indices

for estimating flower head densities in musk thistle; yet, the correlations they produced were non-significant. However, to date, there has been a lack of research attempting to estimate the seed production of *P. australis* through remote sensing methods.

Two biophysical variables, seed production and shoot density, both of which are important inputs to weed demographic models, are studied in this research. With the above considerations in mind, the objectives of this study are defined as follows: to quantitatively estimate seed production as well as shoot density of a *P. australis* canopy using not only close-range images acquired with a digital camera capable of very high spatial resolution, but also by means of spectra generated from field-based radiometers with very high spectral resolution.

METHODS

Field Site

Both digital images (captured by a camera) and spectroradiometric data were collected on the 26th of September, 2011 at a manmade wetland at the Center for Advanced Land Management Information Technologies (CALMIT) field research facilities, located near Mead, Nebraska. The research site is part of the University of Nebraska-Lincoln Agricultural Research Development Center (ARDC), which is approximately 56 km northeast of Lincoln, Nebraska.

P. australis was planted at the ARDC site in 1994, and it has subsequently become a monoculture species in the constructed wetland. Prior to conducting research, the plot was burned in late March, 2011, before the *P. australis* had emerged, for the

purpose of removing the dead biomass which had accumulated during previous growing seasons.

Seventeen, 2 x 2 m sample areas juxtaposed next to one another and representative of the entire *P. australis* canopy were delineated in the wetland. The sample plots were positioned to be within easy reach of sensors and to eliminate issues related to shadowing of the vegetation by the field hardware. Flags were used to mark the target areas very clearly for both image acquisition and spectral scanning.

Instrument Deployment

Photographic images and spectral reflectance data over the sample plots of *P. australis* were acquired using a digital camera and field spectroradiometers mounted on the boom of "Hercules," an all-terrain, motorized platform (Appendix A). Hercules, similar to its predecessor "Goliath" (Rundquist, 2004), provides an ideal platform for collecting remotely sensed data because the configuration of the instrument position is relatively rigid, thus minimizing noise from vibration, and the approach allows repeatable orientation of sensors from one sample site to the next. Once the height of the boom is set relative to the top of the canopy, it remains at that fixed vertical distance above the target. The boom, which may also be rotated to ensure that the sensors are continuously in the principal plane of the sun, extends to a minimum distance of 10 m from the machine, ensuring that reflectance from non-target objects, such as colored clothing worn by an operator, is eliminated. Additionally, Hercules is painted a flat-black color to reduce extraneous scattering from the platform itself. During data collection, Hercules

was positioned directly north of the target canopy being acquired with the boom pointed south to eliminate spurious reflectance measurements caused by shadowing from the platform.

Data Acquisition

Images of the vegetation canopy were acquired with an Olympus C-750 Ultra Zoom (Tokyo, Japan) digital camera. The camera is equipped with a 4.0 megapixel sensor, a 10x optical zoom lens (35 mm equivalent), and is capable of collecting broad-band light in the blue, green, and red spectrum.

Simultaneously with acquisition of digital photographs, spectral data were collected using a dual-fiber optic system, which employs two inter-calibrated Ocean Optics (Dunedin, FL) USB2000 hyperspectral radiometers. The system records spectral data in 2023 individual bands ranging from approximately 400 – 900 nm (visible and near-infrared) with a channel interval of ~.3 nm and a bandwidth of ~1.5 nm. One radiometer, equipped with an optical fiber and cosine diffuser, is pointed upward to measure incident irradiance (E_λ) within a hemispherical field-of-view. The other radiometer, equipped with a 25° field-of-view optical fiber, is pointed downward to measure radiance upwelling from the target (L_λ). A correction factor (CF) is necessary to match the transfer functions and for inter-calibration of the radiometers. This was accomplished by acquiring a spectral measurement of upwelling radiance (L_λ^{cal}) from a Spectralon reference panel (Labsphere, Inc., North Sutton, NH) which is calibrated to

approximately 99% Lambertian reflectance, simultaneously with the measurement of incident irradiance (E_λ^{cal}). The CF can then be calculated as

$$CF_\lambda = \frac{P_\lambda^{cal} \times E_\lambda^{cal}}{L_\lambda^{cal}}$$

[1]

where P_λ^{cal} is the Lambertian reflectance calibrated at each wavelength from the Spectralon panel and linearly interpolated in order to correlate the band centers of the two radiometers. A CF value was calculated at each band center by calculating the median reflectance of daily scans from the calibration panel.

To calibrate the radiance collected from spectral instruments (i.e., acquire L_λ^{cal} and E_λ^{cal}), the downward-looking spectroradiometer was positioned at a height of approximately 30 cm above a 30.5 x 30.5 cm (12 in. x 12 in.) white Spectralon panel. A minimum of eight spectral measurements of upwelling radiance and downwelling irradiance were taken concurrently and the median values for each individual band were calculated.

Spectral reflectance measurements over the 17 sample areas within the *P. australis* experimental plot were acquired near solar noon (between 13:00 and 14:00 local time), when solar diurnal variations in radiation were nearly constant due to a near-vertical zenith angle. The boom of Hercules was positioned at a height of 4.5 m above the vegetation targets, yielding a 2 m instantaneous-field-of-view (IFOV) at the top of the canopy. At each sample area, a minimum of eight spectral measurements of upwelling *P. australis* radiance and downwelling irradiance from the atmosphere were taken

concurrently, and the median values for each band were calculated. Percent reflectance from the *P. australis* canopy (ρ_λ) was determined by the following equation:

$$\rho_\lambda = \frac{L_\lambda}{E_\lambda} \times CF_\lambda \times 100 \qquad\qquad\qquad\qquad [2]$$

After images and spectral data were collected, ground data including inflorescence densities, seed counts, and shoot densities, were collected in each of the 17 plots. Seed production, or the number of florets produced per m^2, was determined by measuring both the average florets per inflorescence and the inflorescence density (inflorescences/m^2). Inflorescence density was calculated by counting the number of seed heads within a 0.75 x 0.75 m quadrat placed in the center of each sample plot. Likewise, shoot density was calculated in conjunction with the inflorescence measurement by counting stems within a 0.5 x 0.5 m quadrat placed in the center of each sample plot. Shoot density was then calculated as the number of *P. australis* culms per m^2. Subsequently, eight plant inflorescences, harvested from different parts of the reedbed and representative of the sample variances within the *P. australis* canopy, were clipped and brought back to a lab where individual seed populations were manually counted. Spikelets were stripped from each pedicel with tweezers and the average number of florets per spikelet was determined (n = 50) per inflorescence.

RESULTS AND DISCUSSION

Digital Sensing of Inflorescence and Shoot Density: Camera Approach

In order to estimate inflorescence density in the canopy by means of digital images acquired by the camera, seed heads were digitally classified. This approach involved quantifying the "inflorescence fraction" (IF), which is essentially defined as the area of the scene or sensor field of view comprised of plant inflorescence. The IF was calculated as the percent of pixels in a particular image (as observed vertically from the top of the canopy) classified as plant inflorescences compared to the total area of non-inflorescence pixels. Thus, the IF was used as a surrogate for estimating inflorescence density.

The IF was estimated with photographic images using similar method to measuring percent green vegetation fraction (Gitelson, et al., 2002; Meyer and Neto, 2008). The sampled area, or IFOV, as observed from the fiber optic connected to the Ocean Optics system, was determined within each photograph and data outside were excluded from the processing. A model was then developed to separate non-vegetative pixels (small green/red ratio) from pixels categorized as green vegetation (large green/red ratio) by applying a user defined threshold to separate the pixels into a binary image. After considerable trial and error, it was determined that the equation (2 * Red − Green), resulted in the best approach for separating plant inflorescence from both green vegetation and other background materials such as shadows and soil. The results from this transformation were visually poor due to a "spectral mixing" of plant inflorescence and non-green plant material. In these circumstances, the model was not able to

discriminate between multiple constituents having largely greater red reflectance than green, as would be more indicative of non-healthy plant matter and plant inflorescence. Therefore, pixels classified as either plant inflorescence or non-healthy plant material using the first transformation were separated from one another using a second transformation (described below).

Visual observation indicated that the *P. australis* flower had less yellow hue than the darker necrosed (but also yellow) leaves. Therefore, in order to more fully elucidate the spectral mixing of plant inflorescence and non-living plant material, hue variations in the yellow components of the photographs were spectrally separated by the following equation: (Red / Green) / (Green / Blue). Figure 4.1 (a) is a digital image acquired over the top of the canopy and Figure 4.1 (b) shows the results of the second transformation, which contrasts nicely the differences between the yellow hue variations in plant inflorescence and necrosed leaves. Once accomplished, IF was calculated as a ratio of pixels identified as plant inflorescence to those pixels which did not correspond with inflorescence.

Estimation of Inflorescence and Shoot Density from Digital Imagery

Correlations among IF, inflorescence density, and shoot density were determined and scatterplots were made to analyze the relationship between the variables tested. The correlation coefficients (r) were tested for significance (a = 0.001) with a t-statistic having $n - 2$ degrees of freedom as shown in Eq. 3:

$$t = \dfrac{r}{\sqrt{\dfrac{1-r^2}{n-2}}}$$ [3]

(Dowdy et al., 2004).

Figure 4.2 displays the relationship between IF and measured inflorescence density. The graph shows a high, positive correlation between inflorescence density and IF ($R^2 = 0.924$; T = 13.289; P < 0.001), thus suggesting that IF, calculated from a digital image, is a good proxy for estimating inflorescence density of the *P. australis* canopy.

Figure 4.3 shows the correlation between inflorescence density and shoot density in the canopy. The graphic demonstrates a positive relationship ($R^2 = 0.797$; T = 7.677; P < 0.001) between the number of inflorescences and the number of shoots present in the sampled plots. The slope of the best fit line indicates that inflorescences can be found on average every 2.6 shoots.

Because of the dense canopy structure, it was not possible to directly estimate the shoot density within the *P. australis* canopy from the digital images. Yet, due to the high correlations between IF and inflorescence density as well as inflorescence density and shoot density, it seemed that IF could be used as a suitable surrogate for estimating shoot density in the canopy. Figure 4.4 shows the relationship ($R^2 = 0.724$; T = 6.248; P < 0.001) between IF and shoot density in the sampled plots of *P. australis*. The positive correlation documents the fact that IF may be used as a proxy for estimating shoot density of the *P. australis* canopy.

Proximal Sensing of Inflorescence and Shoot Density: Spectroradiometer Approach

Spectra of sampled *P. australis* plots acquired by the hyperspectral field radiometers are displayed in Figure 4.5. The graphic shows the reflectance per wavelength of four *P. australis* plots with inflorescence densities ranging from 20 to 36 and shoot densities ranging from 62 to 96. Visual relationships between canopy reflectance and measured inflorescence and shoot density are inconclusive; for example, percent reflectance of the sampled vegetation canopies in the visible (VIS; 400 – 700 nm) and near-infrared (NIR; 700 – 900 nm) do not appear to be consistent with changing inflorescence or shoot densities.

Estimation of Inflorescence and Shoot Density from Reflectance Data

In order to more fully elucidate variations in plant inflorescence and shoot density to changes in canopy reflectance, spectra acquired by the Ocean Optics sensor were correlated to IF, inflorescence density, and shoot density. Figure 4.6 summarizes the relationships involving IF, inflorescence density, and shoot density vs. the reflectance of *P. australis* at each wavelength in the VIS through NIR portions of the spectrum (400 – 900 nm). The graph shows, as expected, a negative correlation between IF, inflorescence density, and shoot density vs. reflectance in the VIS region of the spectrum. There is a pronounced negative correlation in the green (550 nm) and red edge (710 – 720 nm) regions likely due to the higher sensitivity of reflectance in those regions with relation to chlorophyll concentrations as a result of increased shoots and plant biomass (Chappelle et al., 1992; Gitelson and Merzlyak, 1998). Correlations are weaker in the blue (400 – 500

nm) and red (650 – 690 nm) portion of the spectrum due to the pronounced absorption of light from several pigments such as carotenoids and chlorophyll (Chappelle et al., 1992; Gitelson et al., 2003). Correlation coefficients in the NIR approach zero suggesting little or no correlation between the collected ground data and NIR reflectance.

Also seen in Figure 4.6, correlations are stronger between reflectance at each wavelength in the visible spectrum vs. shoot density than either IF or inflorescence density. At the time of season this study was conducted (26th of September), the amount of green vegetation present in the canopy accounted for the largest proportion of area (approximately 50% compared to 20% inflorescence and 30% background) in the canopy structure (see Chapter 3 of thesis); thus, it is reasonable to expect that the *P. australis* culms (or shoot density), which contributed to the fraction of green vegetation, have a stronger correlation than either IF or inflorescence density. The IF provides the lowest correlation to reflectance at each wavelength in the visible spectrum.

Spectral indices, or mathematical transformations, were derived from the reflectance data acquired over the *P. australis* canopy. The normalized difference vegetation index, known as NDVI (Rouse et al., 1973), is the most widely used transformation for monitoring various biophysical parameters associated with vegetation. Alternatively, due to the maximum negative correlations in the green region of the spectrum (explained above), green normalized difference vegetation index (GNDVI) was also considered (Gitelson et al., 1996). Wavelengths used to calculate the indices were derived from the peaks and troughs of the correlation coefficients presented in Figure 4.6. Those correlation maxima and minima tended to be somewhat narrow in spectral range,

so wavelengths were integrated by averaging reflectance values in each of those portions of the spectrum. The average ranges for green (540 – 560 nm), red (660 – 680 nm), and NIR (750 – 800 nm) were employed in calculating the indices.

The selected spectral indices, NDVI and GNDVI, were correlated to inflorescence and shoot density of the *P. australis* canopy. Moreover, because of the lack of published research dealing with the estimation of seed production from spectral indices, IF was also estimated by the same spectral transformations as a means of indirectly estimating inflorescence density. Figure 4.7 (a-c) shows the relationship and best-fit lines of both NDVI and GNDVI vs. a) IF, b) inflorescence density, and c) shoot density. As visually illustrated in Figures 4.7 (a-c), correlations between NDVI and GNDVI to the measured biophysical parameters of *P. australis* were all low and only one correlation, GNDVI vs. shoot density, was found to be even weakly significant ($R^2 = 0.277$; T = 2.398, P = 0.03).

The relationships of NDVI and GNDVI vs. IF and inflorescence density were lower than the relationship between the indices and shoot density. Low correlations between each of the indices and inflorescence no doubt resulted due to spectral mixing of incident light from both plant inflorescence and non-green plant material as it was reflected back to the downward-looking sensor. The total proportion of yellow constituents in each of the *P. australis* plots was calculated using the 2 * Red – Green transformation. As a result, an average of 22.55% of the canopy structure was comprised of plant inflorescence and an average of 14.43% was comprised of other yellow components such as non-photosynthetic plant material. Thus, the yellow constituents caused confusion when attempting to estimate only plant inflorescence.

Assessments of seed production were made from estimated inflorescence densities and seed counts. After seed counts were conducted, it was determined that there was an average of 8,681 seeds per inflorescence. This number is substantially greater than Kettenring et al. (2011) which had average counts of 1,000 – 7,000 florets per inflorescence in several *P. australis* stands in the Chesapeake Bay area, yet much less than the 13,000 florets per inflorescence determined by Maheu-Giroux and de Blois (2006) in Quebec, Canada. These differences in seed production may be largely influenced by rainfall and temperatures, as well as available nutrients (McKee and Richards, 1996). Based on estimates from this research, it was determined that within the tested *P. australis* stand, seed production ranged from approximately 174,000 – 336,000 seeds per m^2. Such a finding underscores the potential for *P. australis* communities to expand their territory in rapid fashion.

CONCLUSIONS

In this study, the analysis of inflorescence and shoot density was assessed using digital images and non-imaging, hyperspectral reflectance data collected at close proximity to the vegetation canopy. It was found that IF, measured as the number of pixels in a digital photo classified as inflorescence compared to those pixels which were not, correlates well to both inflorescence and shoot density. Correlations between vegetation indices derived by basic spectral-reflectance data vs. inflorescence and shoot density measurements were found to be low and statistically non-significant. Altogether, the results suggest that any estimation of seed production or plant density is best

accomplished through the use of a simple digital camera as opposed to the more sophisticated scanning with a hyperspectral field instrument.

A major factor contributing to the differences in correlations between data acquired by each of the instruments to plant biophysical data was the spatial resolution of the camera pixels vs. the FOV of the Ocean Optics acquired at the top of the canopy. Individual yellow components, such as inflorescence and necrosed plant material, within an image captured by the camera were able to be spatially distinguished because of its very high spatial resolution (cm to mm). However, with spectra collected from the radiometer, which integrates the upwelling radiation within a FOV of 2 m, it was not possible to distinguish the individual yellow components. Thus, correlations involving the spectral indices were much lower than those involving the images derived from the camera system.

Another factor affecting the accuracy of each of the two instruments relating to the plant biophysical measurements involved the method of defining plant inflorescences. For example, the identification of plant inflorescences by means of the digital camera system was accomplished visually and, to a large extent, was based on qualitative reasoning on the part of the user by establishing a threshold level to separate yellow components from the others found within an image. This subjective measurement was exclusive to each of the sampled plots of *P. australis* and may have led to more accurate measurements of inflorescence density than was possible by means of hyperspectral data. The analysis of the spectral-reflectance data acquired by the Ocean Optics systems, which were transformed to well-documented indices, was based purely on quantitative

techniques for estimating plant inflorescence. This non-imaging method involved each reflectance dataset from the sampled plot of *P. australis* being passed through the transformation with no decision making on the part of the user. This automated approach led to a generalized estimation of plant inflorescence, which very likely caused the resulting low correlations.

Further research should be aimed at extending the temporal period wherein the seed production and shoot density are investigated. If spectroradiometer data had been collected shortly prior to senescence, it is likely that the results may have allowed for more accurate estimations of seed production and shoot density because less spectral mixing would have been observed between plant inflorescence and non-living plant matter in the vegetation canopy. It should also be pointed out that the results presented in this research may vary in habitats with different weather and climate regimes, available nutrients, elevations, and other variables which could influence the plant vigor and densities within individual stands (Haslam, 1972). Moreover, research should be conducted to examine the relationship between estimated seed production and shoot density in other vegetation canopies with structural canopy characteristics similar to those of *P. australis*.

REFERENCES

Bart, D., David B., R. Chambers, and J. M. Hartman. 2006. Human Facilitation of *Phragmites australis* Invasions in Tidal Marshes: A Review and Synthesis. *Wetlands Ecology and Management*, 14 (1): 53–65.

Belzile, F., J. Labbé, M.-C. LeBlanc, and C. Lavoie. 2009. Seeds Contribute Strongly to the Spread of the Invasive Genotype of the Common Reed (*Phragmites australis*). *Biological Invasions*, 12 (7): 2243–2250.

Brisson, J., É. Paradis, and M.-È. Bellavance. 2008. Evidence of Sexual Reproduction in the Invasive Common Reed (*Phragmites australis* Subsp. *australis*; *Poaceae*) in Eastern Canada: A Possible Consequence of Global Warming. *Rhodora*, 110 (942): 225–230.

Brown, R. B. and S. D. Noble. 2005. Site-Specific Weed Management: Sensing Requirements: What Do We Need to See? *Weed Science*, 53 (2): 252–258.

Buhler, D. D., R. G. Hartzler, and F. Forcella. 1997. Implications of Weed Seedbank Dynamics to Weed Management. *Weed Science*, 45: 329–336.

Chappelle, E. W., M. S. Kim, and J. E. McMurtrey. 1992. Ratio Analysis of Reflectance Spectra (RARS): An Algorithm for the Remote Estimation of the Concentrations of Chlorophyll A, Chlorophyll B, and Carotenoids in Soybean Leaves. *Remote Sensing of Environment*, 39 (3): 239–247.

Dowdy, S. M., S. Wearden, and D. M. Chilko. 2004. Statistics for research. Hoboken, N.J.: Wiley-Interscience.

Fiala, K. 1976. Underground Organs of *Phragmites communis*, Their Growth, Biomass and Net Production. *Folia Geobotanica & Phytotaxonomica*, 11 (3): 225–259.

Gervais, C., R. Trahan, D. Moreno, and A.-M. Drolet. 1993. Le *Phragmites australis* Au Québec: Distribution Géographique, Nombres Chromosomiques Et Reproduction. *Canadian Journal of Botany*, 71 (10): 1386–1393.

Gitelson, A. A., Y. Gritz, and M. N. Merzlyak. 2003. Relationships Between Leaf Chlorophyll Content and Spectral Reflectance and Algorithms for Non-destructive Chlorophyll Assessment in Higher Plant Leaves. *Journal of Plant Physiology*, 160 (3): 271–282.

Gitelson, A. A., Y. J. Kaufman, and M. N. Merzlyak. 1996. Use of a Green Channel in Remote Sensing of Global Vegetation from EOS-MODIS. *Remote Sensing of Environment*, 58 (3): 289–298.

Gitelson, A. A., Y. J. Kaufman, R. Stark, and D. Rundquist. 2002. Novel Algorithms for Remote Estimation of Vegetation Fraction. *Remote Sensing of Environment*, 80 (1): 76–87.

Gitelson, A. A. and M. N. Merzlyak. 1998. Remote Sensing of Chlorophyll Concentration in Higher Plant Leaves. *Advances in Space Research*, 22 (5): 689–692.

Gonzalez-Andujar, J. L. and C. Fernandez-Quintanilla. 1991. Modeling the Population Dynamics of *Avena sterilis* Under Dry-land Cereal Cropping Systems. *Journal of Applied Ecology*, 28: 16–27.

van Groenendael, J. M. 1988. Patchy Distribution of Weeds and Some Implications for Modeling Population Dynamics: a Short Literature Review. *Weed Research*, 28 (6): 437–441.

Hara, T. 1994. Growth and Competition in Clonal Plants-persistence of Shoot Populations and Species Diversity. *Folia Geobotanica*, 29 (2): 181–201.

Haslam, S. M. 1972. *Phragmites communis* Trin. (Arundo *Phragmites* L.,? *Phragmites australis* (Cav.) Trin. ex Steudel). *Journal of Ecology*, 60 (2): 585–610.

Kettenring, K. M., M. K. McCormick, H. M. Baron, and D. F. Whigham. 2009. *Phragmites australis* (Common Reed) Invasion in the Rhode River Subestuary of the Chesapeake Bay: Disentangling the Effects of Foliar Nutrients, Genetic Diversity, Patch Size, and Seed Viability. *Estuaries and Coasts*, 33 (1): 118–126.

Kettenring, K. M., M. K. McCormick, H. M. Baron, and D. F. Whigham. 2011. Mechanisms of *Phragmites australis* Invasion: Feedbacks Among Genetic Diversity, Nutrients, and Sexual Reproduction. *Journal of Applied Ecology*, 48 (5): 1305–1313.

Kettenring, K. M. and D. F. Whigham. 2009. Seed Viability and Seed Dormancy of Non-native *Phragmites australis* in Suburbanized and Forested Watersheds of the Chesapeake Bay, USA. *Aquatic Botany*, 91 (3): 199–204.

Kiviat, E. 2010. *Phragmites* Management Sourcebook for the Tidal Hudson River and the Northeastern States. Annandale, NY: Hudsonia Ltd.

Lamb, D. W. and R. B. Brown. 2001. PA—Precision Agriculture. *Journal of Agricultural Engineering Research*, 78 (2): 117–125.

Lenssen, J. P. M., F. B. J. Menting, and W. H. van der Putten. 2004. Do Competition and Selective Herbivory Cause Replacement of *Phragmites australis* by Tall Forbs? *Aquatic Botany*, 78 (3): 217–232.

Lu, S., Y. Shimizu, J. Ishii, S. Funakoshi, I. Washitani, and K. Omasa. 2009. Estimation of Abundance and Distribution of Two Moist Tall Grasses in the Watarase Wetland, Japan, Using Hyperspectral Imagery. *ISPRS Journal of Photogrammetry and Remote Sensing*, 64 (6): 674–682.

Lutman, P. J. W. 2002. Estimation of Seed Production by *Stellaria media*, *Sinapis arvensis* and *Tripleurospermum inodorum* in Arable Crops. *Weed Research*, 42 (5): 359–369.

Maheu-Giroux, M. and S. de Blois. 2006. Landscape Ecology of *Phragmites australis* Invasion in Networks of Linear Wetlands. *Landscape Ecology*, 22 (2): 285–301.

McCormick, M. K., K. M. Kettenring, H. M. Baron, and D. F. Whigham. 2009. Extent and Reproductive Mechanisms of *Phragmites australis* Spread in Brackish Wetlands in Chesapeake Bay, Maryland (USA). *Wetlands*, 30 (1): 67–74.

McKee, J. and A. J. Richards. 1996. Variation in Seed Production and Germinability in Common Reed (*Phragmites australis*) in Britain and France with Respect to Climate. *New Phytologist*, 133 (2): 233–243.

Meyer, G. E. and J. C. Neto. 2008. Verification of Color Vegetation Indices for Automated Crop Imaging Applications. *Computers and Electronics in Agriculture*, 63 (2): 282–293.

Mirik, M., K. Steddom, and G. J. Michels. 2006. Estimating Biophysical Characteristics of Musk Thistle (*Carduus nutans*) With Three Remote Sensing Instruments. *Rangeland Ecology & Management*, 59 (1): 44–54.

Pellegrin, D. and D. P. Hauber. 1999. Isozyme Variation Among Populations of the Clonal Species, *Phragmites australis* (Cav.) Trin. Ex Steudel. *Aquatic Botany*, 63 (3-4): 241–259.

Rice, D., J. Rooth, and J. C. Stevenson. 2000. Colonization and Expansion of *Phragmites australis* in Upper Chesapeake Bay Tidal Marshes. Wetlands 20 (2): 280–299.

Rouse, J. W., R. H. Haas, J. A. Schell, and D. W. Deering. 1973. Monitoring Vegetation Systems in the Great Plains with ERTS. *In Third ERTS Symposium, ed. S. C. Freden and M. A. Becker*, 1:309–317.

Rundquist, D. C., S. Narumalani, and R. M. Narayanan. 2001. A Review of Wetlands Remote Sensing and Defining New Considerations. *Remote Sensing Reviews*, 20 (3): 207–226.

Rundquist, D. C., R. Perk, B. Leavitt, G. Keydan, and A. A. Gitelson. 2004. Collecting Spectral Data over Cropland Vegetation Using Machine-positioning Versus Hand-positioning of the Sensor. *Computers and Electronics in Agriculture*, 43 (2): 173–178.

Sakai, A. K., F. W. Allendorf, J. S. Holt, D. M. Lodge, J. Molofsky, K. A. With, S. Baughman, et al. 2001. The Population Biology of Invasive Species. *Annual Review of Ecology and Systematics*, 32 (1): 305–332.

Tucker, G. C. 1990. The Genera of *Arundinoideae* (*Gramineae*) in the Southeastern United States. *Journal of the Arnold Arboretum*, 71.
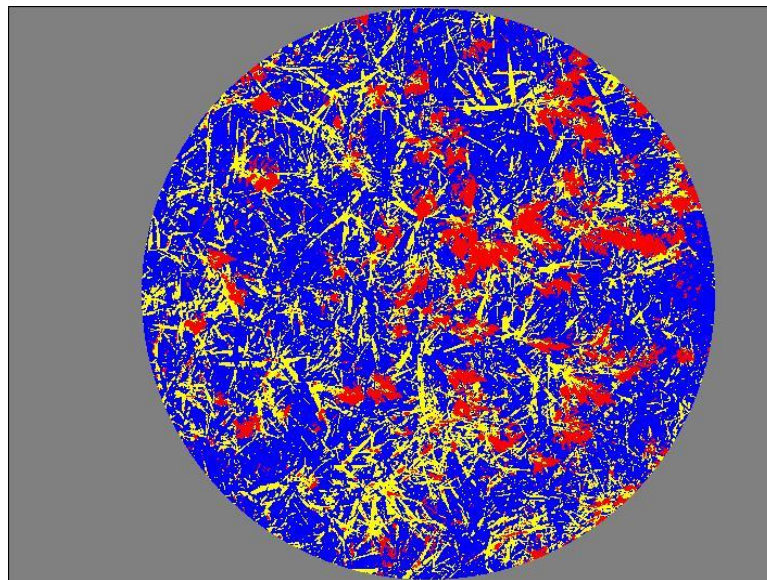
Figure 4.1 (a)

Figure 4.1 (b)

Figure 4.1 (a-b). Figure 4.1 (a) is a digital photograph taken over the *P. australis* canopy sampled in support of the research. Figure 4.1 (b) is the result of applying a user defined threshold to the image after the second transformation {(Red / Green) / (Green / Blue)} had been applied. The image is classified into four categories with gray representing areas outside the Ocean Optics IFOV, blue representing green vegetation and background material, yellow representing yellow leaves, and red representing plant inflorescences.
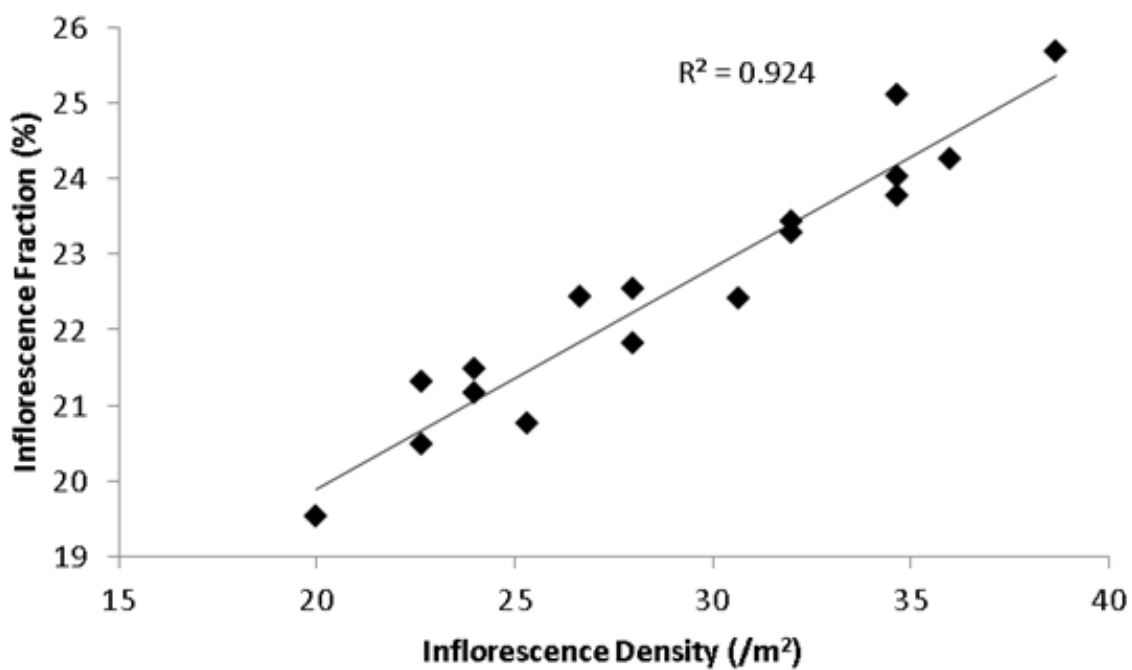
Figure 4.2. Linear regression of Inflorescence Density vs. Inflorescence Fraction. Note the strong, positive linear correlation between inflorescence density and inflorescence fraction (R^2=0.924).
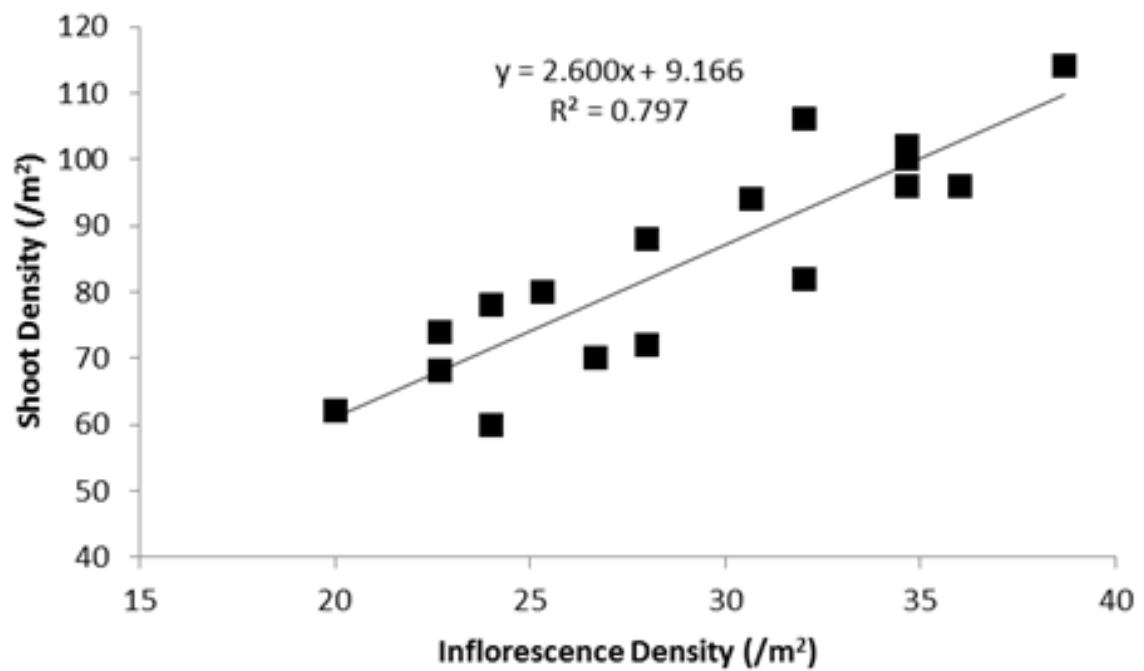
Figure 4.3. Linear regression of Inflorescence Density vs. Shoot Density. Note the strong, positive linear correlation between inflorescence density and shoot density (R^2=0.797). The slope of the best-fit line indicates that there is an average of 2.6 *P. australis* culms for every inflorescence observed.
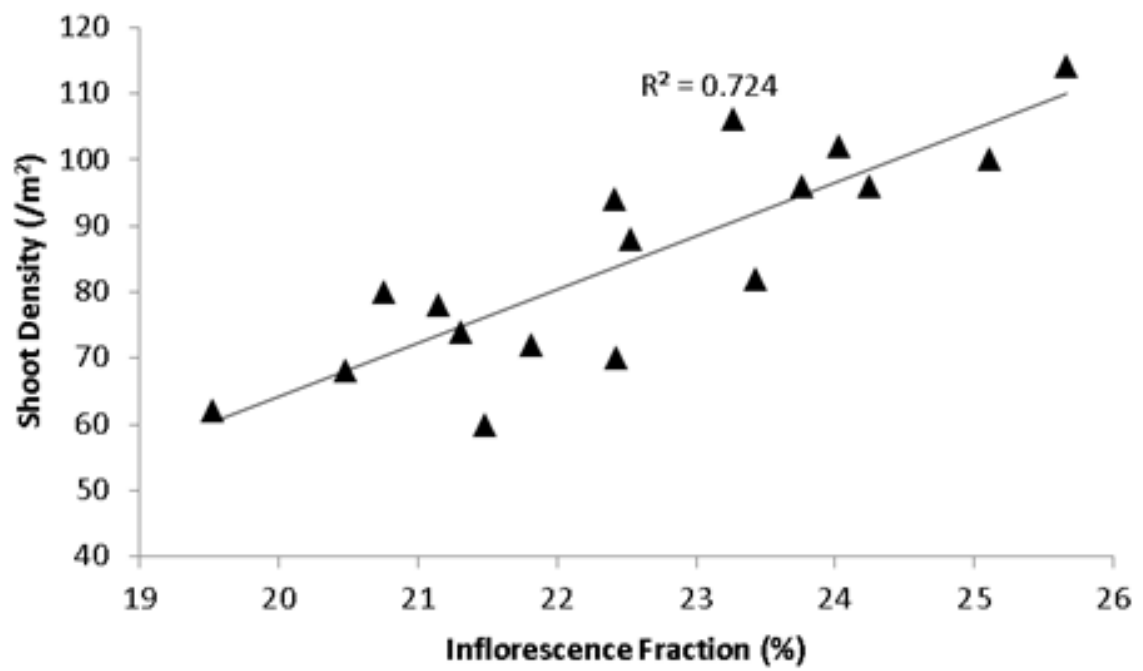
Figure 4.4. Linear regression of Inflorescence Fraction vs. Shoot Density. Note the strong, positive linear correlation between inflorescence fraction and shoot density (R^2=0.724).
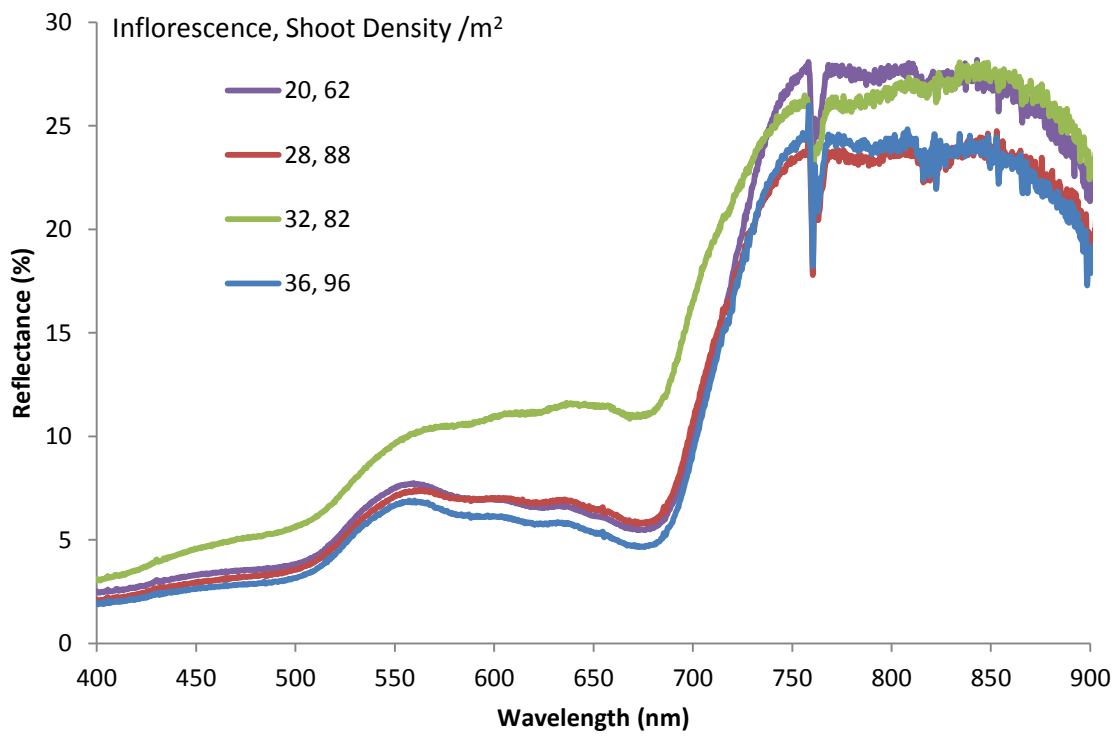
Figure 4.5. Reflectance spectra (Ocean Optics) of the *P. australis* canopy between 400 – 900 nm with changes in inflorescence density and shoot density.
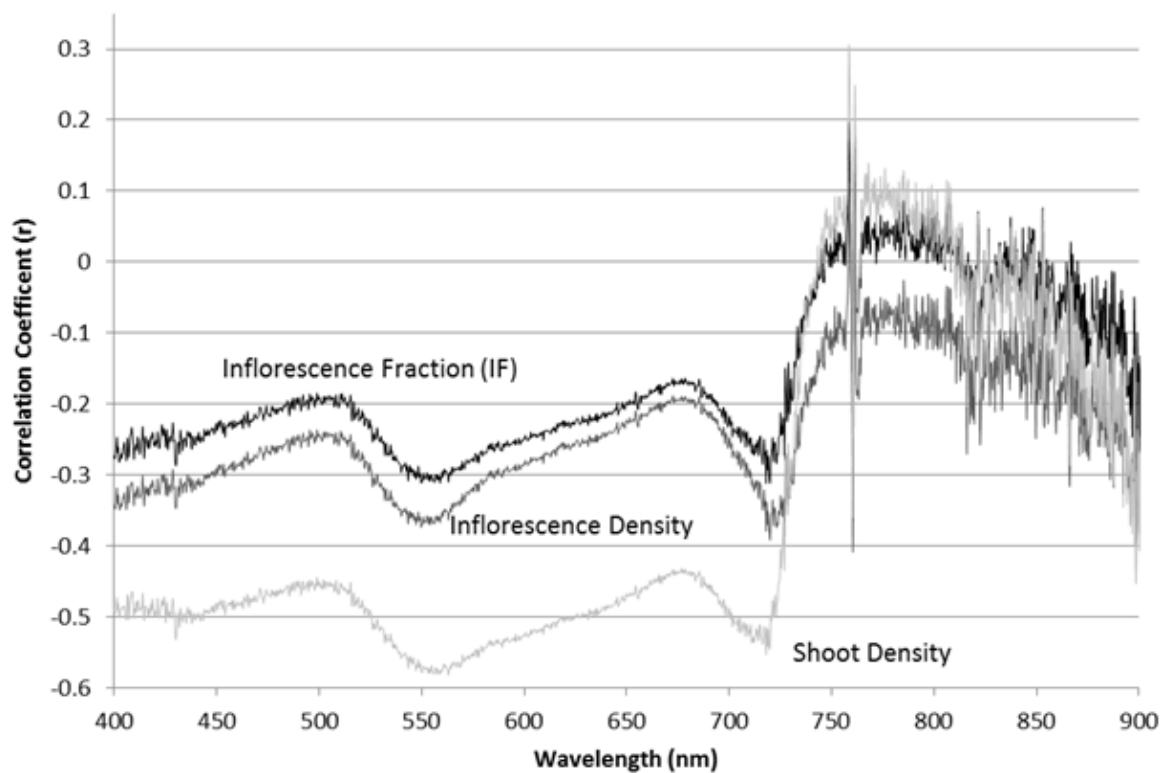
Figure 4.6. Correlation coefficients between recorded measurements of inflorescence fraction, inflorescence density, and shoot density vs. reflectance in the VIS through NIR (400 – 900 nm) spectrum. Correlations are negative in the visible range (400 – 700 nm), with the highest negative correlations observed in the green (540 – 560 nm) and red edge (710 – 720 nm) ranges. The correlations in the NIR (750 – 800 nm) are near zero with little variability.
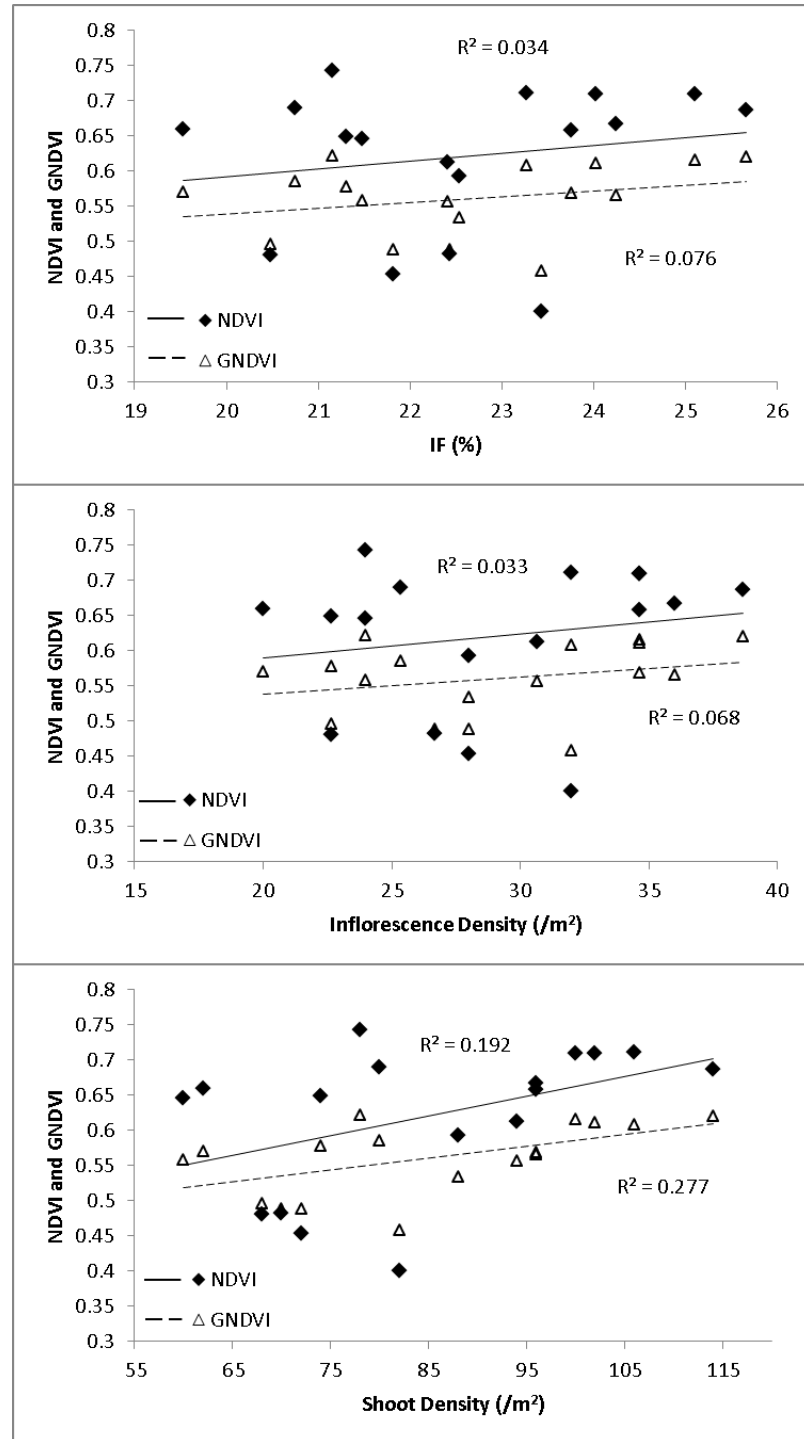
Figure 4.7 (a-c). Correlations of NDVI and GNDVI vs. a) inflorescence fraction, b) inflorescence density, and c) shoot density. Relationships between the indices and measured biophysical variables were all non-significant ($\alpha = 0.01$) except GNDVI vs. shoot density, in which a weak, positive correlation resulted.

CHAPTER 5

CONCLUSION

INTRODUCTION

Proximal sensing is a vital diagnostic tool for understanding the spectral response of an individual plant species. Therefore, the research performed in this paper presents a method for not only studying *Phragmites australis* in some considerable detail at one point in time, but the technology also allows one to monitor the plant community over an extended period of time; for example, an entire growing season. Thus, the general goal of this thesis was to demonstrate the manner in which two very different types of sensors, a sophisticated hyperspectral field radiometer as compared to a simple digital camera, are capable of providing valuable information with regard to the morphology, phenology, and reproductive/spread characteristics of the invasive plant, *P. australis.*

CHAPTER 2: REFINING METHODS FOR SPECTRAL CALIBRATION IN THE FIELD

Chapter 2 was developed in response to resolve errors discovered in the multi-temporal reflectance data acquired over the *P. australis* canopy during the 2011 field campaign. The specific objectives of that chapter were as follows:

1) Review the challenges in matching inter-calibrated radiometers.

Prior to identifying the cause behind the discrepancy in the spectral profiles was to review and understand the rudimentary mechanics behind operating dual spectroradiometers in a concurrent mode, and relating those procedures to quality control regarding data collection. Therefore, Chapter 2 was a summary of the many of the complexities and details concerning the use of proximal sensing systems, and the document emphasized guidelines that must be followed in order to obtain accurate, scientifically valid spectral data.

2) Identify the cause(s) of the problem noted that implied the lack of precise radiometric matching of the two sensors used in data collection (which led to measurement errors).

Because apparent spurious measurements were found in the spectral curves of *P. australis*, it was determined that moisture condensing under the cosine diffuser attached to the upward-looking radiometer was the probable cause of the non-equality in sensor performance.

3) Suggest a potential method to correct the errors in acquired spectral data (i.e., thus preventing data loss).

As a means of providing a correction to the erroneous reflectance measurements caused by moisture contaminating the signal acquired by the upward-looking radiometer, the collected downwelling irradiance impinging upon the *P. australis* canopy during the 2011 field season was normalized to photon flux data acquired simultaneously by a pyranometer. The adjusted spectral signature for *P. australis* appeared much more

congruent with a reflectance profile of a typical vegetation canopy, and allowed for the quantitative analyses undertaken in the chapter which followed.

CHAPTER 3: REMOTE MONITORING OF PHENOLOGY AND VEGETATION FRACTION IN *PHRAGMITES AUSTRALIS*

Chapter 3 was focused on monitoring the growth of *P. australis* by means of summarizing multi-temporal hyperspectral reflectance collected in close proximity to the canopy. Specifically, the objectives of this chapter were

1) Characterize the spectral response of a canopy of *P. australis* over an entire growing season.

The chapter presented and described the variability observed in the hyperspectral reflectance from the *P. australis* canopy over a period of seven months. With respect to changes in the canopy reflectance, four phenological stages were clearly identified in spectra: emergence, vegetative growth, flowering, and senescence.

2) Relate the multi-temporal spectra to changes in fraction of vegetative cover.

As vegetation fraction, or percent canopy coverage, increased during the emergence and vegetative growth stages, reflectance in the visible decreased while reflectance in the near-infrared decreased. Reflectance in the red region remained more sensitive to changes in vegetation fraction. Further analysis showed that canopy albedo, or the combination of visible light reflecting from the vegetation, was higher during the vegetative growth than the flowering stage even at equal amounts of vegetation fraction.

Thus, objective 3 of the chapter was initiated in order to understand why this phenomenon was occurring.

3) Deconvolve the primary components that make up the composite spectral signature of both living and non-living material comprising an individual sensor field of view.

By deconvolving the primary constituents (vegetation, inflorescence, shadows, and background litter) comprising of the upwelling spectral signal emanating from a plant canopy, it was possible to determine the percent coverage of each component. From this analysis, it was determined that changes in the canopy albedo (noted in objective 3) between the vegetative growth and flowering stages were primarily caused by differences in the observable area of plant inflorescence versus soil background. As a result, a new spectral transformation, termed Albedo Corrected Vegetation Index (ACVI), was generated in order estimate vegetation fraction without bias towards differences in reflected albedo caused by changes in the canopy structure.

4) Examine selected spectral transformations (i.e., vegetation indices) for determining which appears best for continued monitoring of the canopies using remotely sensed data.

The new index, ACVI, was tested alongside Normalized Difference Vegetation Index (NDVI) and Visibly Resistant Atmospheric Index (VARI) for estimating vegetation fraction in the *P. australis* canopy. The results showed a high positive correlation between ACVI and vegetation fraction and the accuracy exceeded the other indices tested.

CHAPTER 4: REMOTE SENSING OF SEED PRODUCTION AND PLANT DENSITY IN *PHRAGMITES AUSTRALIS*

Chapter 4 summarizes the testing of two proximal sensing systems, a hyperspectral radiometer and a simple digital camera, for:

1) Estimating seed production (number of florets produced/m^2) of a *P. australis* canopy.

Inflorescence density, (inflorescences/m^2), was used as a surrogate for estimating seed production. In order to estimate the inflorescence density with a digital camera, inflorescence fraction (IF), or area of inflorescence classified in a digital photograph, was determined. The results of this analysis ($R^2 = 0.924$) showed promising potential for estimating seed production of the *P. australis* canopy with use of a digital camera. Vegetation indices, including and Green Normalized Difference Vegetation Index (GNDVI), were examined as possible means to estimate seed production using the radiometer approach; however, the results were poor.

2) Estimating shoot density (number of culms/m^2) of a *P. australis* canopy.

Methods similar to Objective 1 of this chapter were employed for estimating shoot density within the *P. australis* canopy. Because high correlations were observed between IF vs. inflorescence density and between inflorescence density vs. shoot density, IF was used as a surrogate for estimating shoot density with the use of the digital camera. The results suggest that IF may be used as a proxy for estimating shoot density as determined by the high correlation ($R^2 = 0.724$). However, NDVI and GNDVI vs. shoot

density were again poor; suggesting that the hyperspectral radiometer approach was inadequate for estimating either of the biophysical plant characteristics.

IMPLICATIONS OF RESEARCH

The study of the morphology of a vegetation species based upon a sensor operating with hyperspectral resolution, and in close proximity to the target of interest, is invaluable to understanding the basic species-specific reflectance characteristics as well as light interactions within the canopy. Therefore, in this study, I have sought to understand the basic spectral signature of a particular vegetation canopy and analyze the acquired data from a quantitative point of view. My hope was that the results are somehow useful for land managers.
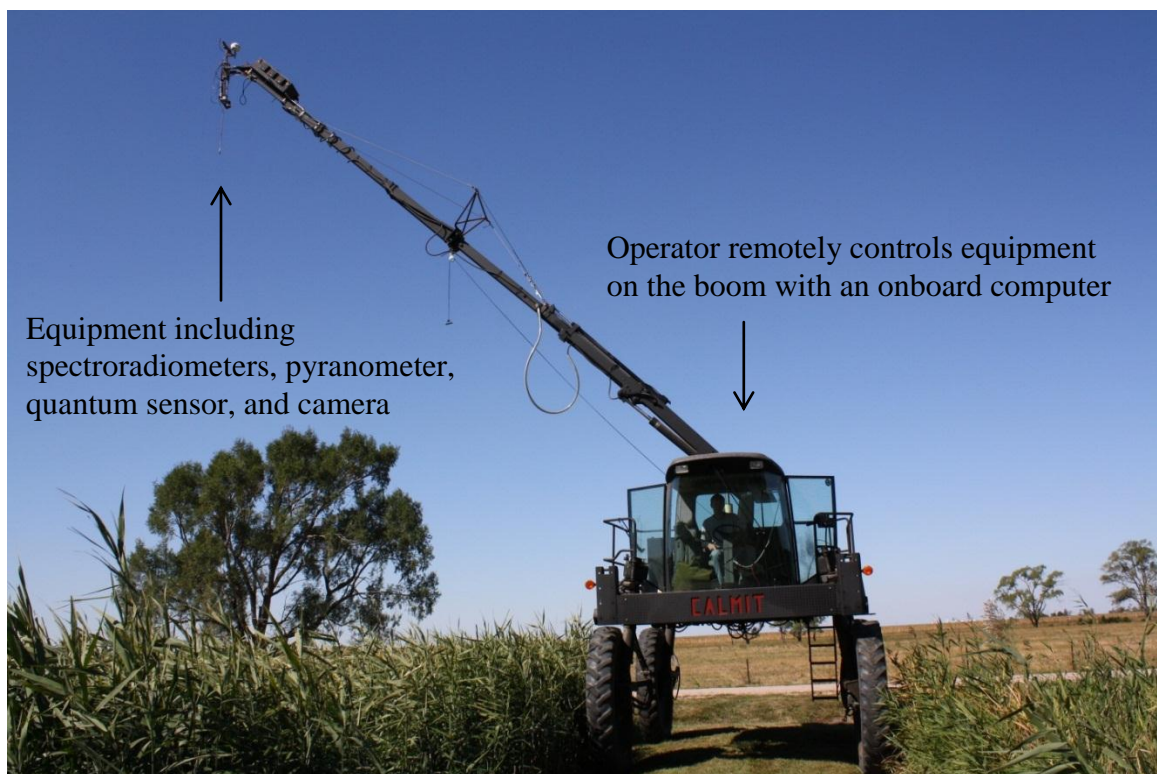
The high spectral, spatial, and temporal resolution of the data acquired in support of this research through proximal sensing techniques, provides the first spectral library that describes and characterizes the growth of *P. australis*. This information should be useful for better understanding spectral information acquired from aerial or satellite platforms.

Characterizing biophysical parameters of a plant canopy, including VF, shoot density, and inflorescence density, are important for understanding the growth and development of the vegetative stand. The research presented in this thesis has demonstrated the potentiality for estimating VF, shoot density, and inflorescence density using spectral data acquired by sensors such as dual-linked spectroradiometers and a simple digital camera.

Further implications of this study may relate to the procedures associated with collecting scientifically valid spectral data in a field setting. When undertaking spectroscopy in a field setting, the procedures associated with obtaining useful and meaningful data are quite challenging as well as intricate. Researchers must be cognizant of extraneous factors that may affect the composite reflectance signal, including condensation as discovered in this study, which may create difficulty in the inter-calibration of two radiometers operating in tandem.

FURTHER RESEARCH

Further research is needed where monitoring the growth and physiology of *P. australis* is accomplished at a broader scale, such as with aerial or satellite platforms. Furthermore, spectral signatures acquired in this research should be compared very carefully to those acquired in similar fashion over canopies of other invasive plant species. In addition, the spectral index, here termed ACVI, which was developed specifically for this study as an improved means of quantifying vegetation fraction, needs further analysis to determine its robustness for use with other plant canopies. Finally, the results presented in this paper may be intrinsic to the site-specific growing conditions. Future research should consider examining differences in the biophysical characteristics of *P. australis* studied herein to those of other geographic locales and changes in climatic conditions, as well as differences in canopy structure.

APPENDIX

Equipment including spectroradiometers, pyranometer, quantum sensor, and camera

Operator remotely controls equipment on the boom with an onboard computer

Appendix A. CALMIT's all-terrain research vehicle, "Hercules", collecting spectral data above *P. australis* canopy near Mead, NE in September 2011.